EFFECT OF SHOT PEENING COVERAGE ON MICROSTRUCTURE AND MECHANICAL PROPERTIES OF THE PLASMA NITRIDED AISI 316L STAINLESS STEEL

Thesis

Submitted in partial fulfilment of the requirements for the degree of

DOCTOR OF PHILOSOPHY

by

JAYALAKSHMI M.

DEPARTMENT OF METALLURGICAL AND MATERIALS ENGINEERING

NATIONAL INSTITUTE OF TECHNOLOGY KARNATAKA, SURATHKAL, MANGALORE – 575025

March, 2019

DECLARATION

I hereby *declare* that the Research Thesis entitled **"EFFECT OF SHOT PEENING COVERAGE ON MICROSTRUCTURE AND MECHANICAL PROPERTIES OF THE PLASMA NITRIDED AISI 316L STAINLESS STEEL"** which is being submitted to the **National Institute of Technology Karnataka, Surathkal** in partial fulfilment of the requirements for the award of the Degree of **Doctor of Philosophy** in the **Department of Metallurgical and Materials Engineering** is a *bonafide report of the research work carried out by me*. The material contained in this Research Thesis has not been submitted to any University or Institution for the award of any degree.

JAYALAKSHMI M.
Register Number: 123012MT12F03

Department of Metallurgical and
Materials Engineering

Place: NITK Surathkal, Srinivasnagar

Date:

C E R T I F I C A T E

This is to certify that the Research Thesis entitled **"EFFECT OF SHOT PEENING COVERAGE ON MICROSTRUCTURE AND MECHANICAL PROPERTIES OF THE PLASMA NITRIDED AISI 316L STAINLESS STEEL"** submitted by **Ms. Jayalakshmi M. (Register Number: 123012MT12F03)** as the record of the research work carried out by her, *is accepted as the Research Thesis submission* in partial fulfilment of the requirements for the award of degree of **Doctor of Philosophy.**

Research Guides

Prof. Udaya Bhat K.   Prof. B. Ramachandra Bhat
Professor   Professor
Dept. of Metallurgical and   Dept. of Chemistry
Materials Engineering

Chairman – DRPC

Dedicated

to

the Almighty God

ACKNOWLEDGEMENTS

ABSTRACT

In this study, surface nanocrystallization produced by air-blast shot peening is used as a pretreatment step to enhance the kinetics of plasma nitriding. Hot-rolled plates of AISI 316L grade stainless steel samples were subjected to air-blast shot peening. Peening was carried out at different peening coverage, from conventional to severe; to assess the effect of coverage on surface nanocrystallization and subsequent diffusion. This was followed by plasma nitriding in the temperature range of 300-500 °C for the duration of 4 hours. Microstructural characterization was carried out by using scanning electron microscope, X-Ray diffractometer, transmission electron microscope, while mechanical properties of the treated layer was analysed by using microhardness and nanoindentation testers.

Peening process lead to the formation of deformation induced martensite (DIM), and its fraction was found to increase with the peening coverage. Depth of the nanostructured layer and surface microhardness also increased with the increase in coverage. Severe shot peening generated about 500 μm thick gradient nanostructured (GNS) layer at the peened surface. The hot-rolled parent austenitic microstructure having grain size in the range of 40–80 μm was refined to dislocation cell- type martensite of cell size in the range of 100–140 nm. Nucleation of DIM was not limited to shear band intersections. Martensite units found to nucleate at multiple locations in the austenite; like parallel to shear bands, within the shearbands, across the shearbands, at the grain boundary, etc.

Nitriding temperature of 300 °C was found insufficient to produce continuous nitride layer in spite of the severe peening pre-treatment; while nitriding at 500 °C resulted in the precipitation of the chromium nitride phase. Nitriding of un-peened and severe peened samples at 400 °C did not show chromium nitride precipitation. Significant improvement in nitride layer thickness was obtained at this temperature; from less than 1 μm for the un-peened sample to about 50 μm for the severe peened sample. Transmission electron microscopy affirmed that the nitride layer in the severe peened nitrided sample was largely martensitic in nature. Synergetic effect of selection of

right nitriding temperature, surface nanocrystallization, drastic increase in the number of dislocations and other defects, deformation induced transformation of austenite to martensite, etc. are opined to be reasons for enhanced diffusion kinetics.

Hardness of the treated surface evaluated by microhardness method showed that the surface hardness increase with increase in the peening coverage and a similar trend was observed upon nitriding as well. These results were found to be in accordance with the results of scratch testing. Nanoindentation and nano-scale wear tests of the base metal, severe peened and severe peened-nitrided sample (nitrided at 400 °C) affirmed the improvement in the properties after the duplex treatment of shot peening and plasma nitriding.

CONTENTS

List of Figures

List of Tables

NOMENCLATURE

ABSP	Air-blast shot peening
AISI	American iron and steel institute
ASM	American society for metals
ASTM	American society for testing of materials
BCC	Body centered cubic
CrN	Chromium nitride
DIM	Deformation induced martensite
EDS	Energy dispersive spectroscopy
γ_N	Expanded austenite
FCC	Face centered cubic
GNS	Gradient nano-structured
HCP	Hexagonal close packing
OM	Optical microscopy
SAED	Selected area electron diffraction
SEM	Scanning electron microscopy
SMAT	Surface mechanical attrition treatment
TEM	Transmission electron microscopy
XRD	X-ray diffraction

CHAPTER 1

INTRODUCTION

Austenitic stainless steels are the most versatile class of alloys which find applications in automobile, aerospace, domestic, medical, nuclear industries and many more diverse domains. Moderate strength, good formability and excellent corrosion resistance at ambient service conditions are major properties of this class of stainless steels which make them find widespread applications. However, austenitic stainless steels reportedly have lower surface hardness and wear resistance (Sun and Bell 1998, Menthe et al. 2000).

Nitriding of austenitic stainless steels is a well-established surface modification process used for the improvement of wear resistance of the industrial components. It is a technique in which a hard, wear resistant nitride layer will be formed on the component surface while properties of the core remain unaltered. Amongst the nitriding techniques available plasma nitriding offers unique advantages, like lower nitriding temperatures, dimensional stability, uniform case depth, possibility of automation, environmentally benign, etc. (Surface engineering ASM handbook 1994, Larisch and Spies 1999).

During plasma nitriding, nitrogen is transferred to the sample surface in the plasma environment and further it diffuses inside to form a modified layer consisting of various nitride phases. Plasma nitriding has advantages over other nitriding techniques in nitriding of austenitic stainless steels, as it is capable of removing the adherent Cr_2O_3 layer; thus improving the nitriding efficiency significantly. With plasma nitriding technique, low temperature nitriding of austenitic stainless steels are viable. It is known that the higher nitriding temperatures would result in the precipitation of the chromium nitride (CrN). Precipitation of the CrN is deleterious as it impairs the corrosion resistance. There are reports indicating that nitriding temperature less than 450 °C prevents formation of the chromium nitride (Zhang and Bell 1985) (Blawert et al. 1996) (Gil et al. 2006). However, the case depth achieved

1

would be significantly lower owing to slower diffusion kinetics of the nitrogen through the austenite lattice.

Surface nanocrystallization refers to the formation of the nano-sized grains on the component surface through severe deformation processes. During the process, original coarse grain structure would be replaced by the ultra-fine grains. The nanostructured surface is associated with higher surface energy due to presence of the increased dislocation density, higher fraction of the grain boundaries, triple junctions, etc. Hence, such a surface is proven to be beneficial during diffusion based surface modification techniques, like nitriding (Tong 2013), nitrocarburizing (Wu and Yan 2011), boriding (Yang et al. 2013), etc. Higher defect concentration in the surface and sub-surface region is known to improve the kinetics of the diffusion. Specific to austenitic stainless steels, deformation induced martensitic transformation is highly probable upon severe deformation. Martensite being the open structure further enhances the diffusion kinetics. Hence, several attempts were made to utilize severe plastic deformation techniques as pre-treatment methods for low temperature plasma nitriding of the austenitic stainless steels.

Surface nanocrystallization of the austenitic steels is achieved popularly through the processes, like surface mechanical attrition treatment (SMAT) (Lin et al. 2006) (Laleh et al. 2013) (Chemukhi et al. 2013) (Baluswamy et al. 2013), air-blast shot peening (Hashemi et al. 2011) (Ji et al. 2005) (Shen et al. 2010), laser shock peening (Lu et al. 2000), high pressure torsion (HPT) (Ferkel et al. 2003), cold rolling (Nishimoto et al. 2009) etc. Severe plastic deformation followed by plasma nitriding, found to yield appreciably thick nitride layers.

Air-blast shot peening is the most widely adopted and industrially viable process; which bears unique advantages over other techniques to induce surface nanocrystallization. Though the conventional shot peening is basically adopted to impart the compressive residual stresses in the material, it could be used for grain refinement by increasing the peening severity. However, in the literature, reports related to application of severe shot peening as pre-treatment to plasma nitriding are rather limited; with some of them (Shen et al. 2010) (Hashemi et al. 2011) being

2

associated with the problem of CrN formation. Considering the cost-effectiveness and versatility of shot peening process, it is relevant to understand the effect of conventional to severe peening processes on the surface nanocrystallization, improvement in the nitride layer thickness upon low temperature plasma nitriding and assessment of mechanical properties of the treated surface after the duplex treatment.

It is also relevant to study the microstructural development during severe shot peening to gain insights about the mechanism of the grain refinement and the martensitic transformation. On the other hand, study of the literature indicates that no common opinion exists amongst the researchers about the phases formed during plasma nitriding of the pre-deformed austenitic stainless steels. Detailed microstructural characterization is necessary to analyze the surface layer formed during duplex treatment as well.

Hence, the present study is focused on studying the effect of the shot peening pre-treatment on microstructural and mechanical properties of the AISI 316L grade stainless steel subjected to low temperature plasma nitriding process. The details of the study are represented in this thesis as different chapters. Second chapter discusses the literature relevant to the study. This chapter also defines the objectives and scope of the study. Details of the equipments and process parameters related to experimental procedures and characterization are mentioned in chapter three. Results of microstructural and mechanical characterization are documented in chapter four. Relevant discussions on the results obtained; with reference to the reported literature, are elaborated in chapter five. Inferences from the present study are summarized in chapter six.

CHAPTER 2

LITERATURE REVIEW

This chapter discusses the review of the literature in the areas of plasma nitriding of the austenitic stainless steels, effect of surface severe deformation by various peening methods, effect of pre-treatment on plasma nitriding of the stainless steels, etc. After discussing the relevant research papers in the area, objectives of the present study are listed along with the scope of the work.

2.1 Nitriding

Nitriding is a well known surface modification technique used for improving the hardness, wear resistance and fatigue resistance of the components. It involves diffusion of nitrogen into the component surface from an atmosphere of higher nitrogen potential; resulting in a hard nitride layer on the component surface. The nitriding process was developed in early 19th century by Adolph Machlet, who was working as a metallurgical engineer for the American Gas Company. Since then, nitriding has been a popular industrial technique for surface hardening of ferrous and non-ferrous systems along with other diffusion based surface hardening techniques like carburizing, borizing, nitrocarburizing, etc.

Three main types of nitriding treatment are (ASM handbook Vol.5 1994)

1. Gas nitriding

2. Salt bath nitriding

3. Plasma nitriding

In gas nitriding process, nascent nitrogen for diffusion is obtained through the dissociation of ammonia gas at 500-570 ⁰C. Kinetics of ammonia dissociation is relatively low and hence, longer nitriding duration is needed to achieve considerably thick nitride layer on the component surface. The nitriding kinetics is largely

dependent on the surface conditions and additional surface activation would be necessary in the case of stainless steels having higher chromium content.

In salt bath nitriding process, the diffusion of nitrogen is facilitated through the dissociation of the nitrogen containing salts. Cyanide salts are widely used in the process. Process offers uniform case depth, as well as shorter nitriding durations compared to gas nitriding. However, application of the process is limited as cyanide salts are highly toxic. Disposal of the salts used for nitriding will result in serious environmental hazards.

During plasma nitriding, nascent nitrogen required for the nitriding process is obtained from the ionization of a gas mixture containing nitrogen. This process offers unique advantages over the other variants of nitriding and hence, is popular in the recent times.

The advantages of plasma nitriding process over other nitriding processes are listed below (ASM handbook Vol.5 1994)

(a) Environmentally benign

(b) Uniform case depth

(c) Shorter cycle time

(d) Better tailoring of nitride layer thickness and characteristics by precise control of process parameters

(e) Capability of nitriding stainless steels and titanium alloys

(f) Better dimensional stability.

2.2 Plasma nitriding

Process of plasma nitriding was developed by German physicist Dr. Wehnheldt in 1932 while it gained world-wide industrial acceptance in mid 1970s. The process is also called as glow discharge nitriding and ion nitriding. It is based on the generation of the plasma by ionizing the gas mixture and subsequent inward diffusion of the

nitrogen into the surface of the component to be nitrided. Figure 2.1 depicts the schematic diagram of plasma nitriding process.
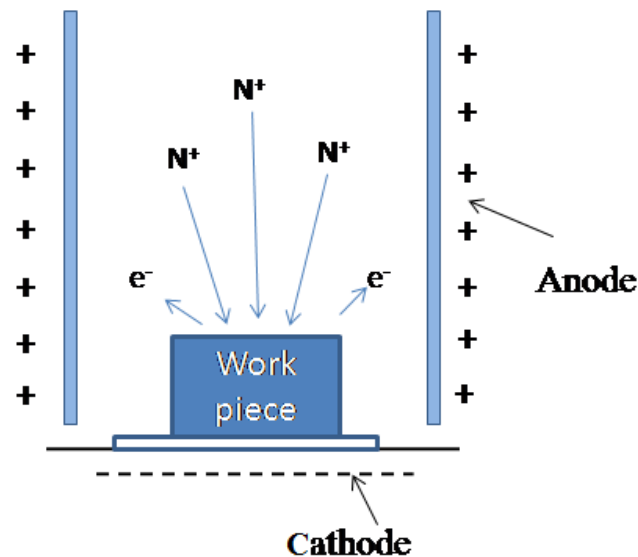
Fig. 2.1 Schematic diagram showing the principle of plasma nitriding process

During the process, the nitriding chamber is evacuated to a pressure of 0.05 to 0.1 torr in order to drive out the atmospheric air and the contaminants. The chamber is heated to nitriding temperature by the use of resistance heaters. Subsequently, a mixture of nitrogen and hydrogen gases at desired ratio is introduced into the chamber. Process gas pressure is maintained in the range of 1 to 10 torr such that the molecular mean free path is optimum to produce and sustain glow discharge on the component surface (Dossett and Totten 2013).

If the chamber pressure is high, energy produced on the molecular impact is low and plasma cannot be used to materialize the nitriding process. If the pressure is significantly lower; then the molecular mean free path will be higher. This would generate high energy during molecular impacts. However, the plasma generated will be intermittent in nature due to lesser number of collisions. In the presence of process gas mixture, the work piece is maintained at a high negative dc potential (500 to 1000 V) with respect to the vessel, which is grounded. Under this condition, the nitrogen gas is dissociated, ionized, and accelerated toward the component.

Within a short distance of the work-piece, the positively charged nitrogen ion acquires an electron from the cathode (work-piece) and thus emits a photon. This photon

emission during the return of the nitrogen ions to their atomic state results in the visible glow discharge that is characteristic of plasma techniques. Upon impact on the work-piece, kinetic energy of the nitrogen atoms is also converted into heat, which can totally bring the load to nitriding temperature. Auxiliary heating elements are also used to maintain the desired nitriding temperature. Nitrogen diffuses into the work piece at high temperature. Inward diffusion of the nitrogen during the nitriding cycle leads to the development of the nitride layer on the surface of the work piece (Dossett and Totten 2013).

2.3 Plasma nitriding of the austenitic stainless steels

This section elaborates the advantages of plasma nitriding technique for austenitic stainless steels, phases in the nitride layer formed upon plasma nitriding and the effect of process parameters on the properties of the nitride layer.

2.3.1 Advantages of plasma nitriding

Austenitic stainless steels are important class of ferrous alloys which find wide-spread applications in automobile, nuclear, food and chemical industries. Hardness and wear resistance of these steels are rather limited. Hence, the components are usually subjected to nitriding treatment. Presence of tenacious chromium oxide layer on the surface of the stainless steel suppresses the nitriding efficiency in the case of the gas nitriding and salt bath nitriding processes. Instantaneous removal of the oxide layer during nitriding is a major challenge in these techniques and hence, it is difficult to get thick and uniform nitride layer. Additionally, higher nitriding temperature promotes the formation of the chromium nitride (CrN) precipitates in the nitride layer. This result in the depletion of the chromium content in the matrix; leading to a decrease in the corrosion resistance.

These drawbacks of the conventional nitriding techniques have rendered the plasma nitriding as an efficient technique for nitriding of the austenitic stainless steels. During plasma nitriding, bombardment of ions in plasma helps in instantaneous removal of the native Cr_2O_3 layer on the steel surface and facilitates the efficient in-

take of the nitrogen. This in turn, helps in carrying out nitriding at relatively lower temperatures than gas / liquid bath nitriding (ASM handbook Vol.5 1994).

In literature, there are many studies regarding the plasma nitriding of austenitic stainless steels which elaborate on the phase formation, effect of process parameters, improvement in mechanical properties, etc.

2.3.2 The phase formation

Iron-nitrogen binary phase diagram is shown in Fig. 2.2. It could be observed that the maximum solubility of the nitrogen in the BCC-Fe is 0.1 wt%. Thus, diffusion of the nitrogen leads to formation of the Fe_4N, Fe_2N and FeN in ferritic steels. In contrast, maximum solubility of nitrogen in FCC-Fe is 2.8 wt%. Thus nitriding of austenitic steels lead to formation of interstitial solid solution of nitrogen in austenite.
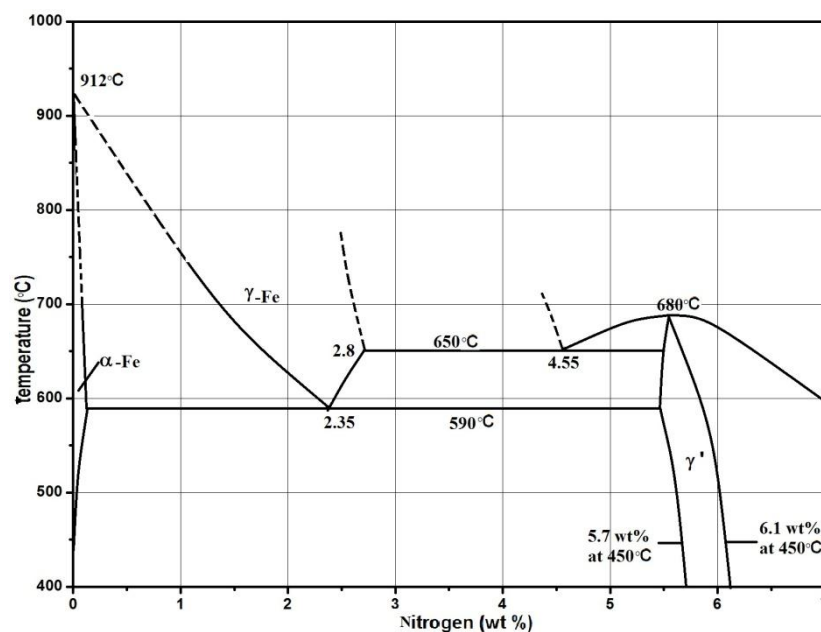
Fig. 2.2 Portion of the Fe-N binary phase diagram from Fe-rich side (Redrawn from the work of Frisk 1987)

The pioneering work in the field of plasma nitriding of the austenitic stainless steel was carried out by Zhang and Bell (1985). In the study, AISI 316 stainless steel was subjected to plasma nitriding over a range of nitriding temperatures. It was reported that plasma nitriding at 570 ℃ resulted in a duplex surface layer of γ' phase and austenite while low temperature plasma nitriding at 400 °C produced a nitride layer

9

which had a corrosion resistance equivalent to that of the original material; along with higher hardness. This phase was termed as S-phase/ expanded austenite by several researchers (Ichii and Fugimura 1986) (Menthe et al. 1995) (Samandi 1995). It was not characterized according to the ASTM X-ray Diffraction Index as it was a supersaturated solid solution of nitrogen in FCC-Fe.

Detailed XRD study of the S-phase was carried out by Sun et al. (1999) using low temperature (400–500 $^\circ$C) plasma nitriding of the AISI 316, 304 and 321 grade austenitic stainless steels. Thin, hard and corrosion resistant layers were produced in case of all three grades; exhibiting similar X-ray diffraction patterns corresponding to the S-phase. But the positions of the major diffraction peaks varied with nitriding temperature and the nitrogen concentration profile. Peaks from the S-phase deviated in a systematic way from those for an ideal FCC lattice. Detailed analysis of the deviation suggested that very high compressive residual stresses and stacking faults were developed in the layers, resulting in a highly distorted and disordered FCC structure. The lattice parameter of the distorted and disordered S-phase was found to increase with the increase in the nitrogen concentration.

Marchev et al. (1998) suggested that ion nitriding of the 316L SS in the range of 400-510 °C for 6- 96 hours lead to formation of the expanded martensite phase (m-phase) which has a tetragonal structure. It is characterized by a doublet peak, i.e. (101) and (110) in the range of 40-47°. The paper emphasizes on the fact that the S-phase reported in the previous studies is not having FCC structure instead it was a tetragonal structural.

Mingolo et al. (2006) studied the plasma nitriding behavior of the AISI 316 austenitic stainless steel at low (400 °C) and high temperatures (550 °C) under different nitriding gas mixtures. Nitrided surfaces were characterized by using XRD. Expanded austenite (S-phase) with minor volume fractions of Fe_3N, Fe_4N and Cr_2N were identified in the nitride layer. Authors opine that the supersaturation of the nitrogen in the austenite leads to distortion of the lattice so that the structure would be closer to a triclinic unit cell. Nitriding at 550 °C lead to the formation of high volume fraction of Fe_4N, Cr_2N and CrN phases, leading to a low distortion of the parent austenitic phase,

maintaining the original cubic lattice. It was observed that different nitrogen and hydrogen gas mixture ratios did not had major effect on the phase formation.

2.3.3 Effect of nitriding on physical and mechanical properties

The work of Gil et al. (2006) assesses the corrosion performance of the 316L austenitic stainless steel subjected to ion nitriding for 8 hours. The corrosion resistance was evaluated in 0.9% sodium chloride solution by using potentiodynamic polarization and linear polarization techniques. Though nitriding treatment found to improve the surface hardness, it found to be prone to localized corrosion. This was found to be due to the precipitation of the deleterious CrN which decreases the chromium content in the matrix necessary to provide the corrosion resistance. This suggests that the process parameters of the nitriding treatment should be chosen meticulously to avoid the chromium nitride precipitation.

Menthe et al. (2000) studied the effect of the plasma nitriding parameters on the mechanical properties of the AISI 304L austenitic stainless steel. Samples were subjected to plasma nitriding treatment by using pulsed-DC plasma unit. Experiments were carried at the nitriding temperature range 375 °C- 475 °C using different nitrogen and hydrogen gas ratio mixtures and nitriding duration. No delamination of the nitride layer was observed upon indentation and scratch hardness measurements. Five-fold improvement in the microhardness was observed upon nitriding. Residual compressive stress on the surface is found to enhance the fatigue life. Significant improvement in the wear resistance was also evident after plasma nitriding. These improvements were attributed to the formation of the S-phase at the nitriding temperature of 400 °C. Hence the authors opine that nitriding temperature has major influence on the nitride layer properties than other process parameters.

Effect of process parameters on the microstructures and wear resistance was assessed by Wang et al. (2009) through plasma nitriding of the 304L SS. Process parameters under consideration were nitriding temperature, time and pressure. A hard and wear-resistant nitride layer was produced on the surface of the stainless steel and analysis of the nitride layers showed that the expanded austenite phase (S-phase) was formed at

temperatures in the range of 350 and 400 °C, whereas CrN layer was formed at 480 °C. The microstructures of the nitride layer were strongly dependent on the nitriding temperature, but not on the nitriding chamber pressure. The effect of nitriding time, over the range from 4 to 8 hours in the present study, was insignificant. S-phase layers found to exhibit improved dry-sliding wear resistance. Similar results were obtained by Li et al. (2008) during plasma nitriding of the 316L stainless steel.

Evaluation of the fatigue properties and texture evolution of the AISI 316 austenitic stainless steel during plasma nitriding treatment was assessed by Stinville et al. (2010) at a nitriding temperature of 400 ℃. Through the use of electron back scattered diffraction study, it was observed that nitriding enhances the crystallographic texture of <001> and <111>. It was also observed that the fatigue strength of the nitrided samples improved in the low cycle fatigue regime; which is attributed to presence of the compressive residual stresses in the nitride layer.

It can be summarized that plasma nitriding of the austenitic stainless steels results in the formation of the expanded austenite phase. Nitriding temperature is the most important process parameter which decides the structure and properties of the nitride layer. Formation of the deleterious CrN precipitates could be hindered by nitriding at low temperatures (below 450 ℃).

2.4 Significance of plastic deformation prior to nitriding

Low temperature plasma nitriding hinders the plasma nitriding kinetics and hence, the case depth obtained would be relatively less. In order to achieve higher case depth, the nitriding duration should be increased. Since nitriding is a process of industrial relevance, increased duration will render the process uneconomical. The first work of Tong et al. (2003) demonstrated that prior deformation could significantly decrease the duration of the nitriding for obtaining a specific case depth; compared to the un-deformed counterparts. With detailed study, it was observed that the nanocrystalline grain structure on the surface of the component to be nitrided enhances the nitriding kinetics.

Surface nanocrystallization is a process of obtaining nanocrystalline / ultra-fine grain structure on the surface by severe plastic deformation processes, such as high pressure torsion, rolling, shot peening, laser peening, surface mechanical attrition treatment (SMAT), etc. Nanostructured surface consists of higher fraction of grain boundaries along with other defects like dislocations, deformation twins, triple junctions, etc. and hence, exhibit greater atomic diffusivity. This helps in faster diffusion of nitrogen through the component there by enhancing the nitriding kinetics. As a result, thicker case depths could be achieved in shorter duration during low temperature plasma nitriding process.

In the work of Tong et al. (2003), pure iron was subjected to the SMAT process to obtain nanostructured surface layer. It was found that homogenous coarse grains of about 100 µm diameter converted to grains of 13 nm diameter upon SMAT. Further, the SMAT and un-SMAT samples were subjected to nitriding at 300 $^\circ$C for 9 hours. It was observed that 10 µm thick nitride layer was obtained in the SMAT sample while there was no observable nitride layer in the un-SMAT counterpart.

2.5 Surface nanocrystallization in austenitic stainless steels

Severe plastic deformation of the austenitic stainless steels, in particular, leads to the transformation of the austenite to the strain induced martensite; in addition to surface nanocrystallization. Martensite being a more open structure than the austenite, it promotes faster diffusion of the nitrogen through its lattice (Yu et al. 2002). Hence prior deformation in the case of austenitic steels has pronounced effect on the kinetics of the plasma nitriding; apart from the advantages stated in section 2.4.

Various peening processes are effective and versatile to bring about surface nanocrystallization. Three major peening techniques used commonly in practice; namely, ultrasonic peening, laser peening and air-blast shot peening. In the present section, effect of these peening processes on the nanocrystallization and martensitic transformation is elaborated.

2.5.1 Ultrasonic peening

Ultrasonic peening is the peening method in which the shots are resonated by using the vibration of an ultrasonic transducer. Here, the ultrasonic energy is used to impart the kinetic energy to the shots. There are several studies on the effect of the ultrasonic peening on the austenitic stainless steels.

The work of Liu et al. (2000) showed that ultrasonic peening could effectively induce surface nanocrystallization in the 316L stainless steel. About 5 μm thick nanocrystalline layer was found to form on the surface; containing randomly oriented grains having average grain size of about 10 nm. The sub-surface layer extending upto about 30 μm was found to consist of deformation features with grains in the range of 10-100 nm. No deformation induced martensitic transformation was observed upon peening. With detailed transmission electron microscopy study, authors opine that the mechanism of the grain refinement is primarily attributed to activity of the high density of dislocations.

In the work of Roland et al. (2006), the effect of a nanocrystalline layer produced by surface mechanical attrition treatment (SMAT) on the fatigue behavior of AISI 316L austenitic stainless steel was studied. It was observed that the microstructural modification upon nanostructuring of the surface could successfully impede the motion of the dislocations. This helps in delaying the crack initiation as the cracks responsible for fatigue failure originate from the surface. The nanocrystalline regions as well as the plastically deformed zone lead to the development of compressive residual stresses in the surface and sub-surface region of the sample. This is found to delay the propagation of the fatigue crack. Marked improvement in the magnitude of the yield strength and the fatigue limit were achieved after the peening treatment. In the subsequent study, authors (Roland et al. (2007)) have also observed that the nanocrystalline structure was stable upto the temperature of 600 °C.

Similar study was carried out by Baluswamy et al. (2013) in which the AISI 304 stainless steel was subjected to surface mechanical attrition treatment. Grain refinement and strain induced martensitic transformation was observed in the

specimen with generation of the residual compressive stresses at the treated layer. However, corrosion resistance was found to be lowered upon peening treatment.

2.5.2 Laser peening

During laser peening, laser pulses of high energy of the order of several GW cm^{-2} are made to bombard the surface of a metal to be hardened. The sample surface will be covered by two layers- one is called the absorbing layer and the other is water confining layer. When the laser pulse passes through the transparent confining layer and hits the metallic substrate, the absorbent material undergoes vaporization to form plasma. Until the end of the peening process, the plasma continues to absorb the laser energy. It will be entrapped in between the sample surface and the transparent confining layer. This generates surface high pressure waves and propagates through the subsurface of the material as a shockwave. Metal surface will be plastically deformed when the pressure of the shockwave exceeds the yield strength of the metal. This leads to grain refinement and nanocrystallization of the sample surface (Gujba and Medraj 2014). There are a few reports in which laser peening is used to enhance the surface mechanical properties of the austenitic stainless steel.

Laser peening process was carried out on the surface of the AISI type 316L stainless steel and its effect on the electrochemical behavior was studied in saline environment by Peyre et al. (2000). Deformation induced martensitic transformation was not observed during the process; as a result of which moderate work hardening was evident. Marginal reduction in the corrosion resistance was observed due to increased surface roughness after peening.

Grain refinement mechanism of the AISI 304 grade stainless steel was studied by Lu et al. (2010) upon multiple laser shock peening process. Upon detailed transmission electron microscopic study, the authors opine that the grain refinement occurs through four major steps: formation of planar dislocation arrays and multidirectional deformation twins, formation of submicron triangular blocks by twin intersections, transformation of mechanical twin matrices into subgrain boundaries and evolution of the nanostructured grains by continuous dynamic recrystallization process. The paper

highlights the crucial role of the high strain and strain rate during the grain refinement process.

Zhou et al. (2016) studied the nanocrystallization and deformation-induced martensitic transformation in AISI 304 stainless steel upon laser shock peening treatment. The microstructural characterization was carried out by using transmission electron microscopy and electron back-scattered diffraction. Upon three laser shot impacts, nanocrystalline surface layer with grain size in the range of 50 to 300 nm was formed on the surface. It was found that ultra-high strain rate of more than 10^7 s^{-1} was experienced during multiple laser shot impacts. Based on the microstructural study authors opine that multidirectional mechanical twins as well as the deformation induced martensitic transformation are responsible for grain subdivision and nanocrystallization.

2.5.3 Air-blast peening

Air-blast shot peening is yet another method of peening; used for several decades to improve the surface finish and to induce compressive residual stresses on the industrial components. In this technique, peening occurs through bombardment of the cast steel balls projected towards the sample surface through the jet of compressed air. Increase in peening severity will result in grain refinement of the surface and sub-surface regions of the components. Hence severe peening is also considered as one of the techniques to bring about surface nanocrystallization.

Severity of the shot peening process is influenced by many process parameters, such as hardness, size and material of the shots, shot velocity, nozzle diameter, angle of shot flow, air pressure, peening time, etc. Effect of shot peening is also dependant on properties of the material undergoing shot peening treatment. These properties include hardness, crystal structure, stacking fault energy, flow behavior of the material, etc.

It is the industrial practice to determine the severity of the shot peening through two factors: peening intensity and peening coverage. Shot peening intensity is measured by using the Almen intensity scale. It represents the combined influence of process parameters on the severity of the process. It is defined as the amount of energy that is

deposited on to the standard test sample; known as the Almen strip. During the peening process, these Almen strips are placed at the same location and orientation relative to the peening nozzle as that of the work piece.

Three types of Almen strips are used in practice: A, N and C. Almen A strips are used for most of the peening processes while N and C are used for typical lower and higher intensity applications respectively. When one side of an Almen strip is peened, the surface stresses generated during the process will result in the arching of the strip. The arc height is plotted as a function of the peening duration. The intensity is defined as the spot on the curve where a two-fold increase in the peening time results in 10% increase in height. The value is typically reported as the arc height (as measured by a calibrated Almen gauge) in thousandths of an inch.

Coverage is the percentage of total surface area that is dimpled by the shot peening process. Peening coverage is to be 100% when the entire surface to be peened has at least one dent covering it. Since the shot impacts on the surface are random in nature, when more than 98% of the surface is dimpled, it is defined as 100% coverage. Determining the time required for the 100% coverage at a fixed Almen intensity is only done empirically through 10x-30x objective lens or through the software. Once the time for 100% coverage is determined, higher coverage is obtained by linearly increasing the time required for 100% coverage.

100% is the typical coverage level used in conventional shot peening to generate an appropriate compressive residual stress on the surface of the components. The literature (Bagherifard et al. 2012) (Hassani-Gangaraj et al. 2015) suggests that coverage levels of over 650% represents the severe shot peening regime, which produces significant grain refinement and eventually leads to surface nanocrystallization.

Many studies have shown that increase in the peening severity can successfully bring about nanocrystallization in the austenitic stainless steels.

AISI 304 austenitic stainless steel which was subjected to air-blast shot peening was studied by Altenberger et al. (1999) to assess the effect of shot peening on the

microstructure and fatigue behavior. Microstructural characterization through transmission electron microscopy revealed that the shot peening treatment leads to formation of complex near-surface microstructure consisting of ultra-fine grains, shearbands, deformation induced martensite and high dislocation density. The peening treatment found to decrease both the crack initiation and propagation rate; thus improving the fatigue limit of the material.

Mahagoankar et al. (2008) studied the effect of the process parameters on the microhardness of the AISI 316L stainless steel by the design of experiments method. It was found that peening time, nozzle distance, shot size and peening pressure have profound effect on the improvement in the hardness levels.

Effect of shot peening on the AISI 301LN steel was studied by Fargas et al. (2015). Deformation induced martensitic transformation was observed in the steel; with martensite content upto a level of 30% was observed upon shot peening. Ultra-fine grained region extending upto a depth of about 1 μm was observed in the cross-sectional scanning electron microscopy. But the surface was found to consist of numerous microcracks as a result of which effect of residual stress was counterbalanced in improving the fatigue limit of the material.

In the study of Azar et al. (2010), AISI 316L stainless steel was subjected to shot peening at different peening durations. Deformed layer, hardness and fatigue resistance was found to improve due to peening treatment. Electrochemical study depicted that resistance to pitting corrosion in Ringers solution was found to improve at higher peening duration.

The work of Bagherifard et al. (2016) suggests that apart from nanocrystallization, severe air-blast shot peening of 316L stainless steel induces compressive residual stresses and work hardening. Peening process also found to enhance the wettability and surface roughness. Authors also opine that these features will favourably contribute to the biological compatibility by increasing the cell adhesion to the metallic implant substrate (Sara et al. (2015)).

2.6 Plasma nitriding of the austenitic stainless steels with prior deformation

In literature there are several investigations exploiting various severe plastic deformation techniques as pre-treatment step for the low temperature plasma nitriding.

In the work of Lin et al. (2006), AISI 321 austenitic SS specimens were subjected to SMAT to produce nanocrystalline structure on the top surface. Martensite formation was evident on the top surface by both XRD and selected area electron diffraction (SAED) pattern analysis. Both, un-SMAT and SMAT samples were subjected to plasma nitriding at 400 °C for 4 hrs. XRD of samples after nitriding clearly indicates the presence of the S-phase in the sample but it is stated that TEM observations indicate the co-existence of the austenite and the ferrite. However no detailed analysis is presented in the paper and it focuses more on the improvement in the wear resistance of the samples.

In the study of Ferkel et al (2003), high pressure torsion (HPT) was used to produce severe plastic deformation prior to RF plasma nitriding at 400 °C for Fe and Fe based alloys. Amongst them, one alloy was X5CrNi1810, which was largely austenitic (initially) with small amount of martensite due to processing. After HPT, relatively coarse-grained structure is transformed into fine-grained structure; along with complete transformation of the austenite to the martensite. Shear banding and curling of shear bands were observed due to severe plastic deformation. Plasma nitriding of the untreated steel resulted in the formation of the S-phase along with that of the austenite and the martensite. Sample with HPT pre-treatment showed a broad peak between 40-45° and a sharp peak at martensite position. Authors opine that this could be either from the deformation induced martensite originating from the HPT-process or due to the decomposition of the metastable expanded austenite into ferrite/martensite phase and CrN. It is also stated that the sharp peak at 45° could be from the martensite or CrN as their individual peak positions are overlapping. Hence, authors strongly emphasize on the detailed TEM studies to understand the microstructural evolution and to identify the phases formed after plasma nitriding of the samples subjected to severe plastic deformation.

The work of Yu et al. (2002), describes two step transformation of the martensite to the expanded austenite. In the study, martensite in 304SS was obtained by mechanical polishing and this was subjected to plasma nitriding at 400 °C for different times starting from 30 min to 4 hrs. The phase formation was identified through XRD studies. It was observed that the amount of martensite gradually reduced and the austenite increased till nitriding time was about 90-120 minutes. Further nitriding resulted in appearance of the expanded austenite phase. This was not merely due to the heating effect as martensite to austenite reversion temperature for 18-8 stainless steels was found to be above 500 °C. Martensite being an open structure, diffusion coefficient of the nitrogen in the martensite lattice is 50-folds more than that of the austenite. Due to mechanical polishing, matensite was mostly confined to the surface. This suggests that the major amount of nitrogen would be dissolved in the martensite phase. Since nitrogen is an austenite stabilizer, it brings down the reverse transformation temperature. As a result, martensite gets converted to austenite and then it transforms into expanded austenite by further incorporating the nitrogen into the lattice. This is the two-stage mechanism proposed by the authors to explain the formation of the expanded austenite phase in the case of nitriding of the pre-deformed samples.

Laleh et al. (2012) used SMAT as a pre-treatment for plasma nitriding of the 316L SS. Nanocrystalline layer of about 200 μm was obtained with average diameter of the grains in the range of 10 nm on the top surface. No martensite formation was observed on the surface. Plasma nitriding of the samples was carried out by a low-frequency pulse-excited plasma unit at 300 ˚C for 4 hours. It is found that the pre-SMAT sample developed a nitride layer twice as thick as that on the as-received sample; along with higher hardness, excellent wear resistance and corrosion resistance. The pre-SMAT sample showed the presence of the S-phase on the surface while untreated sample showed both the austenite (from the base) as well as the S-phase. Nitriding at higher temperature (500 ˚C) found to favour the formation of the Fe_4N phase along with the traces of the deleterious CrN.

In the study of Chemuki et al (2013), medical grade F138- 316L SS was subjected to plasma nitriding at 425 °C for 20 hrs with SMAT pre-treatment. After SMAT,

samples were subjected to 20 hrs of annealing at 425 °C to confirm the thermal stability of the nanocrystallised layer and no drastic change was observed in the average grain size of the sample subjected to SMAT. Prior to plasma nitriding, for one set of samples, top 3 μm surface layer was removed by polishing to ensure removal of the surface oxides that might have formed during SMAT process. Case depth after plasma nitriding was highest for SMAT-polished samples while un-polished sample yielded a discontinuous case. No martensite was observed after SMAT. However, authors suspect that the strongest peak observed in the XRD to be either from the (111) plane of the austenite phase or from the (110) plane of the martensite or ferrite or from (200) plane of the CrN. However no specific reason is mentioned throughout the paper for the validity of such an assumption.

In the study by Baluswamy et al. (2013) 304 SS samples were subjected to plasma nitriding at 500 °C for 8 hours with SMAT pre-treatment. The un-SMAT samples were purely austenitic while SMAT samples showed presence of the strain induced martensite. Upon plasma nitriding, XRD data suggested the presence of Fe_4N (111), Fe_3N (111), CrN (200) and α-ferrite (110) phases in the untreated 304 SS. Peaks of Fe_3N (111), CrN (200) and α-ferrite (110) phases were observed in the SMAT-nitrided samples. These observations suggest that, the above mentioned phases might have formed following the decomposition of the γ_N phase at conditions employed for nitriding in the said study. It was also reasoned that the presence of the nano-grains, slip bands and dislocations in the 304 SS subjected to SMAT enables the migration of the chromium and promotes formation of the higher amounts of the CrN phase than the untreated one under similar conditions of nitriding. The increase in the hardness after nitriding is attributed to the formation of the iron and chromium nitrides. Similar observations are reported by Atul et al. (2016) in which ultrasonic peening was used as the pre-treatment to plasma nitriding.

In the work of Bottoli et al. (2015) two grades of austenitic stainless steels, namely AISI 304 and EN 1.4369 in annealed and plastically strained conditions were surface hardened by low-temperature nitriding. Gas nitriding was carried out for 20 hours at temperatures in the range of 430 °C to 470 °C. It was observed that, on plastic deformation, strain-induced martensite developed in AISI 304, while EN 1.4369

remained austenitic up to maximum equivalent strain of 0.5 encountered in the study. This was irrespective of the degree of deformation or the mode of deformation (tensile, shear, plane strain compression). It was observed that the strain-induced martensite promotes faster growth of the nitride layer, while plastic deformation of the austenite without martensite formation had no measurable effect on the case depth. Study also showed that the strain-induced martensite promoted the pre-mature nucleation of deleterious CrN precipitates.

Borgioli et al. (2016) studied the plasma nitriding behavior of 200 and 300 series austenitic steels at 400 and 430 °C for 5 hours. The 300 series steels were possessing austenitic microstructure with a small amount of the strain induced martensite. The nitride layer was found to consist of S-phase after treatment at 400 °C while precipitation of the CrN occurred at 430 °C. Few samples of 304 SS were strained to 0.5 equivalent tensile strain and the alloy found to develop strain induced martensite due to deformation. Expanded austenite was found to form after gas nitriding at 430 °C for 20 hrs with a change of preferred orientation from (220) to (200) due to lattice rotation. Reduction in the diffracted intensity of the martensite peak suggested that a portion of the martensite has been converted into expanded austenite during nitriding. Glancing Incidence X-Ray Diffractometry (GIXRD) showed the presence of small amount of CrN and α-Fe. Nitriding at 450 °C resulted in abundant growth of CrN into the nitriding layer. XRD also detected peaks of CrN and α-Fe with small amount of expanded austenite. This suggests that strain induced martensite would yield expanded austenite as suggested by Yu et al. (2002) at temperatures below 450 °C while CrN formation takes place at higher temperatures.

The effect of surface mechanical attrition treatment (SMAT) on corrosion resistance and plasma nitriding behavior of 304L stainless steel was studied by Gatey et al. (2016). SMAT intensity was increased by increasing the number of balls used for peening. Formation of defects and martensitic transformation found to increase with increasing intensity. Plasma nitriding was carried out at 500 °C for 10 hours. Both peened and nitrided samples found to produce expanded austenite, chromium nitride and Fe_3N phases. The study showed that corrosion resistance improved upon SMAT process.

It can be summarized that severe plastic deformation-plasma nitriding duplex treatment of austenitic stainless steels results in thicker nitride layers at shorter durations compared to plasma nitriding alone. However, there exists ambiguity amongst various investigators over the phase formation in the nitride layer. Further, nitriding temperature more than 450 °C found to result in the CrN precipitation. It is reasoned that the high diffusivity paths, like grain boundaries, triple junctions, dislocations, etc. which enhance the diffusion of nitrogen will also help in the diffusion of Cr to the surface to facilitate CrN formation. But, if the temperature is below 400 °C, diffusion of Cr is found to be minimal as CrN precipitation is seldom observed.

2.7 Plasma nitriding with shot peening pre-treatment

Severe deformation processes, like high pressure torsion, rolling with large thickness reduction, etc. are often associated with a dimensional change. It is also possible that they affect the grain structure of the bulk materials as well; which may be undesirable for certain applications. In contrast, in most of the peening processes, deformation will be restricted to surface and sub-surface regions of the component. Hence, they are more often exploited as pre-treatment techniques for plasma nitriding. In literature, there are numerous studies on the application of SMAT as a pre-treatment to plasma nitriding. Though SMAT successfully produces nanocrystallization and which in turn produces thicker nitride layers; the process poses limitation on the size of the components to be peened. Also, the process is currently having limited industrial applications due to size limitations. Use of laser peening also bears similar disadvantages.

In contrast, air-blast shot peening (ABSP) is a well established and economical surface engineering technique; widely used for the improvement of fatigue resistance of the industrial components. Conventional shot peening treatment mainly induces compressive residual stress and work hardening; along with altering the surface topography.

Changes in the properties of work piece upon shot peening treatment are listed below:

- Shot peening increases the roughness of the well-polished sample inducing dimples on the sample surface

- Change in the crystallographic texture of the sample

- Inducing compressive residual stress close to the sample surfaces

- Increase in the fraction of lattice defects, increase in the dislocation density, twin density and hardness

- Peening can initiate deformation induced phase transformations on the sample surface

- Over-peening can induce microcracks on the surface which adversely affects the corrosion and fatigue resistance

With growing interest in surface nanostructured materials by severe plastic deformation processes, shot peening is also viewed as a tool to achieve surface nanocrystallization. Many studies (Bagheri et al. 2009, Unal et al. 2014, Hassani Gangaraj et al. 2015) have shown the formation of nano-sized grains in the surface layer of metallic materials upon severe shot peening. But only limited studies have exploited the possibility of using shot peening technique as a pre-treatment to plasma nitriding of the austenitic stainless steels.

Ji et al. (2005) studied the influence of plastically deformed layer caused by pre-shot peening on plasma nitriding of the AISI 304 austenitic stainless steel in the temperature range from 380 to 450 °C. After severe peening, the top surface was found to consist mainly of strain induced martensite with a strong (110) preferred orientation. After nitriding, though enhanced nitride case depth was observed, there was no clear evidence which indicates the formation of the expanded austenite (S-phase) in the nitride layer. Since the XRD peaks are observed over the range of 45-55°, authors opine that the nitride layer may consist predominantly of (Fe, Cr, Ni)$_{2-3}$N or nitrogen-containing martensite or their mixtures.

Shen et al. (2010) used shot peening as the pre-treatment for low temperature nitriding of 304SS. After shot peening, the surface layer consisted of strain induced martensite

with only a small fraction of the austenite. However, after plasma nitriding at 400 °C, the major phase formed was the expanded austenite. This was justified through the work of Yu et al. (2002) which infers that considerable amount of nitrogen atoms dissolve and supersaturate the martensite during short time and facilitate its transformation to austenite and then to expanded austenite. Smaller fraction of the martensitic peaks detected in the XRD results was attributed to the reflection from the substrate material for the case of very thin nitrided layers (about 5 μm).

In the work of Hashemi et al. (2011) medical grade 316L stainless steel samples were subjected to gas nitriding at 570 °C with pre-shot peening treatment. Paper reported improvement in the wear resistance, increase in the nitride case depth and microhardness with pre-treatment which are attributed to the strain induced martensite formation and also, to increased amount of surface defects which enhance the nitrogen diffusion. Phases formed after nitriding were identified to be Fe_4N and CrN. However, the paper doesn't discuss about the mechanism responsible for transformation of the martensite to Fe and Cr nitrides after nitriding.

2.8 Objectives of the study

It can be summarized based on the literature review that shot peening technique can be used as a pre-treatment step to plasma nitriding of the austenitic stainless steels. It is known that the conventional shot peening mainly imparts compressive residual stresses while severe shot peening produces a nanostructured layer. But in the available literature, the effect of peening coverage is not emphasized. Also, structure of the nanocrystalline layer obtained on the sample surface after shot peening, which subsequently enhances the nitriding kinetics, is not studied in detail. Work of Lu et al. (2010) suggests that grain sub-division by deformation twinning and continuous dynamic recrystallization (DRX) is responsible for nanocrystallization. DIM formation isn't evident in the study. However, Zhou et al. (2016) opine that the mechanical twins as well as the DIMs are equally responsible for grain refinement process. Bhagerifard et al. (2016) observed that layers of DIM gets embedded in the austenite matrix. Recent report by Bahl et al. (2017) suggested that microbands and shear bands are formed during peening. Deformation twinning and DRX within these

shear bands are responsible for nanocrystallization. This suggests that the microstructural development depends on peening technique and process parameters. To the best of knowledge, there is no detailed layer-by-layer study of gradient nanostructured layer formed in the AISI 316L SS subjected to severe shot peening.

There also exists an ambiguity amongst the various studies about the structure of the nitride layer formed during duplex treatment. In the study of Laleh et al. (2013) Chemuki et al. (2013), no martensite is reported after pre-treatment while austenite directly transforms to S-phase after plasma nitriding. Few authors opine that the strain induced martensite formed during the deformation gets converted into expanded austenite on plasma nitriding; which further transforms into α-Fe and CrN upon nitriding at higher temperatures for longer durations (Lin et al. 2006) (Wang et al. 2006). In few cases, Fe_4N phase is also reported (Hashemi et al. 2007). Yu et al. (2000) proposed a two- step transformation mechanism from martensite to expanded austenite. It suggests a complete transformation of strain induced martensite to austenite initially, followed by the transformation of austenite to S-phase. Study by Ferkel et al. (2003) and Ji et al. (2005) suggests that the nitride layer is a mixture of ferritic and/or martensitic phases along with Fe and/or Cr nitrides.

Considering the cost effectiveness and industrial applications of shot peening technique, it is relevant to understand microstructural evolution during the low temperature plasma nitriding of the austenitic stainless steel with prior severe shot peening.

Hence, the following objectives are defined:

- To study the effect of coverage of shot peening pre-treatment on plasma nitriding of the AISI 316L austenitic stainless steel

- To study the mechanism of nanocrystallization during severe shot peening process

- To study the phase formation in severe peened-plasma nitrided 316L stainless steel.

o To understand the role of high diffusivity paths created during shot peening on the plasma nitriding process.

2.9 Scope of the study

Study will help in understanding the effect of peening coverage on the microstructural development in 316L stainless steel and on subsequent plasma nitriding. Understanding the mechanism of nanocrystallization helps in tailoring the grain structure on the surface of the material which, in turn, governs the surface properties. It also enables to understand the role of defects on the sample surface which facilitate the easier in-take on nitrogen during plasma nitriding process.

CHAPTER 3

EXPERIMENTAL METHODS

Experimental details regarding the air-blast shot peening (ABSP) technique and plasma nitriding on the surface of the AISI 316L grade stainless steel are given in this chapter. Along with that, details of the techniques used for microstructural and mechanical characterization are also briefed.

3.1 Base material

Base material used in the study was AISI 316 grade austenitic stainless steel procured from M/s Bharath Aerospace Ltd., Mumbai. Material was in the form of sheets of 5 mm thickness which was processed by hot rolling. The chemical composition of the base material is given in Table 3.1. Nominal composition is given in the parenthesis.

Table 3.1 Average chemical composition of the base metal (all in wt %)

Cr	Ni	C	Mn	Mo	Si	S	P	Fe
16.9	10.1	0.014	0.85	2.03	0.44	0.002	0.032	Bal.
(16-18.5)	(10-14)	(<0.03)	(<2)	(2-3)	(<1)	(<0.03)	(<0.045)	

3.2 Air blast shot peening

Coupons of 15 cm X 10 cm X 5mm were cut from the base material sheet and polished metallographically to a surface roughness of 0.2 μm. The specimens were cleaned ultrasonically in ethyl alcohol and distilled water. Air blast shot peening (ABSP) treatment was carried out at M/s Curtiss Wright Surface Technologies Ltd, Bangalore.

Air blast shot peening is the widely used industrial peening process in which the shots are bombarded towards the component surface by the aid of the compressed air. The schematic diagram of the ABSP process is illustrated in Fig. 3.1.
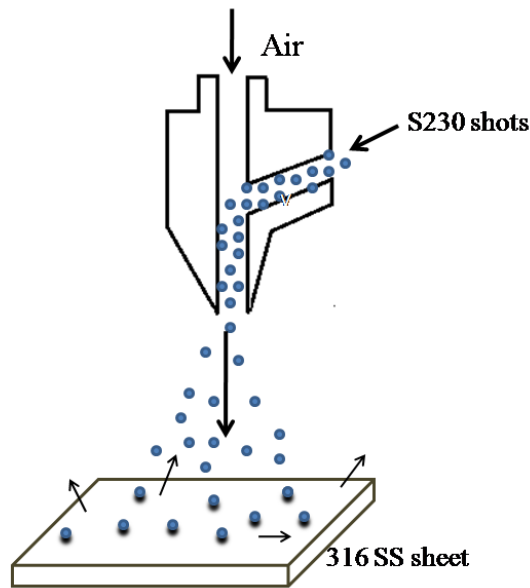
Fig. 3.1 Schematic diagram of the air blast shot peening technique (Re-drawn from the work of Bagheri and Guagliano 2009)

In the present study, cast steel shots (S230) were used for the peening process. Cast steel shots are classified by the mesh opening size which retains 80-85% of the shots. This magnitude is given in ten thousandths of an inch. Thus, for the case of S230 shots, the mesh that retains 85% of the shots has openings that are 0.0230" wide. These shots have nominal diameter of about 0.6 mm.

In industrial practice, severity of peening is expressed by two factors: peening intensity and peening coverage. Peening intensity represents the combined influence of process parameters on the severity of the peening process. It is measured by Almen scale. In the present study, all the samples were peened with Almen intensity of 8A. This indicates that the type-A Almen strip showed a deflection of 0.008".

Coverage is the percentage of total surface area that is dimpled by the shot peening process. 100% is the typical coverage level used in conventional shot peening to generate an appropriate compressive residual stress on the surface of the components. The literature (Bagherifard et al. 2012) (Hassani-Gangaraj et al. 2015) suggests that coverage levels of over 650% represents the severe shot peening regime, which produces significant grain refinement and eventually leads to surface nanocrystallization.

In the present study, shot peening was performed with 100%, 500% and 1000% coverage. The samples thus peened were termed as conventional peened, intermediate peened and severe peened, respectively.

Shot peening parameters are summarized in the Table 3.2.

Table 3.2 Process parameters employed during the shot peening treatment

Shot type	S230, cast steel shots
Nominal shot diameter	0.6 mm
Shot flow Velocity	25 kg/min
Air Pressure	40 psi
Almen Intensity	8A
Coverage	100%, 500% and 1000%
Nozzle diameter	0.5 inch
Angle of shot flow	90 degrees

3.3 Plasma Nitriding

Shot peened specimens as well as the un-peened base metal were subjected to plasma nitriding process at M/s Bhat Metals Research Pvt. Ltd, Pune. Plasma nitriding is the plasma-assisted, diffusion based surface modification technique which allows the diffusion of the nitrogen into the sample surface to produce a hard, wear-resistant case.

Schematic diagram of the plasma nitriding process is given in Fig. 3.2. Prior to nitriding, the specimens were ultrasonically cleaned in acetone and distilled water. During the plasma nitriding process, the nitriding chamber was evacuated to a pressure of 0.05 mbar in order to drive out the atmospheric air and the contaminants. The chamber was heated to nitriding temperature by the use of the resistance heaters. Subsequently, mixture of 450 sccm of the nitrogen gas and 450 sccm of the hydrogen gas was introduced into the chamber. Nitriding chamber pressure was maintained in the range of 0.7-0.8 mbar such that it could produce and sustain glow discharge on the component surface. The work piece was maintained at a high negative dc potential of

700 V with respect to the vessel, which is grounded. Under this condition, the nitrogen gas was dissociated, ionized, and accelerated towards the component. Nitriding was carried out for the duration of 4 hours.
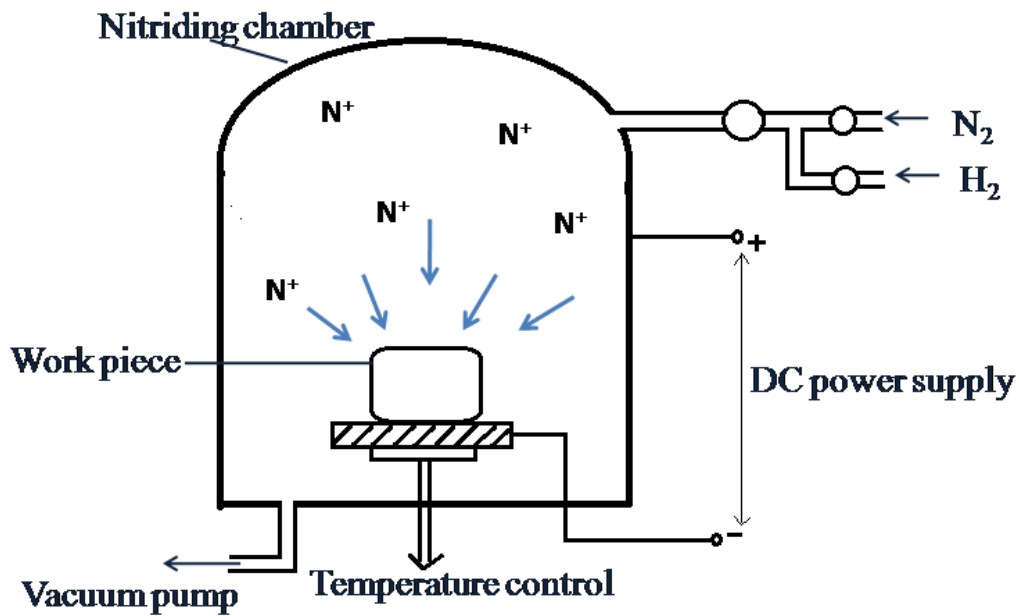
Fig. 3.2 Schematic diagram of the plasma nitriding process (Redrawn from the work of Pye 2003)

Hydrogen gas is used along with the nitrogen gas during nitriding process. It helps in the instantaneous removal of the native oxide layer present on the sample surface thus enabling the nitrogen to diffuse easily into the surface. It also aids in increasing the density of the active nitriding species (Moskalioviene and Galdikas 2015). Both factors enhance the nitriding kinetics. However, if amount of the hydrogen gas exceeds the nitrogen gas content, then it decreases the nitrogen potential. Hence, constant nitrogen to hydrogen gas ratio of 1:1 is maintained for all the plasma nitriding experiments.

Plasma nitriding was carried out at a temperature range of 300-500 °C. This range is selected based on the review of the literature. It is observed that temperature less than 300 °C is ineffective for the diffusion of the nitrogen into the component and the temperature more than 500 °C results in the undesirable precipitation of the chromium carbide phase (Gil et al. 2006).

Plasma nitriding parameters are summarized in Table 3.3.

Table 3.3 Process parameters used during plasma nitriding treatment

Nitriding temperature	$400 \pm 10\ ^{\circ}C$
Time	4 hrs
Chamber pressure	0.7-0.9 mbar
DC voltage	700 ± 20 V
Nitrogen gas flow	450 sccm
Oxygen gas flow	450 sccm

3.4 Characterization

3.4.1 X-ray diffractometry

X-ray diffraction patterns of the base material, shot-peened and nitrided samples were obtained by using X-Ray diffractometer (model JPX 8P, JEOL make, Japan) operated at 30 kV voltage and 20 mA current. Monochromatic copper K_α (λ=0.154 nm) radiation was used for obtaining the diffraction pattern. The diffraction patterns were collected in the range of 30° to 100° at a scanning speed of 2°/min and step size of 0.02°. The output data was analyzed by comparing with the standard JCPDS files to identify the phases present in the sample. Depth-wise XRD results were obtained by removal of the successive layers prior to the experiment by mechanical polishing.

3.4.2 Scanning electron microscopy

Morphological studies of the base material, peened, nitrided and peened-nitrided samples were carried out by using scanning electron microscope (SEM, JSM-6380LA, JEOL). Topographical features of the shot-peened samples were imaged in as-peened condition. Microstructural features and depth of the deformed layer as well as the nitride layer were studied by using the cross-sectional samples. These samples were cut by electro-discharge machining (EDM), followed by standard metallographic polishing and etching. Diluted aqua regia (50% HCL, 25% HNO_3 and 25% distilled water by volume) was used as the etchant for all the samples.

3.4.3 Transmission electron microscopy

Transmission electron microscope (TEM, JEM-2100, JEOL) was used for detailed microstructural analysis of the processed samples. Schematic diagram of TEM sample preparation in the sub-surface regions is shown in Fig. 3.3.
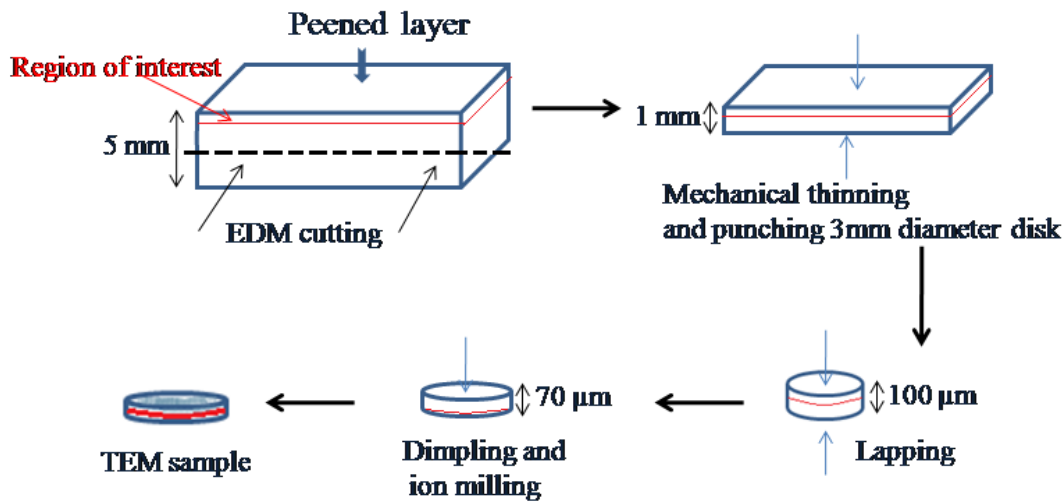
Fig. 3.3 Schematic diagram of TEM sample preparation of the sub-surface regions

Samples containing the region of interest were initially cut from the 5 mm thick peened sample by following electric discharge machining (EDM) technique to a thickness of 1 mm. TEM specimens were prepared by mechanically thinning down to 100 μm thickness. For the samples at top surface, polishing was done from the un-treated side while sub-surface samples were polished from both sides to arrive at the region of interest. Discs of 3 mm diameter were punched from the thinned samples. Punched discs were further thinned down to 70 μm by following the standard lapping procedure. The samples were then dimpled up to 10 μm at the center by using the dimpling unit. Ion milling of the dimpled sample was carried out by using precision ion polishing system (PIPS, Model No. 691, Gatan) with beam energy of 5 keV at beam angle of 7° (rough milling); followed by further milling at 2.5 keV and beam angle of 3° (fine milling). The ion milled samples were analyzed under TEM to reveal microstructural features and selected area electron diffraction (SAED) patterns.

3.4.4 Surface roughness

Surface roughness of the base material, as-peened and as-nitrided samples were measured by using surface profilometer (SJ-301, Mitutoyo). Conical diamond tip having a root radius of 2 μm was used as the stylus. Evaluation length of 4 cm was used for the study. Five readings were taken on the each sample and the average value was reported along with the standard deviation.

3.4.5 Microhardness

Microhardness measurement on the sample surface was carried out by using microhardness testing machine (Model no. HMV-G 20ST, Shimadzu). Vickers indenter was used for the test; which is square based pyramidal indenter with 136 degree angle between the opposite faces. The test was performed by placing the specimen on an anvil and raised till it is close to the indenter point. Constant load of 200 g was then gradually applied to the indenter for 15 s and then removed. A microscope in conjunction with the hardness testing unit was used to determine the size of the indentation. Vickers hardness number (H_v) was directly readout from the machine. Five readings were taken on the each sample and average value was reported along with the standard deviation.

3.4.6 Scratch test

Scratch hardness testing of the samples was carried out by using scratch hardness tester (Lineartester-249, Erichsen). In this method, the sample was drawn against a stylus tip made up of the tungsten carbide insert of 1 mm tip diameter, at a constant load of 20 N. The stroke length and stroke speed were fixed as 3 cm and 25 mm/s, respectively. Scratch width was measured by using the scanning electron microscope (SEM, JSM-6380, JEOL). The scratch hardness (H_s) was calculated by using the formula

$$H_s = \frac{8F_N}{\pi b^2} \text{ (Beegan et al., 2007)}$$

where F_N is the normal force (in N) and b is the average scratch width (in μm).

3.4.7 Nanoindentation study

Nanoindenter (G200, Agilent technologies) was used to perform nanoindentaion, nanoscratch and nano-scale wear tests on the base material, severe peened and severe peened-nitrided samples. For the nanoindentation test, Berkovich indenter was used. Peak load of 300 mN and peak hold time of 10 s were used for all the samples. Surface approach velocity and allowable drift rate were maintained at 10 mm/s and 0.05 mm/s, respectively. Load-displacement data was obtained and hardness was estimated by using Oliver- Pharr method (Oliver and Pharr 1992).

Typical load-displacement plot from the nanoindentaion test and cross-section of the indentation is given in the Fig. 3.4.

(a)

(b)
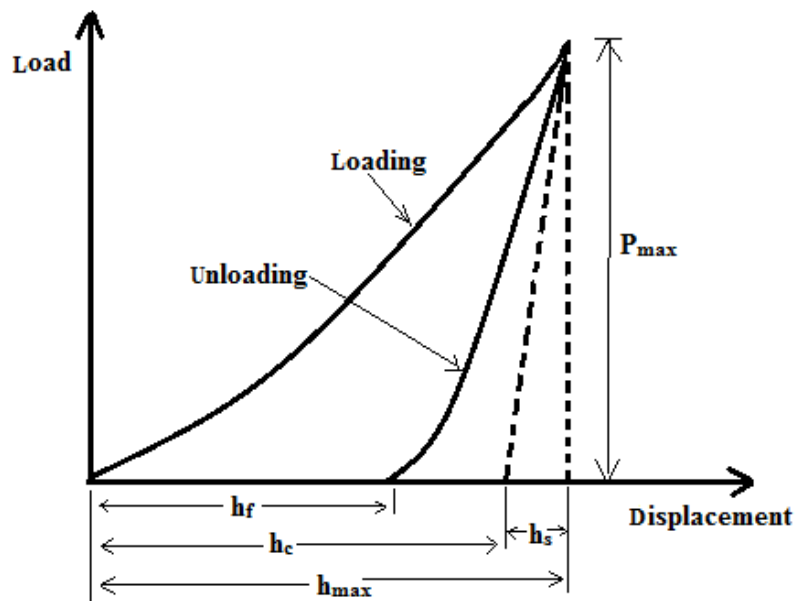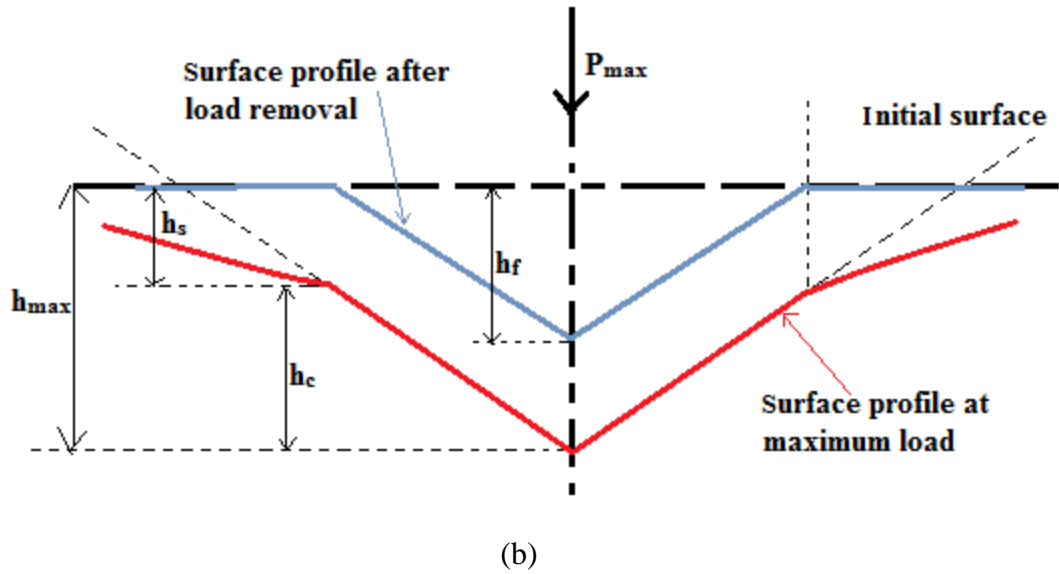
Fig. 3.4 (a) Typical load-displacement plot from the nanoindentation test and (b) cross-section of the indentation (Redrawn from the work of Oliver and Pharr 1992)

Hardness (H_m) is given by the equation,

$H_m = \frac{P_{max}}{A}$ where, P_{max} is the maximum applied normal load and A is the projected area of indentation at maximum load.

Progressive load nano-scratch test was performed upto the peak load of 400 mN. Scratch length and scratch velocity were maintained at 600 μm and 20 μm/s, respectively. Load was applied normal to the sample surface. Pre-scratch and post-scratch profiling was done to obtain the data of penetration into the surface as a function of the scratch distance.

Nano-scale wear test was carried out for 30 cycles to study the maximum wear track deformation. Test was carried out at a constant load of 50 mN. Profiling of the surface was done prior to the loading as well as after 10, 20 and 30 cycles of loading. Profiling load of 50 μN was used to avoid the wear of the surface during profiling.

CHAPTER 4

RESULTS

This chapter presents the results of the microstructural and mechanical characterization of the base metal, peened samples, nitrided samples and peened-nitrided samples under various conditions. Extent of nanocrystallization as a function of severity is studied by increasing the peening coverage. Effect of plasma nitriding temperature on the peening pre-treatment is assessed in the temperature range of 300-500 °C. Depth-wise microstructural study of the severe peened sample is also presented. Chapter also presents the results of assessment of wear-properties of the surface after the duplex treatment.

4.1 Characterization of the base material

Typical SEM micrograph of the base material 316L austenitic SS is shown in Fig. 4.1. Microstructure consists of the austenite grains having the grain size in the range of 40 to 80 μm. Microstructure found to consist of numerous twins. They are the characteristic features of the hot rolled austenitic stainless steel sheets (Li et al. 2017).
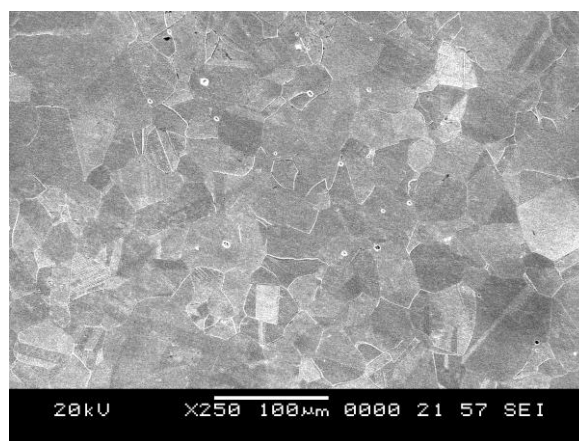
Fig. 4.1 Microstructure of the base material

XRD pattern of the base material is given in Fig. 4.2. XRD data shows presence of four major peaks and they are corresponding to (111), (200), (220) and (311) planes

of austenite phase (identified by JCPDS card no. 33-0397). Deformation induced martensite is not observed in the base metal.
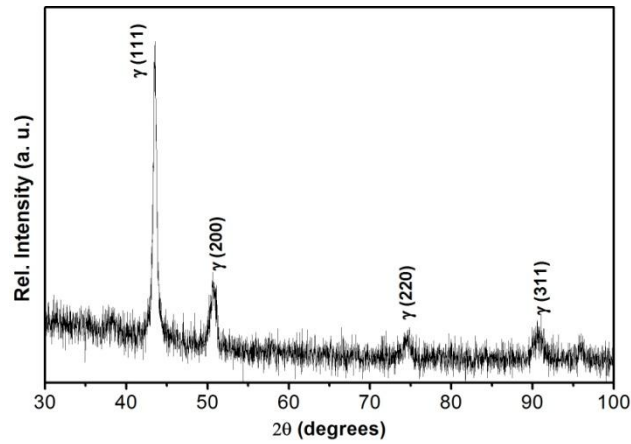
Fig. 4.2 XRD pattern of the base material

Surface roughness of the polished sample is measured to be 0.55 ±0.07 μm and microhardness is measured to be 197.6 ±4.1 H_v.

4.2 Effect of shot peening coverage

Peening coverage is effectively correlated to the peening time where in 100% coverage indicates the time needed to cover the entire surface of the work piece once. For a fixed Almen intensity, the peening severity increases with increase in the coverage. In the present study, sample is subjected to coverage of 100%, 500% and 1000% which represent conventional, intermediate and severe peening domains, respectively.

4.2.1 Surface topography

SEM micrographs of the surfaces of the air blast shot-peened samples at 100%, 500% and 1000% coverage are given in Fig. 4.3 (a-b), (c-d) and (e-f), respectively. Observed roughness on the shot peened surface is due to the dimples formed by the multiple impacts of the steel shots during peening process. Heterogeneities on the sample substrate (indicated by the arrows) are observed more in the conventional and intermediate peened samples in Fig 4.3(a-d). It could be noted that the surface of the sample peened with 1000% coverage appears to be smooth in spite of bearing more

shots. This is due to the flattening of edges of the previously formed dimples with repeated impacts at higher peening coverage. This observation is confirmed with the surface roughness data.

(a)   (b)

(c)   (d)

(e)   (f)
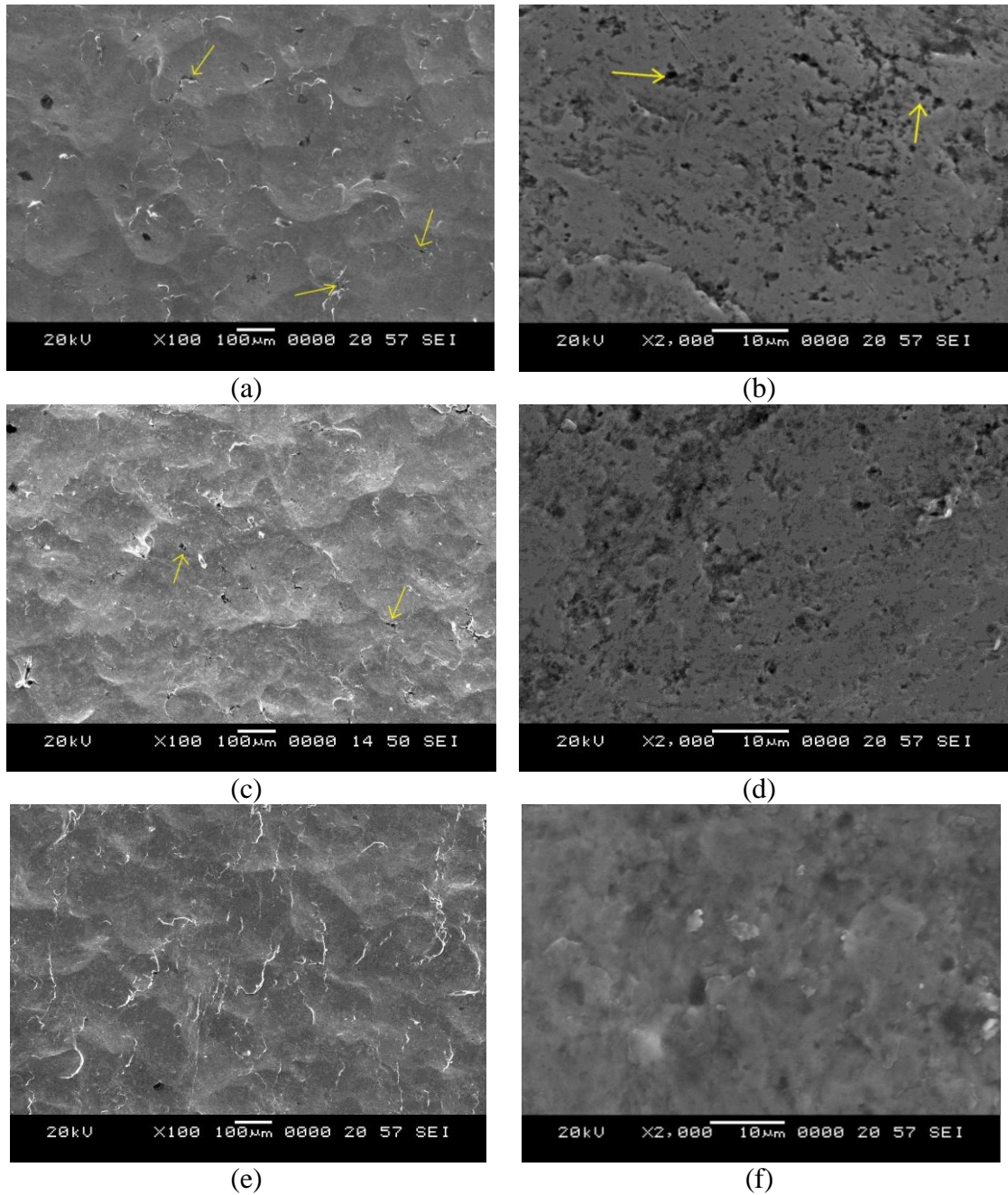
Fig. 4.3 Surface topography of the shot peened samples at (a, b) 100% (c, d) 500% and (e, f) 1000% coverage, respectively

4.2.2 Surface roughness

Variation in the surface roughness for various peened samples is given in the Fig. 4.4. It is observed that the surface roughness of the polished surface increases drastically upon shot peening due to the dimples created by the repeated impact of the steel shots on the surface. But average roughness decreases with increase in the peening coverage. Once the entire sample surface is peened (i.e., after 100% coverage), further impact of the shots fall on the ridges of the previous dimples. This reduces the height of the peak regions; while valley regions will remain largely unaffected (Bagherifard et al. 2012). This is the reason for the observed decrease in the surface roughness.
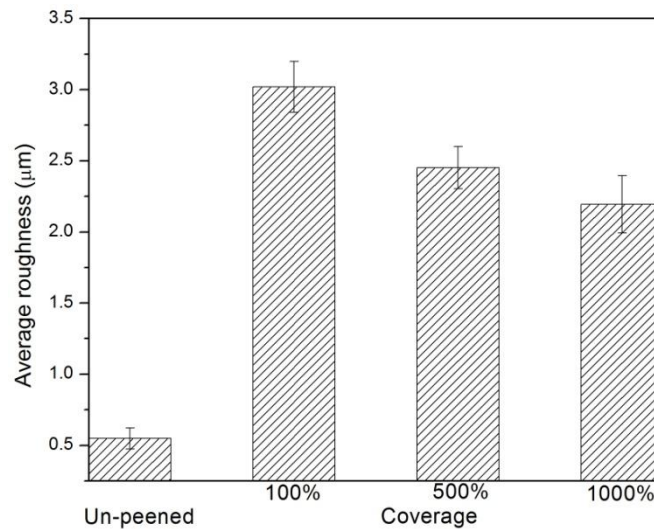
Fig. 4.4 Variation in the surface roughness of the shot-peened samples

4.2.3 Deformed layer

Cross sectional SEM micrographs of the specimen after shot peening to different coverage are shown in Fig. 4.5. It is observed that the top surface has undergone severe deformation due to the continuous bombardment of the shots and the sub-surface consists of deformation features. There exists no sharp boundary between the deformed layer and the base metal; deformation features observed to decrease gradually away from the peened surface. Thickness of deformed layer is minimal in conventional peened sample compared to intermediate and severe peened samples.

Lower magnification SEM micrograph in Fig. 4.5(a) shows that the deformed layer during conventional peening extends to about 20 µm from the top surface during conventional shot peening. Nanocrystalline region is not evident even in the high magnification micrograph shown in Fig. 4.5(b). Thicker deformed layer is visible in the intermediate peened sample, as observed in Fig. 4.5(c-d). Deformed layer of more than 200 µm is observed in Fig. 4.5(e). Higher magnification SEM micrograph in Fig. 4.5(f) shows the presence of nanocrystalline region which extends to about 25-30 µm from the peened surface (shown with the arrow). Transition from the unaffected base material to the nanocrystalline region occurs gradually and this subsurface region consists of several microstructural features which are explained in detail in section 4.3.

(a)

(b)

(c)

(d)

(e)   (f)
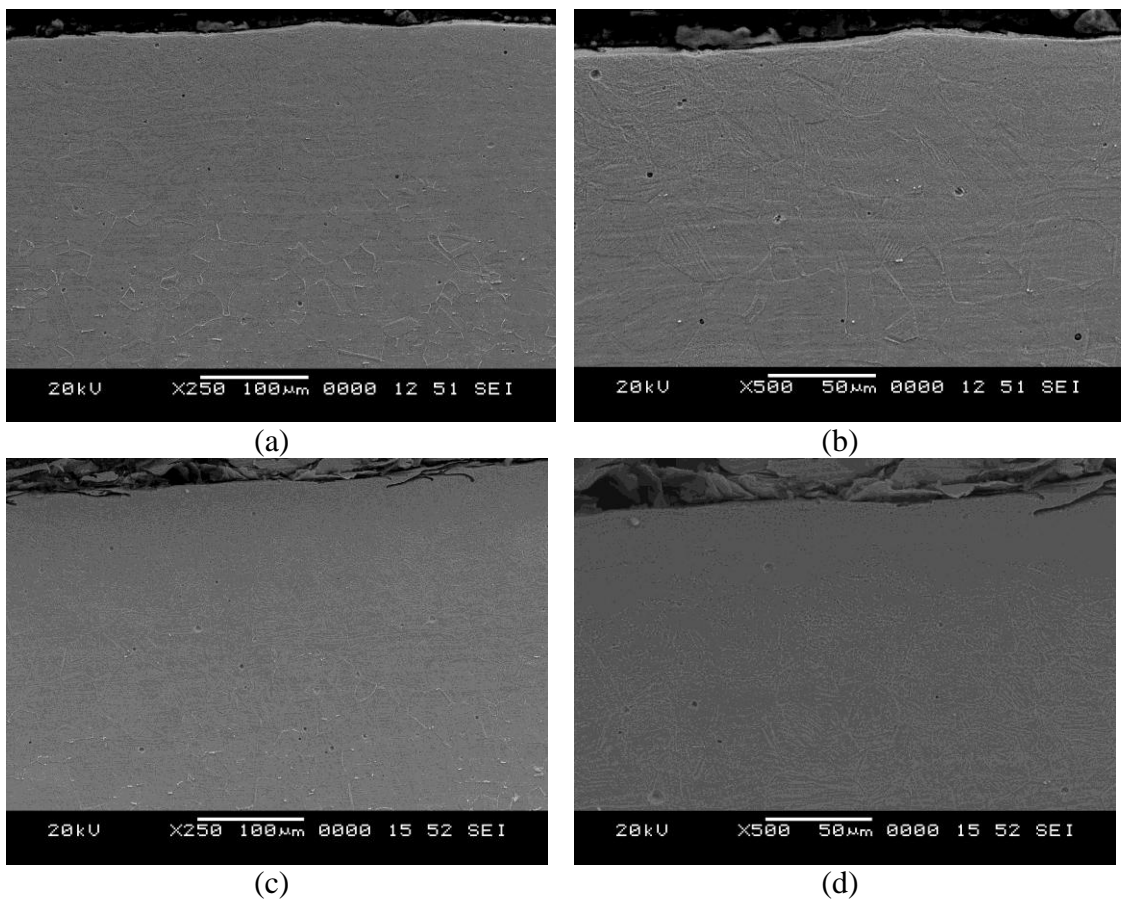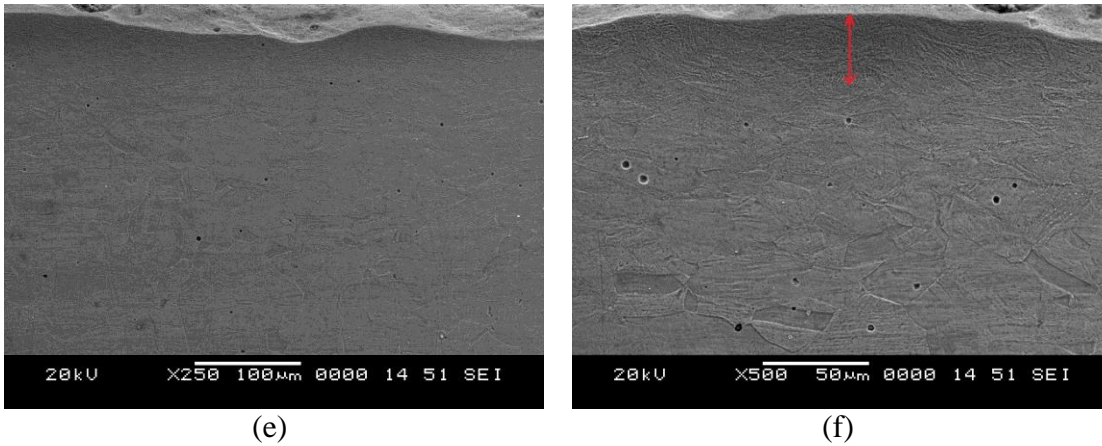
Fig. 4.5 Cross-sectional SEM micrographs of the sample peened at (a, b) 100%, (c, d) 500% and (e, f) 1000%, respectively

4.2.4 Phase analysis

X-ray diffraction patterns of the specimen after shot peening are shown in Fig. 4.6. XRD data from the un-peened base material is given for reference. All peaks of as-received 316L SS are attributed to the austenite phase (JCPDS card no. 33-0397). After peening, peaks of the martensite (JCPDS card no. 35-1375) begin to appear. This indicates the strain induced transformation of the austenite to the martensite due to plastic deformation during shot peening (Fargas et al. 2013). Intensity of the martensite peaks increase with increase in the peening coverage and upon 1000% peening, major phase on the surface would be martensite.
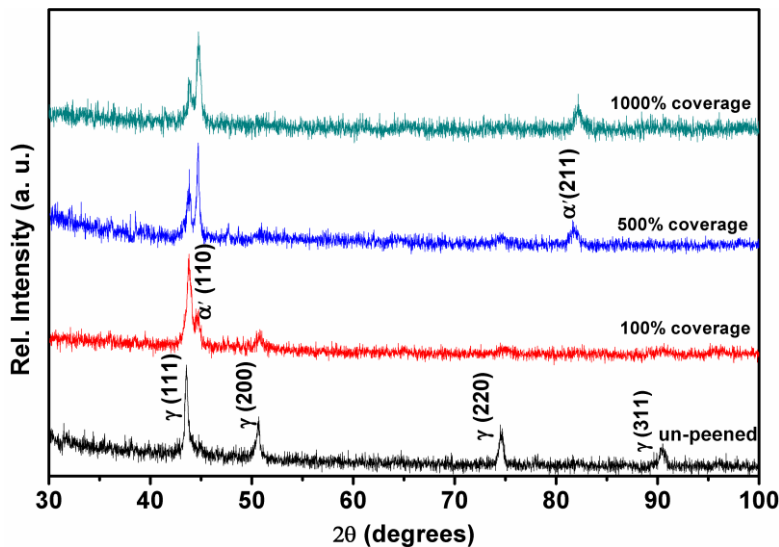
Fig. 4.6 XRD patterns of the samples peened at various coverage level

4.2.5 Microhardness measurement

Figure 4.7 depicts the variation of the microhardness of the sample surface after shot peening treatment at different coverages. It is observed that the surface hardness of the conventionally peened samples is more than 2-times the base material. Also, microhardness is found to increase with the increase in the peening coverage. Improvement in hardness is primarily due to the strain induced transformation of relatively softer austenite phase in the un-peened base metal to harder martensite phase in the peened samples. Thus, increase in the hardness is attributed to increase in the fraction of the martensite formed upon increased severity of peening. It is also widely known that peening process increases the defects, like, dislocations, triple junctions, twins, etc; which collectively enhance the hardness of the peened layer. Residual stress induced during the peening process will also contribute towards increase in the hardness. It was observed in Fig. 4.5(f) that severe peening results in formation of ultra fine/nanocrystalline grains on the surface. It would increase the hardness of the surface.
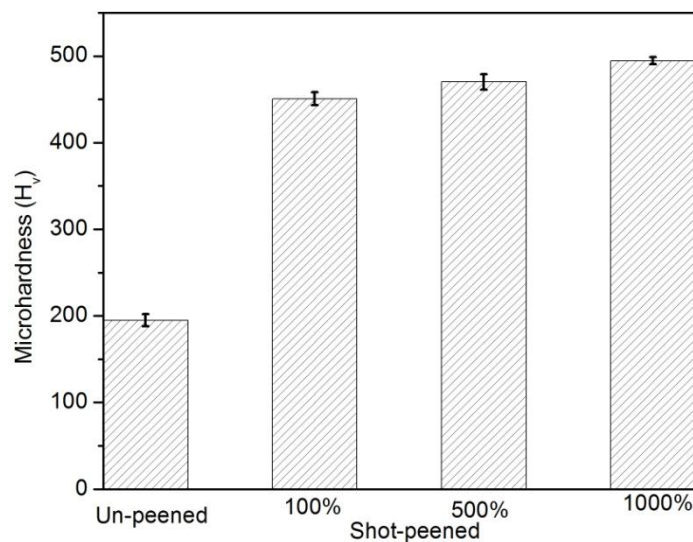
Fig. 4.7 Variation in microhardness of the shot-peened samples

4.3 Microstructural characterization of the peened surface through transmission electron microscopy

Shot peening process induces drastic microstructural changes in the typical hot rolled structure of the un-peened, base material. It involves the formation of nanocrystalline

grains, increase in the defect density, deformation induced martensitic transformation, etc. All these microstructural changes are extremely fine in nature; and hence, studied through transmission electron microscopy.

4.3.1 Microstructure of the base metal

The bright-field TEM micrograph from the surface of the as-received 316L SS sample before peening is shown in Fig. 4.8(a). Selected area electron diffraction (SAED) pattern from the marked region is given in Fig. 4.8(b). Large grains of size in the order of several micrometers are observed; which are separated by well-defined grain boundaries. This is typical of the hot-rolled austenite stainless steel microstructure; having grain size in the range of 40–80 μm. Observed deformation features like dislocations are induced by the mechanical thinning process involved in the TEM sample preparation. SAED pattern corresponds to austenite grain with [011] orientation.

(a)   (b)
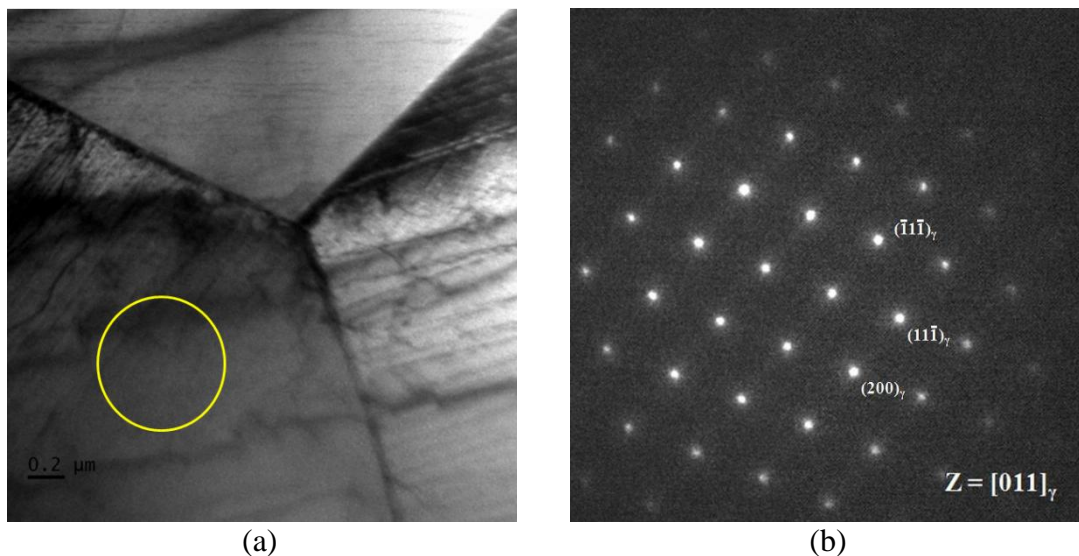
Fig. 4.8 (a) BF-TEM micrograph of the as-received AISI 316L stainless steel (b) SAED pattern from the marked region

4.3.2 Surface after conventional peening

Bright-field TEM micrographs and corresponding SAED patterns from the top surface of the sample subjected to conventional shot peening are given in Fig. 4.9. Multi-directional deformation bands of about 250-300 nm thickness are observed predominantly in Fig. 4.9(a) and (b). SAED pattern in the inset of Fig. 4.9(c) shows

presence of the faint diffraction rings of martensite phase with prominent rings from the austenite phase. This suggests the beginning of deformation induced transformation of the austenite to martensite at certain locations.

(a)   (c)

(c)
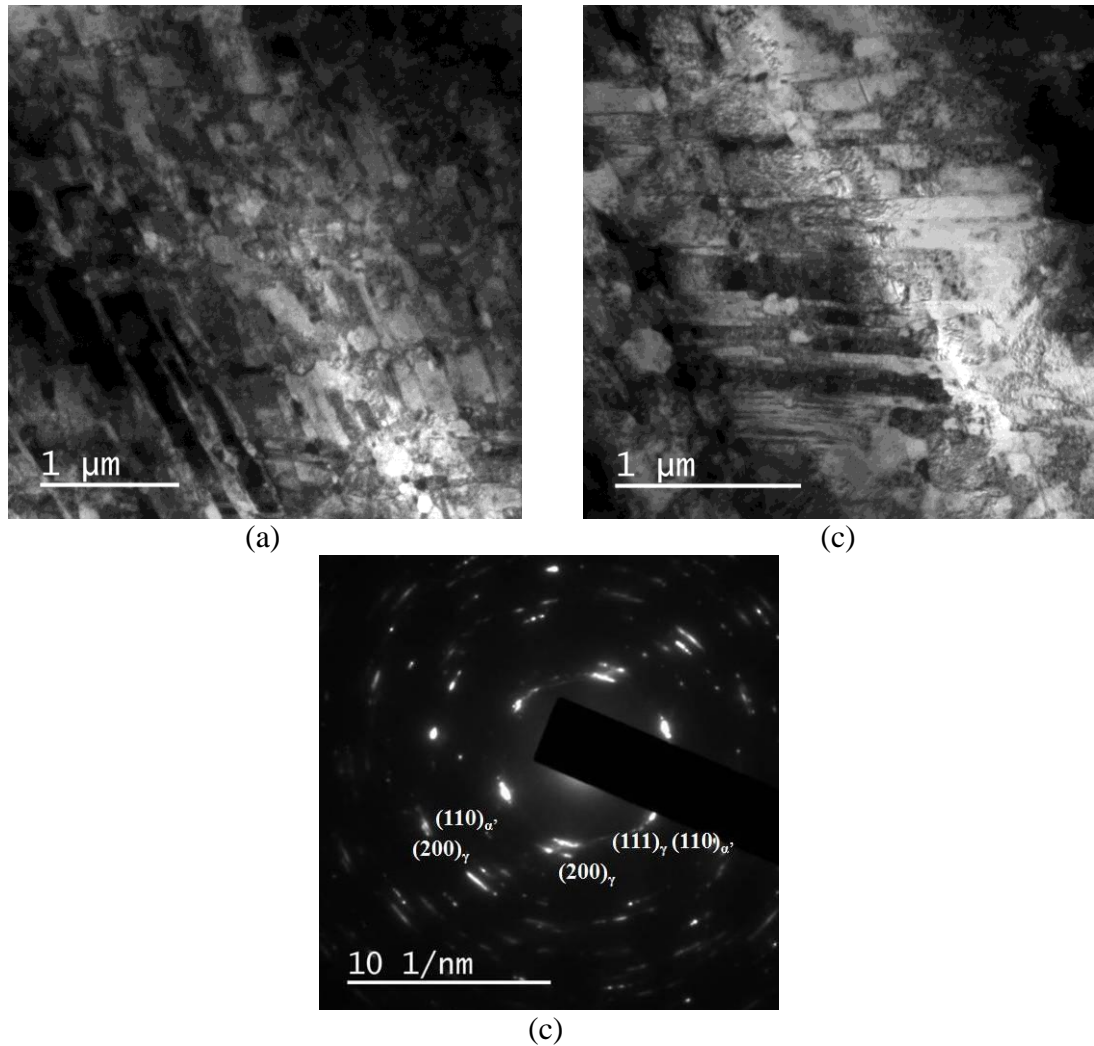
Fig. 4.9 (a, b) Lower magnification BF-TEM micrographs and (c) SAED pattern corresponding to 4.9(b) from the top surface of the 316L SS subjected to conventional shot peening

Higher magnification bright-field TEM micrographs are given in Fig. 4.10. Isolated shear band observed in Fig. 4.10(a) is about 280-300 nm thickness. Huge amount of dislocations are observed inside the shear band. Sub-microscopic shear bands having width in the range of 10-20 nm and length more than 1 μm are observed in Fig 4.10(b) and (c). Presence of huge number of dislocations in the matrix is also evident.

(a)

(b)

(c)
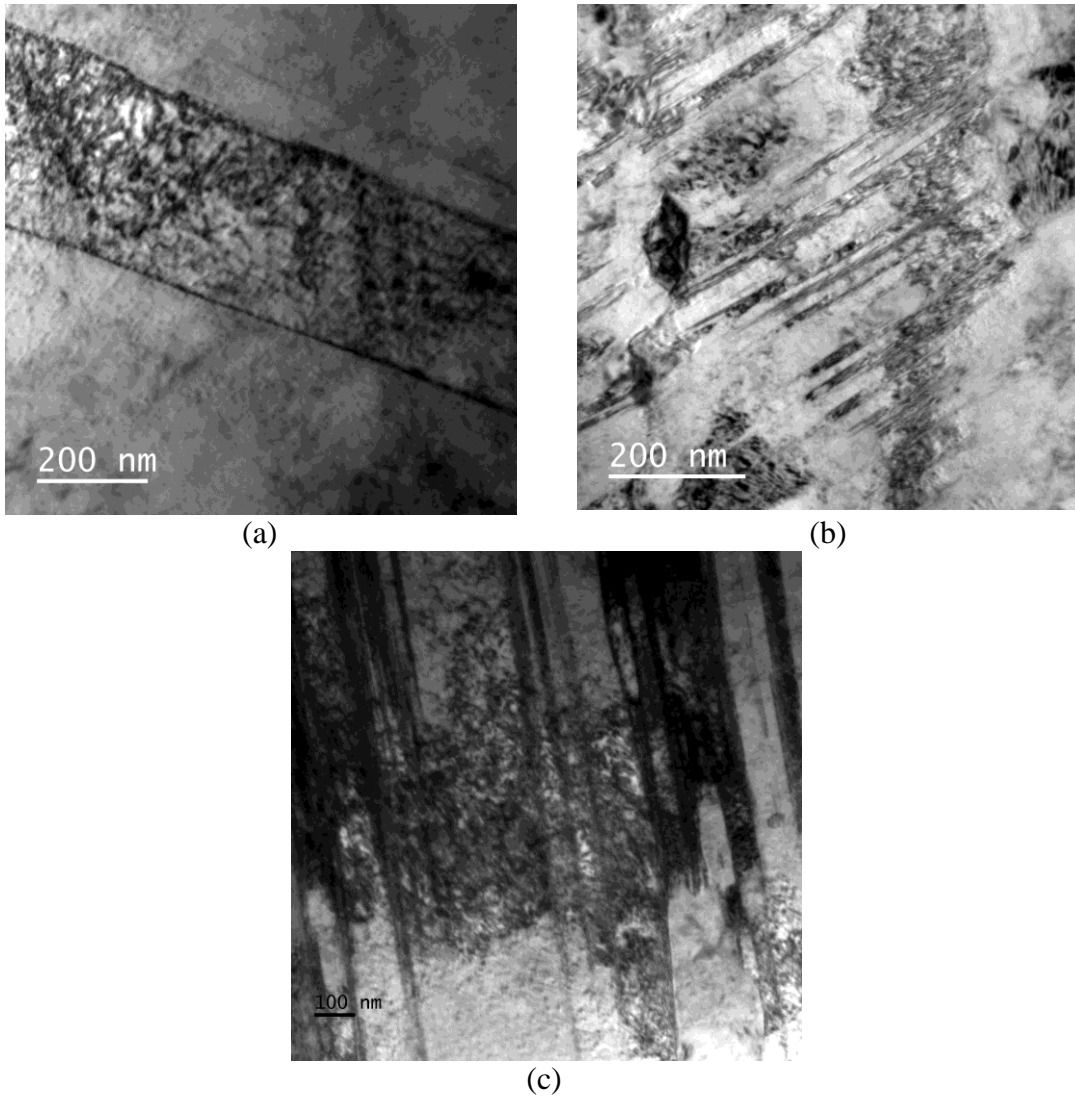
Fig. 4.10 Higher magnification BF-TEM micrographs from the surface of the sample subjected to conventional shot peening

At certain locations in the austenite matrix, dislocations in the highly tangled state are also observed as shown in Fig. 4.11.
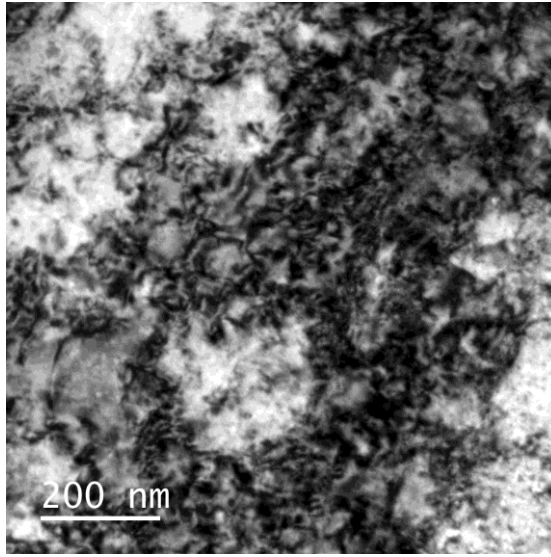
Fig. 4.11 Tangled dislocations in the austenite matrix

4.3.3 Surface after intermediate peening

BF-TEM micrographs shown in Fig. 4.12 are from the top surface of the sample subjected to intermediate peening. Elongated structures of about 100-150 nm thickness are observed in Fig. 4.12(a). They closely resemble the lath structure which is the dominant morphology of the deformation induced martensite in the austenitic stainless steels. In certain locations nearly equi-axed martensite grains are observed as seen in Fig. 4.12(b). SAED pattern in the inset of Fig 4.12(c) indicate that all the diffraction rings are from the martensite phase.
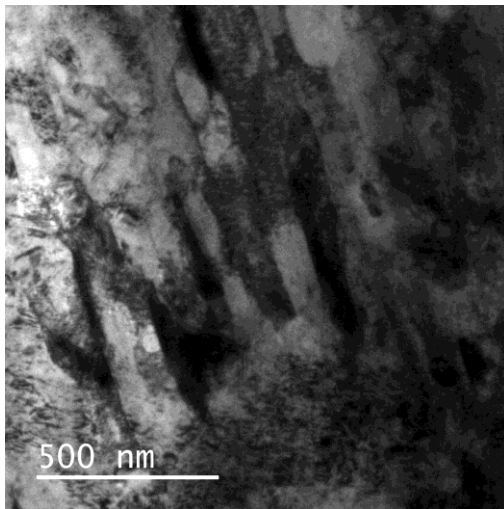
(a)
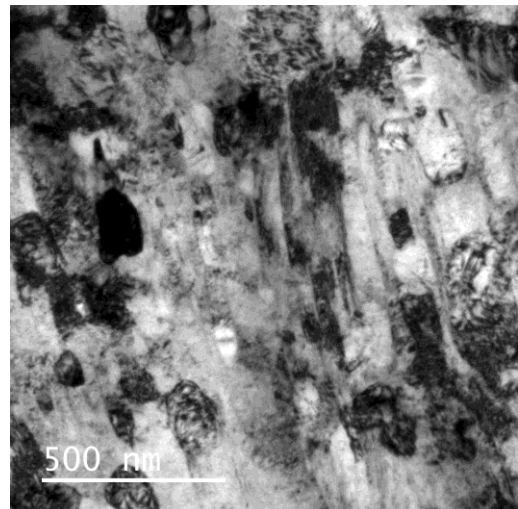
(b)
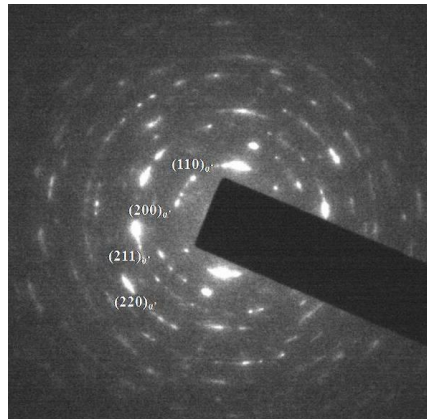
(c)

Fig. 4.12 (a, b) BF-TEM micrographs and (c) SAED pattern corresponding to 4.12(b) from the top surface of the 316L SS after intermediate peening.

Cell-type structures of finer dimension are also observed in certain locations on the surface of the intermediate peened sample, as depicted in bright-field TEM micrograph shown in Fig. 4.13(a). SAED pattern from the region given in Fig. 4.13(b) affirms that the phase is martensite. Higher magnification TEM micrograph shown in Fig. 4.13(c) shows the nearly equi-axed martensite cells having high density of dislocations as indicated by the arrows.
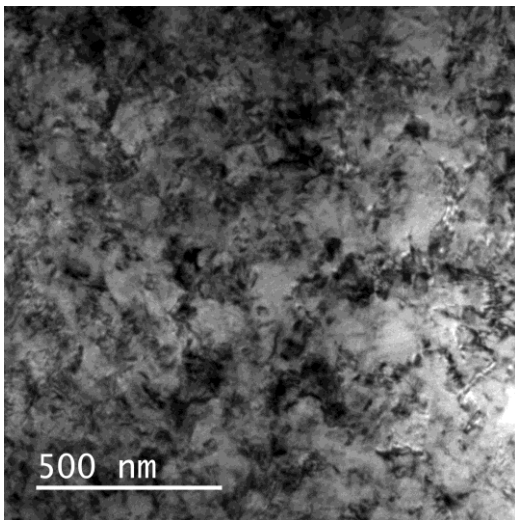
(a)
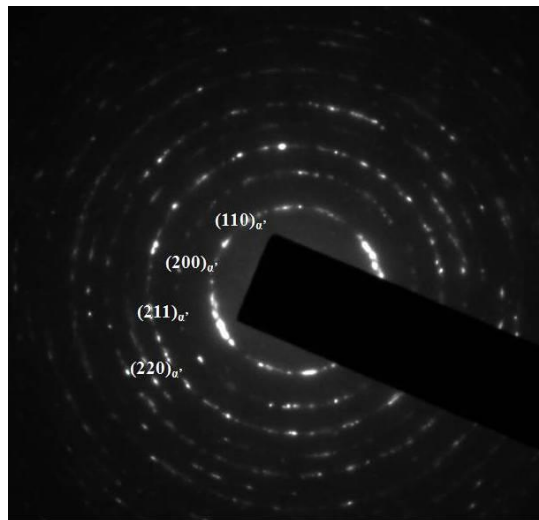
(b)
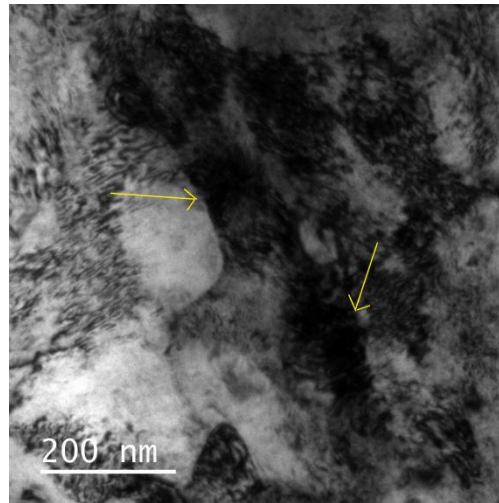
Fig. 4.13 (a) BF-TEM micrograph showing fine martensite crystallites. (b) SAED pattern and (c) higher magnification micrograph showing large dislocation density within the crystallites

4.3.4 Surface upon severe peening

Figure 4.14(a) depicts BF-TEM micrograph from the top surface of the severe peened sample. Corresponding SAED pattern is given in Fig. 4.14(b). Microstructure depicts the presence of dislocation cell type martensite; with cell size in the range of 100-140 nm. Continuous rings of martensite phase are identified in the SAED pattern; affirming the presence of randomly oriented fine martensite crystallites. This morphology is also called blocky martensite (Murr et al. (1998)). Higher magnification micrograph in Fig. 4.14(c) shows presence of huge amount of dislocations inside as well as in the cell boundary of these martensite cells. Drastic grain refinement is observed upon severe peening when compared to the coarse austenite grain structure in the un-peened condition (in Fig. 4.8(a)).

(a)　　　　　　　　　　　　　　　　(b)

(110)ₐ'
(200)ₐ'
(211)ₐ'

(c)
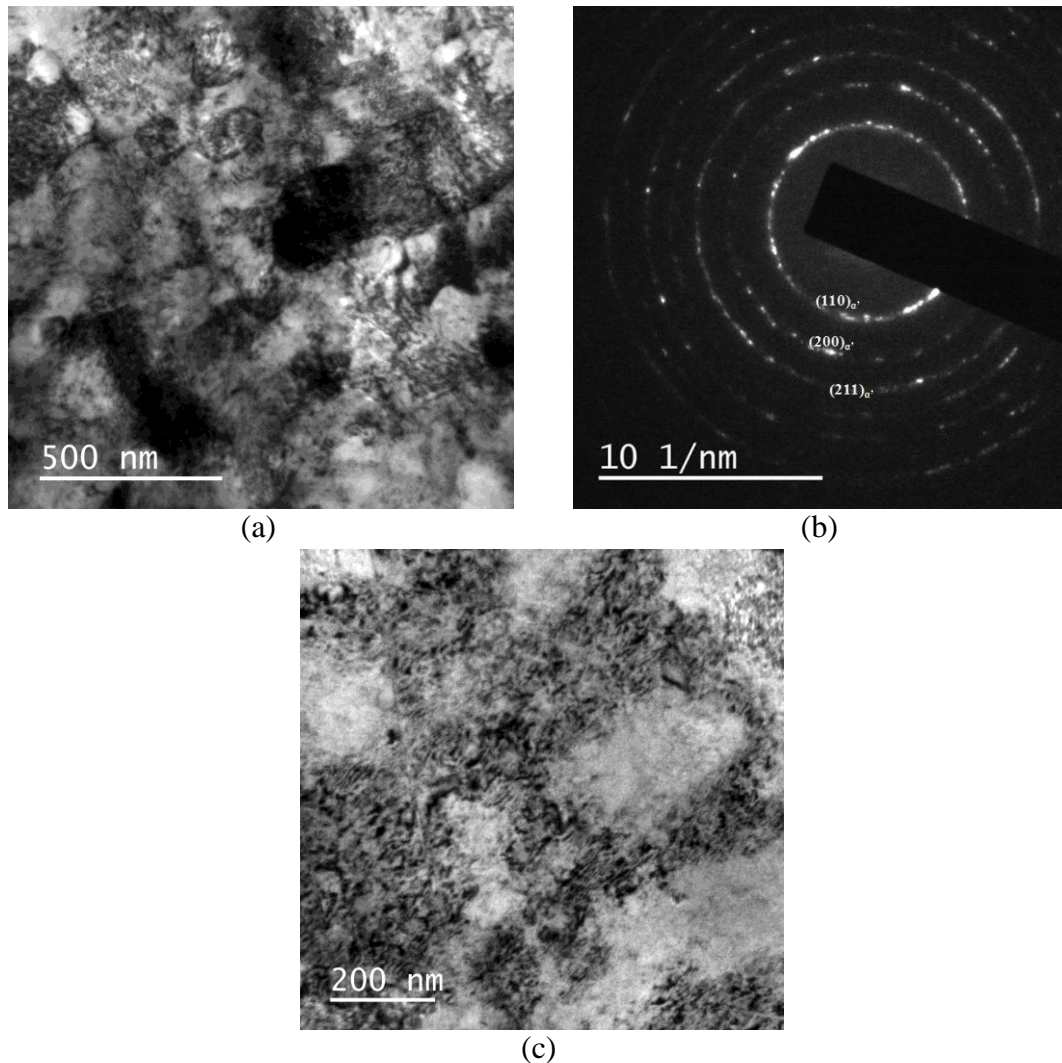
Fig. 4.14 (a) BF-TEM micrograph and (b) SAED pattern from the top surface of the severe peened sample (c) high magnification micrograph showing dislocation cells

4.4 Microstructural evolution in the severe peened sample

It is observed from the cross sectional SEM micrographs in Fig. 4.5 that the extent of the deformed layer increases with increase in peening coverage. Fraction of the austenite transformed to the martensite also found to increase with peening coverage as observed from the results of XRD in Fig. 4.6. This suggests that highest degree of grain refinement and volume fraction of the martensite is present in the severe peened sample. Hence, it would be interesting to study the microstructural evolution in the severe peened sample.

4.4.1 Gradient nanostructured (GNS) layer

Microstructural evolution during severe peening is complex as the process generates gradient nano-structured (GNS) (Huang et al. 2015) layer having layers of differential microstructural features. Deformation induced transformation of the austenite to the martensite further increases the complexity.

Cross sectional SEM micrographs of the sample after severe shot peening are shown in Fig. 4.15. Based on the microstructural features shown in Fig. 4.15(a), two regions are identified in the gradient nanostructured layer (GNS). They are (from the top): region A which has undergone nanocrystallization. This region extends to about 15-20 μm from the peened surface and consists of only martensite phase. Second is the region B; characterized by the presence of structural features induced by the deformation. This region consists of both austenite and martensite. Transition between the regions is gradual. It could be observed from Fig. 4.5(e) that the gradient nanostructured layer extends to about 500 μm from the top surface.

Higher magnification micrograph from the region A in Fig. 4.15(b) indicates that the coarse austenite grains of the base material formed during hot-rolling have undergone severe deformation to form finer grains. Formation of nanocrystalline grains are confirmed through TEM studies. Figure 4.15(c-e) are typical micrographs from the subsurface region B. They indicate the presence of mechanical twins, twin-twin intersections resulting in the formation of the rhombic blocks (Lu et al. 2010) (Zhang, H. W et al. 2003) of 1-5 μm thickness.

(a)   (b)

(c)

(d)

(e)
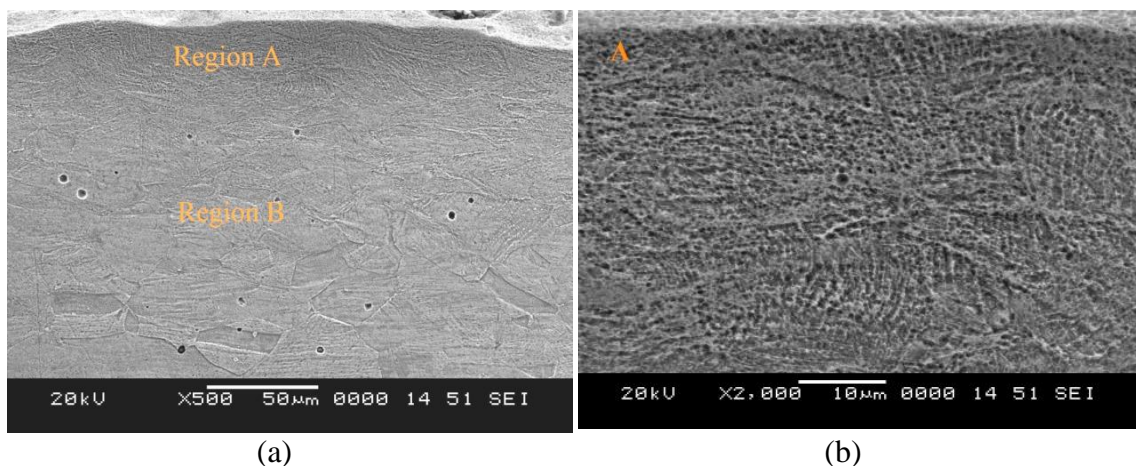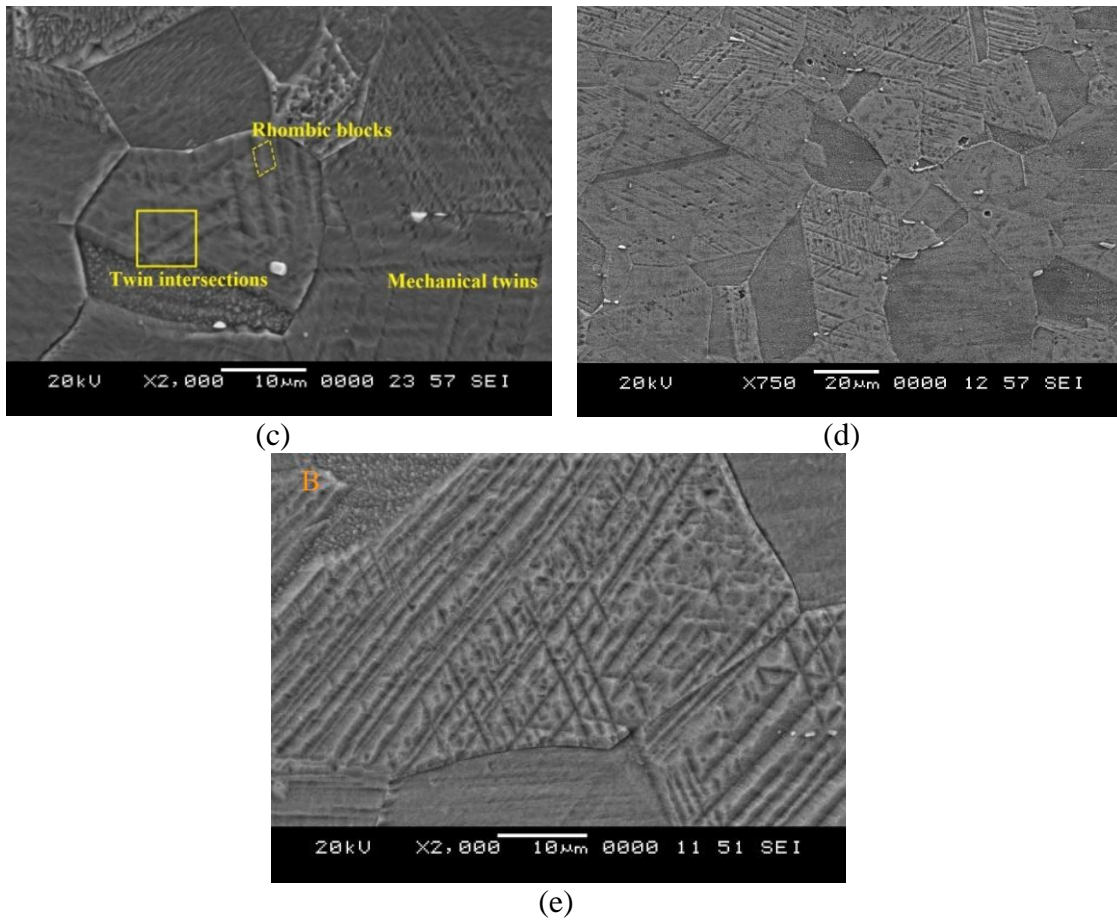
Fig. 4.15 (a) Cross-sectional SEM micrograph of the 316L SS after 1000% shot peening, high magnification micrograph from (a) nanocrystalline region (region A) and (c-e) transition region (region B)

Detailed depth-wise TEM study was carried out to gain insights about the mechanism of nanocrystallization and deformation induced martensitic transformation.

4.4.2 Microstructure below the GNS

Typical bright-field TEM micrograph below the GNS layer (about 500 μm away from the top surface) is shown in Fig. 4.16. Large grains of size in the order of several micrometers are observed; which are separated by well-defined grain boundaries. It should be noted that the base material is a hot rolled sheet consisting of grains in the size range of 40-80 μm. SAED pattern from the marked region is shown in Fig. 4.16(b). It depicts the spot pattern originating from the crystal oriented along [011] zone axis. This indicates that the microstructure below the GNS is essentially the microstructure of the base metal that is not largely affected by the peening process.

<center>(a)   (b)</center>
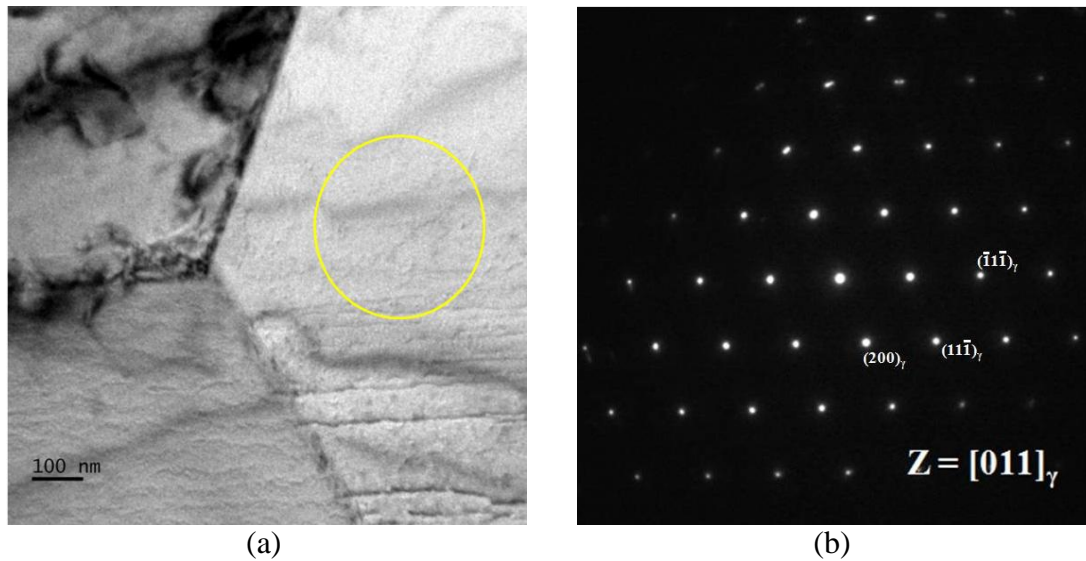
Fig. 4.16 (a) BF-TEM micrograph from the region about 500 μm below the peened surface and (b) SAED pattern from the marked region

4.4.3 Microstructural features in the transition region

All the TEM micrographs in this section are from the transition region of the GNS layer. This region spans from about 20 μm to about 500 μm from the peened surface.

Figure 4.17 depict the bright-field TEM micrographs of the severe peened sample, from a region about 400-500 μm below the peened surface. Presence of mechanical twins, twin-twin intersections and huge amount of dislocations are observed in these micrographs. Similar deformation microstructures are observed by other researchers (Lu et al. 2010; Tao et al. 2003; Zhang et al. 2003) upon severe peening of the austenitic stainless steels. In the literature, different types of planar defects formed during the plastic deformation are collectively termed as "shear bands" (Olson and Cohen 1975; Talonen and Hänninen 2007). Hence, the same term will be used during further discussion. Number of shear bands and their intersections increase towards the peened surface owing to the multidirectional impact of shots on the surface encountered during the peening process (Murr et al. 1982). Martensitic transformation is also observed in this region.

<center>55</center>
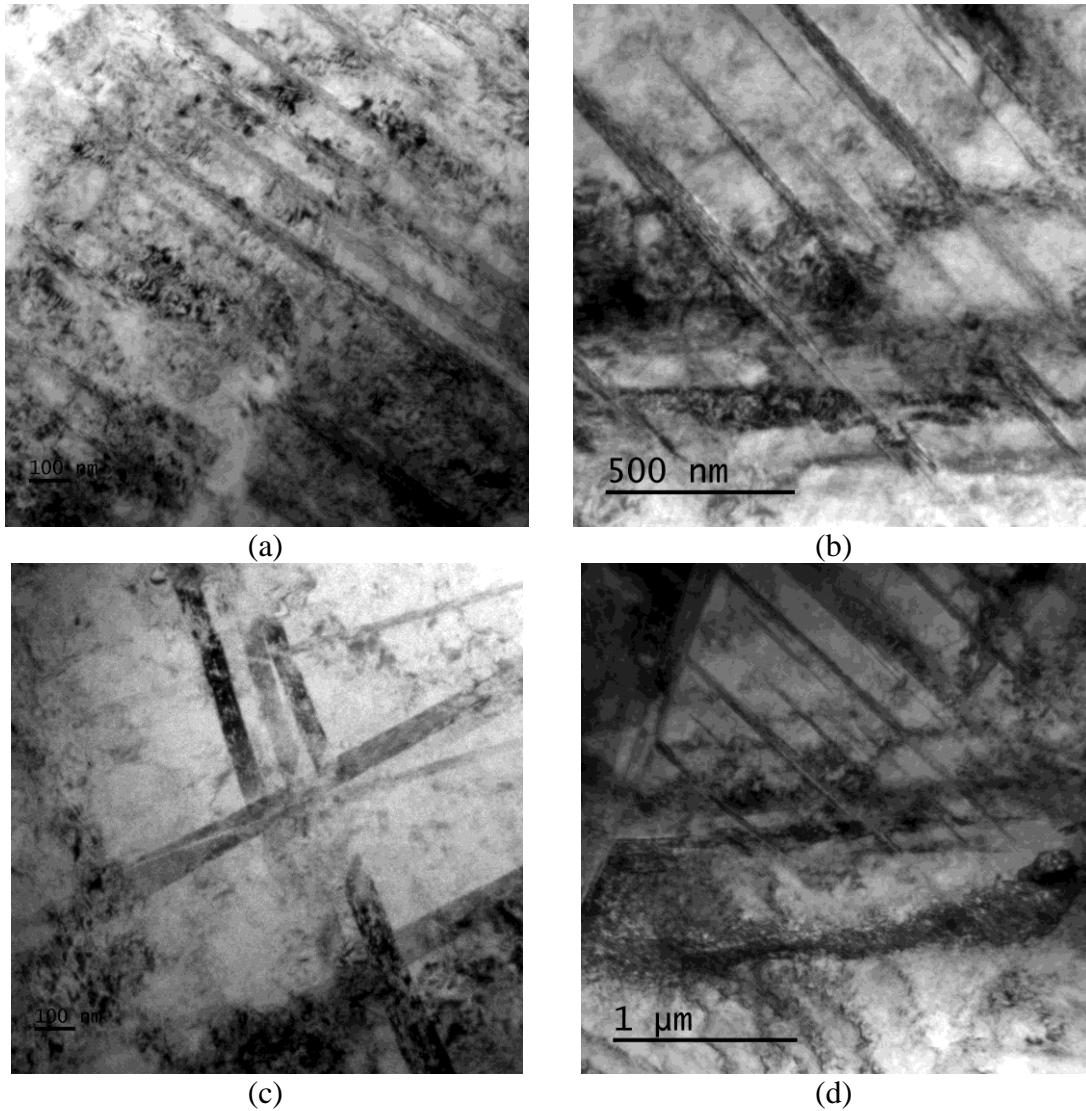
Fig. 4.17 BF- TEM micrographs from about 400-500 μm below the severe peened sample surface showing the presence of (a, b) shear bands and (c, d) multiple shear band intersections

4.4.3.1 Deformation induced martensite formation

When austenitic stainless steel is subjected to deformation, the parent austenite phase may transform directly to α' martensite (having BCC structure) or through an intermediate phase called ε-martensite (having HCP structure). In the present study, ε-martensite is not observed. It is generally advocated that the deformation induced martensite nucleates at the shear band intersections. However, in the present study, martensite is found to nucleate at multiple locations in the matrix.

Bright-field TEM micrograph in Fig. 4.18(a) shows the austenite matrix with multiple shear band intersections. Selected area electron diffraction (SAED) pattern from the marked region is given in Fig. 4.18(b). Along with bright diffraction spots of the austenite along [$\bar{1}12$] zone axis, weaker martensite spots corresponding to [111] zone axis are also visible. Dark-field TEM micrograph from the (110) martensite reflection is given in Fig. 4.18(c). It could be clearly observed that the martensite is nucleated at the shear band intersection (Lecroise and Pineau 1972, Olson 1972).

(a)   (b)

(c)
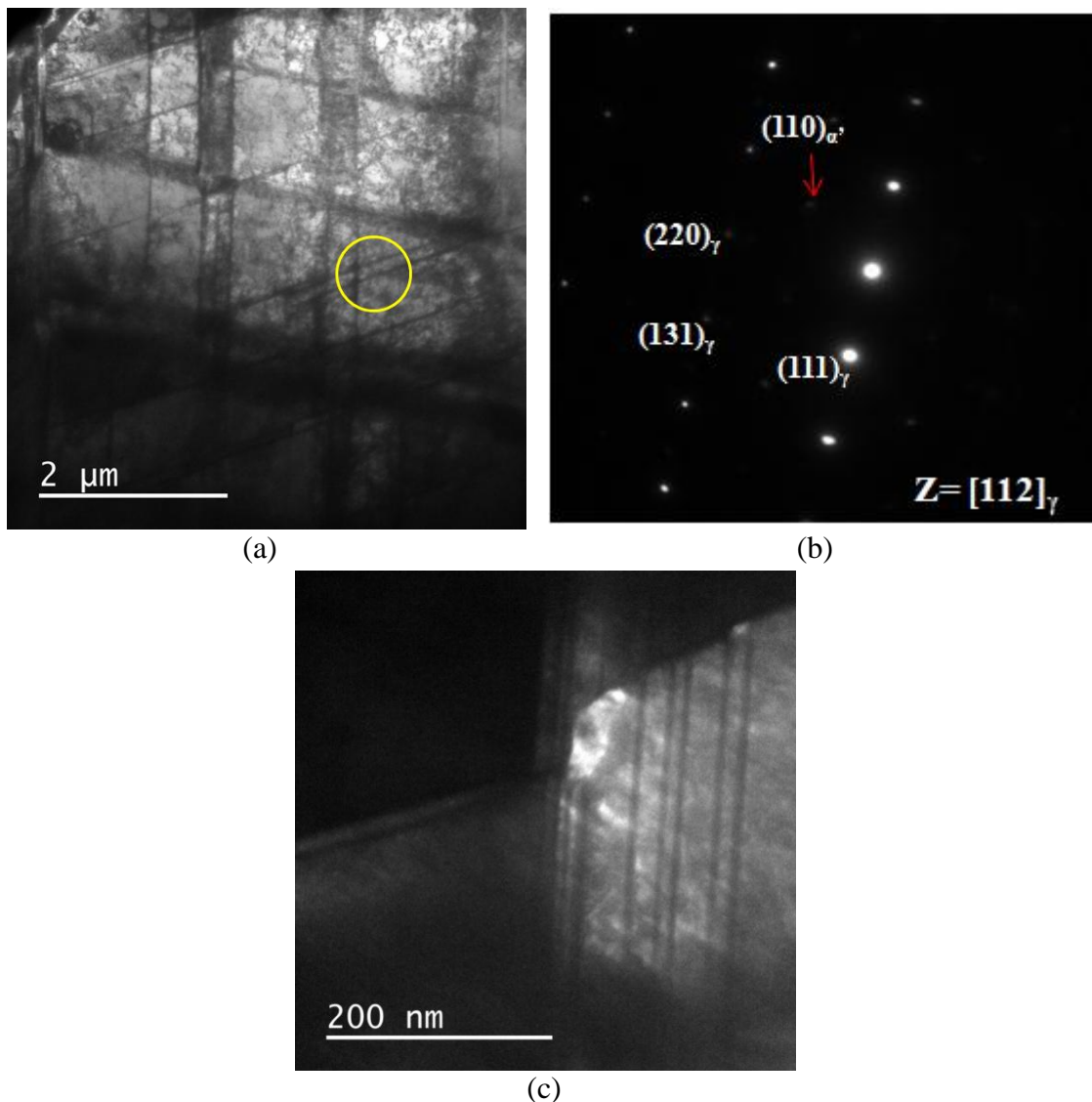
Fig. 4.18 (a) BF-TEM micrograph showing mutiple twin intersections. (b) SAED from the marked region and (c) Dark-field TEM micrograph using (110) martensite reflection

The work of Murr et al. (Murr et al. 1982) suggests that the martensite nuclei formed at shear band intersections close to each other will impinge on each other. This results in the coalescence of the martensite nuclei to form longer martensite laths. It is also justified by Lee et al (Lee and Lin 2002) that martensite embryos overcoming the nucleation barrier will grow as long martensite laths until a barrier for the growth is encountered. It is illustrated by the bright-field TEM micrograph shown in Fig. 4.19(a). The SAED pattern from the marked region in the Fig. 4.19(b) shows the spots corresponding to austenite ($[\bar{1}11]$ zone axis) and martensite ($[111]$ zone axis). Dark-field micrograph in Fig. 4.19(c) from the (110) martensite reflection clearly shows formation of the martensite lath.

(a)

(b)

(c)
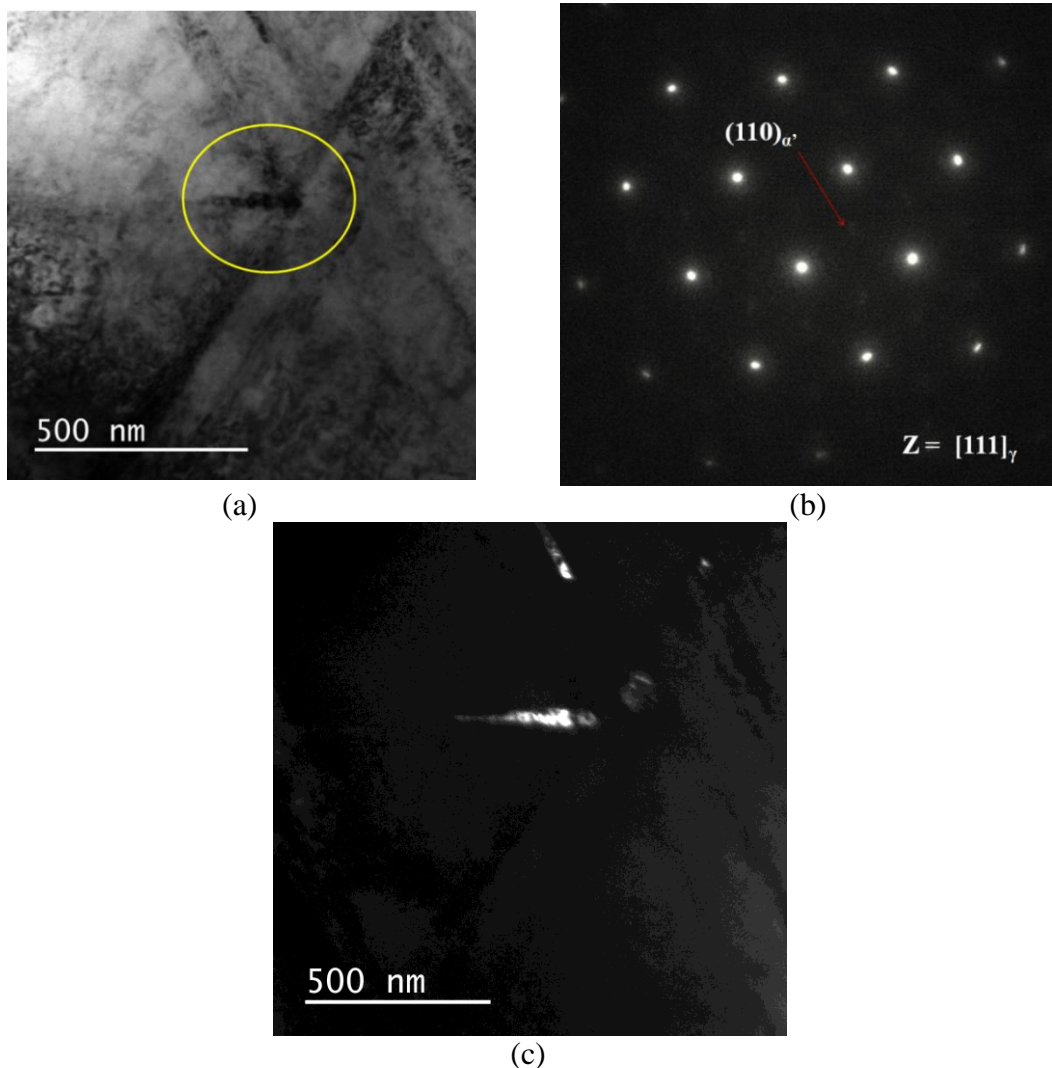
Fig. 4.19 (a) BF- TEM micrograph showing shear band intersection (b) SAED pattern from the marked region and (c) Dark-field micrograph using (011) martensite reflection

However, every shear band intersection need not be a nucleation site for the DIM transformation. It is reported (Staudhammer et al. 1983; Shrinivas et al. 1995) that critical nucleation size and strain invariant conditions should be satisfied at the shear band intersection to facilitate the martensite nucleation. Figure 4.20(a) shows a typical bright-field TEM micrograph depicting the intersection of shear bands. Corresponding SAED pattern from the marked region is given in Fig. 4.20(b). The diffraction spots correspond to [011] zone axis of the austenite phase with twin reflections. It suggests that, in the present case, shear bands are deformation twins in the austenite matrix. Dark-field TEM micrograph using the twin spot in the SAED pattern is given in Fig. 4.20(c). No martensite is evident at the intersection.

(a)

(b)

(c)
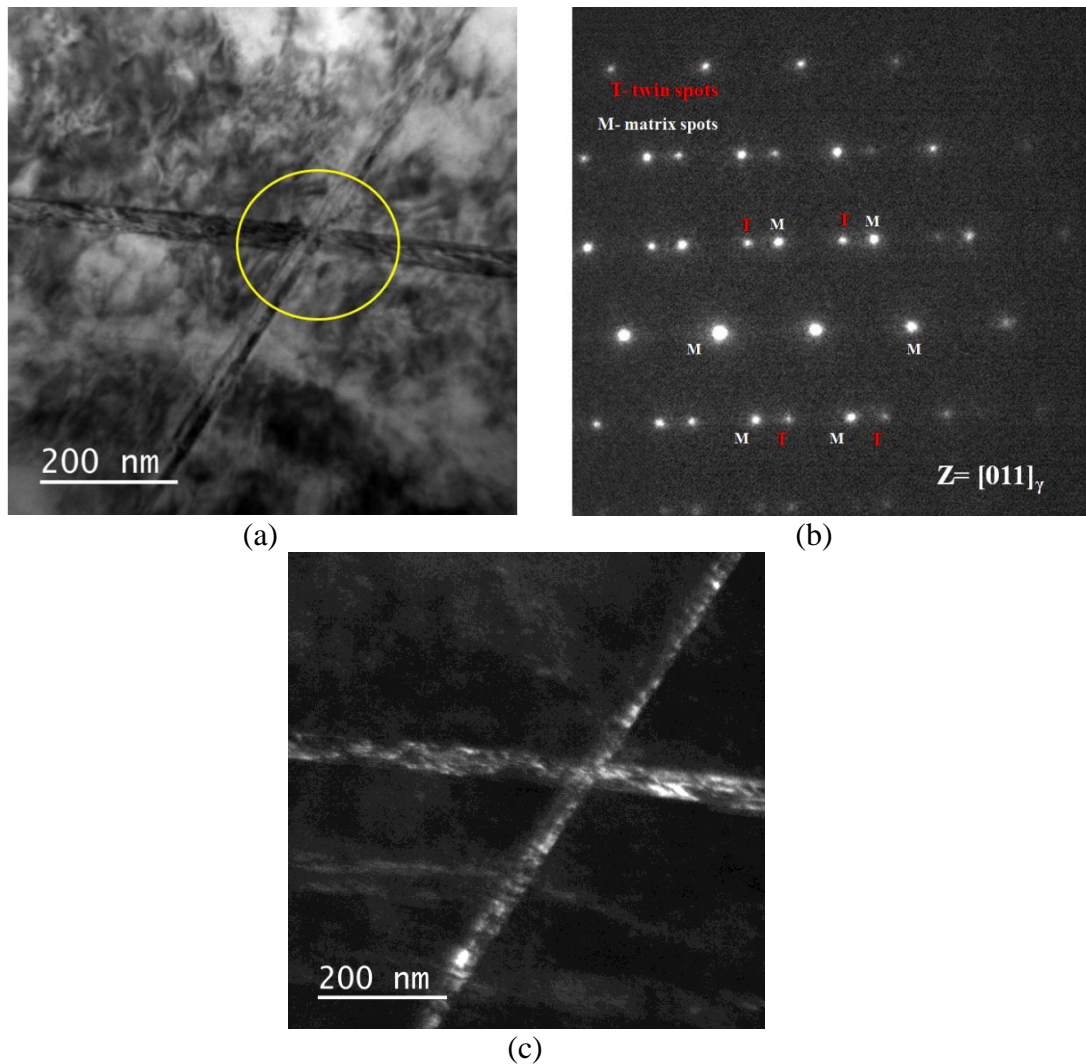
Fig. 4.20 (a) BF-TEM micrograph showing twin intersection (b) SAED pattern from the marked region and (c) DF- TEM micrograph using twin spots

In the study, it is observed that the martensite is nucleated in the locations other than the shear band intersections as well. Figure 4.21(a) shows the presence of parallel shear bands in the austenite matrix and the corresponding SAED pattern is given in Fig. 4.21(b). Major spots in the SAED pattern correspond to the austenite along $[\bar{1}12]$ zone axis while faint spots correspond to the martensite along [111] orientation. The dark-field TEM micrograph from the (110) martensite reflection is given in Fig. 4.21(c). It could be observed that the fine martensite units are formed parallel to the shear band. Width of the martensite formed is in the order of 10-20 nm.

(a)   (b)

(c)
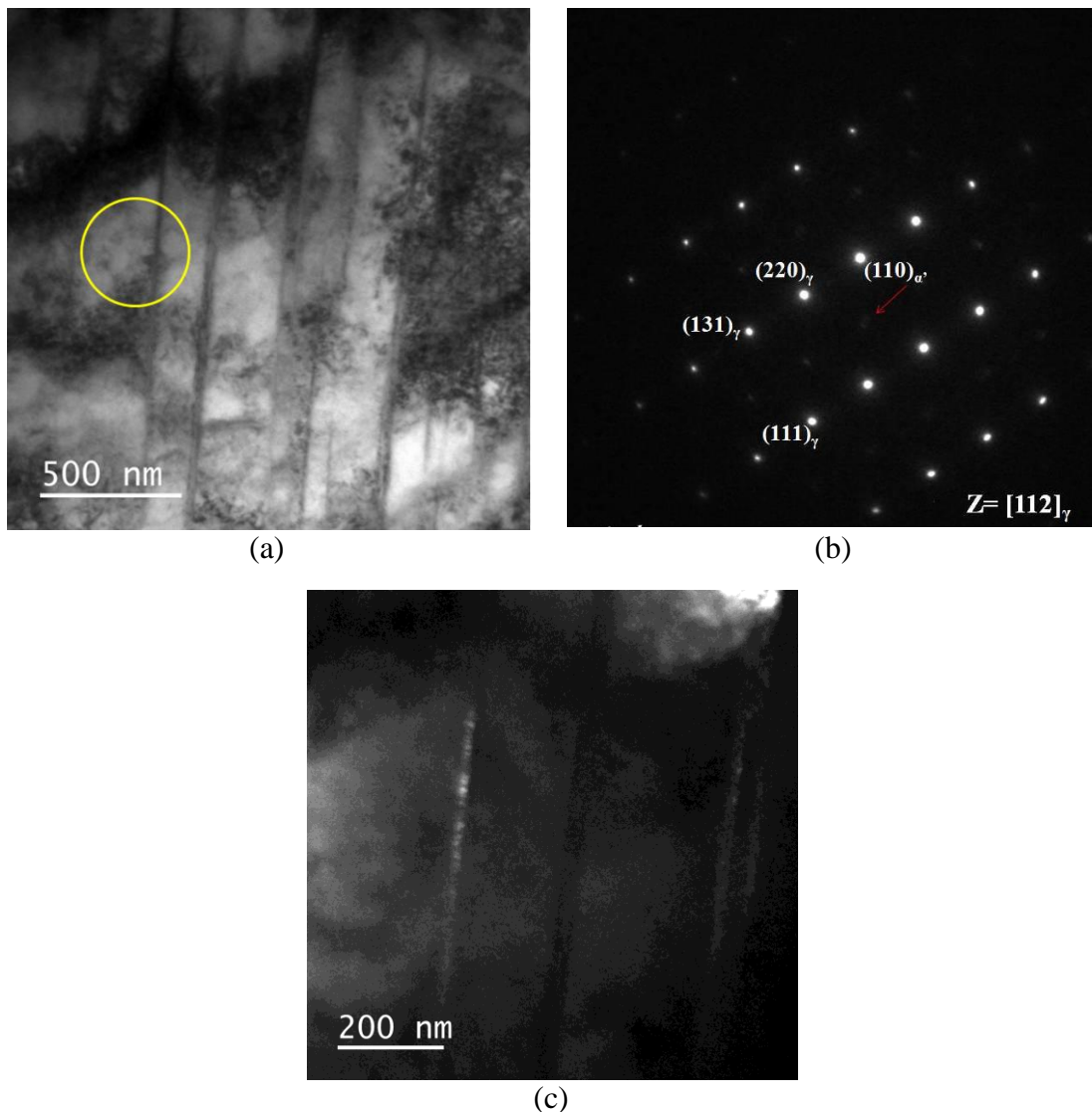
Fig. 4.21 (a) BF-TEM micrograph showing the presence of parallel shear bands (b) SAED pattern from the marked region and (c) Higher magnification DF-TEM micrograph from the (110) martensite reflection

Bright-field TEM micrograph in Fig. 4.22(a) depicts the presence of a shear band in the austenite matrix. SAED pattern from the marked region is given in the Fig. 4.22(b). Presence of a small unit of martensite could be observed inside the shear band. Diffraction spot corresponding to (110) plane of the martensite is also observed in the SAED pattern. The dark-field TEM micrograph from the (110) reflection of the martensite is shown in Fig. 4.22(c). It unambiguously confirms the unit as martensite.

(a)

(b)

(c)
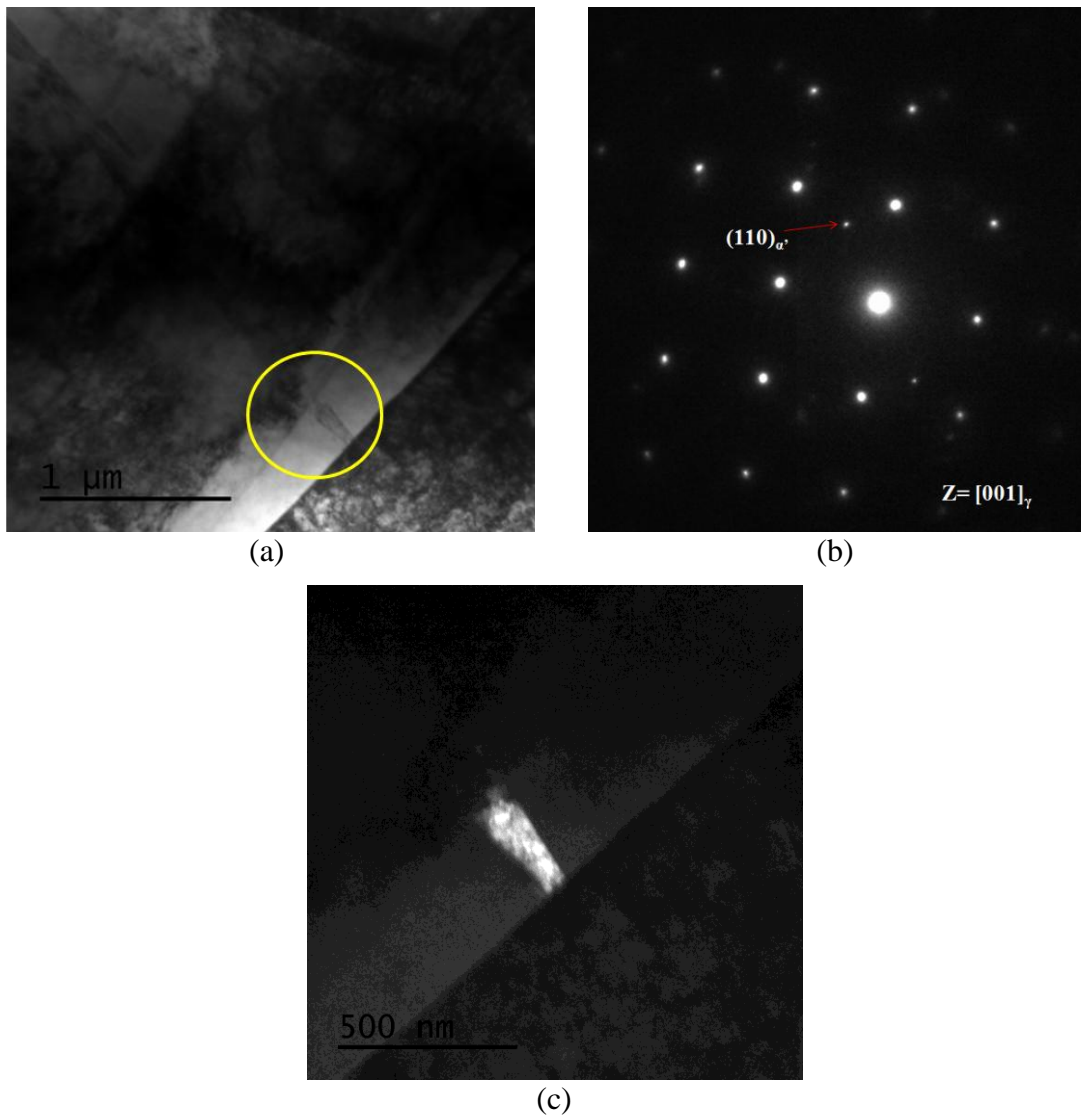
Fig. 4.22 (a) BF-TEM micrograph showing the presence of a shear band (b) SAED pattern from the marked region and (c) Higher magnification DF-TEM micrograph using (110) martensite reflection

Bright-field TEM micrograph in Fig. 4.23(a) shows the presence of parallel nano-scale shear bands in the austenite matrix. It could be observed that a martensite unit of about 150 nm thickness is formed across these bands. Convergent beam electron

61

diffraction (CBED) pattern taken from the marked region is given in Fig. 4.23(b). It corresponds to [111] zone axis of the martensite. This suggests that the martensite could also be formed across the nano-scale shear bands.

<div align="center">(a)   (b)</div>
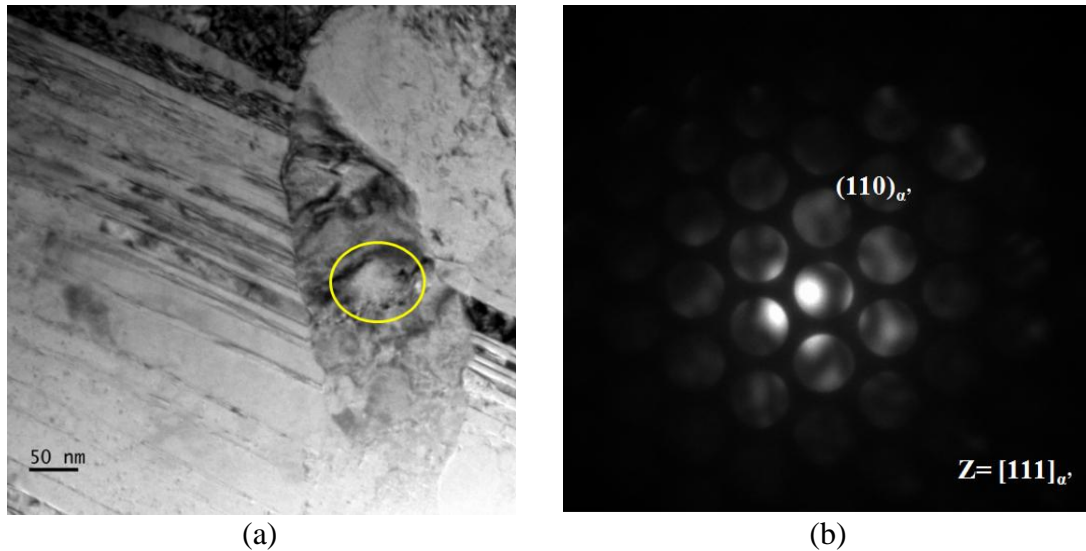
Fig. 4.23 (a) BF-TEM micrograph showing nano-scale shear bands and (b) CBED pattern from the marked region

Figure 4.24(a) depicts a bright-field TEM micrograph from the transition region of the GNS layer. SAED pattern from the marked region is given in Fig. 4.24(b). SAED pattern consists of reflections from the austenite as well as from the martensite phases. Dark-field TEM micrograph using (200) martensite reflection in Fig. 4.24(c) indicates the presence of lath martensite unit of about 200 nm thickness. Lower magnification dark-field TEM micrograph in Fig. 4.24(d) suggests that the martensite lath is closer to the grain boundary. This indicates that grain boundary could be the nucleation site for DIM transformation. There are reports in the literature (Das et al. 2008; Naraghi et al. 2011) suggesting that deformation induced martensite could nucleate at grain boundaries.
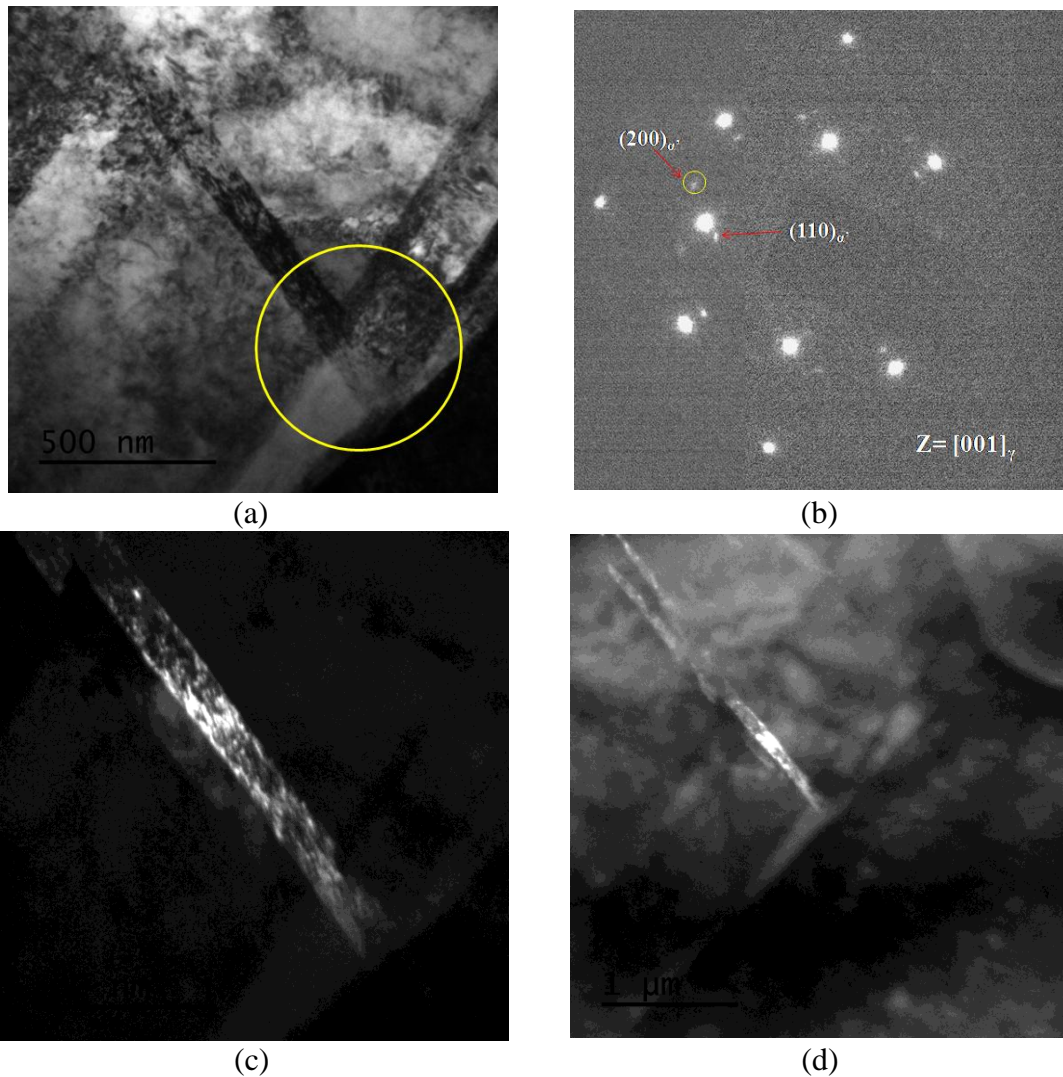
Fig. 4.24 (a) BF-TEM micrograph from the transition region of the GNS. (b) SAED pattern from the marked region (c-d) DF- TEM micrographs using (200) martensite reflection

Bright-field TEM micrograph in Fig. 4.25(a) shows the presence of the parallel shear bands spaced a few hundreds of nanometers apart in the austenite matrix. There are indications of nano-scale shear bands existing between these; along with the dislocations. SAED pattern taken from the area between two shear bands is given in the Fig. 4.25(b).

(a)

(b)

(c)
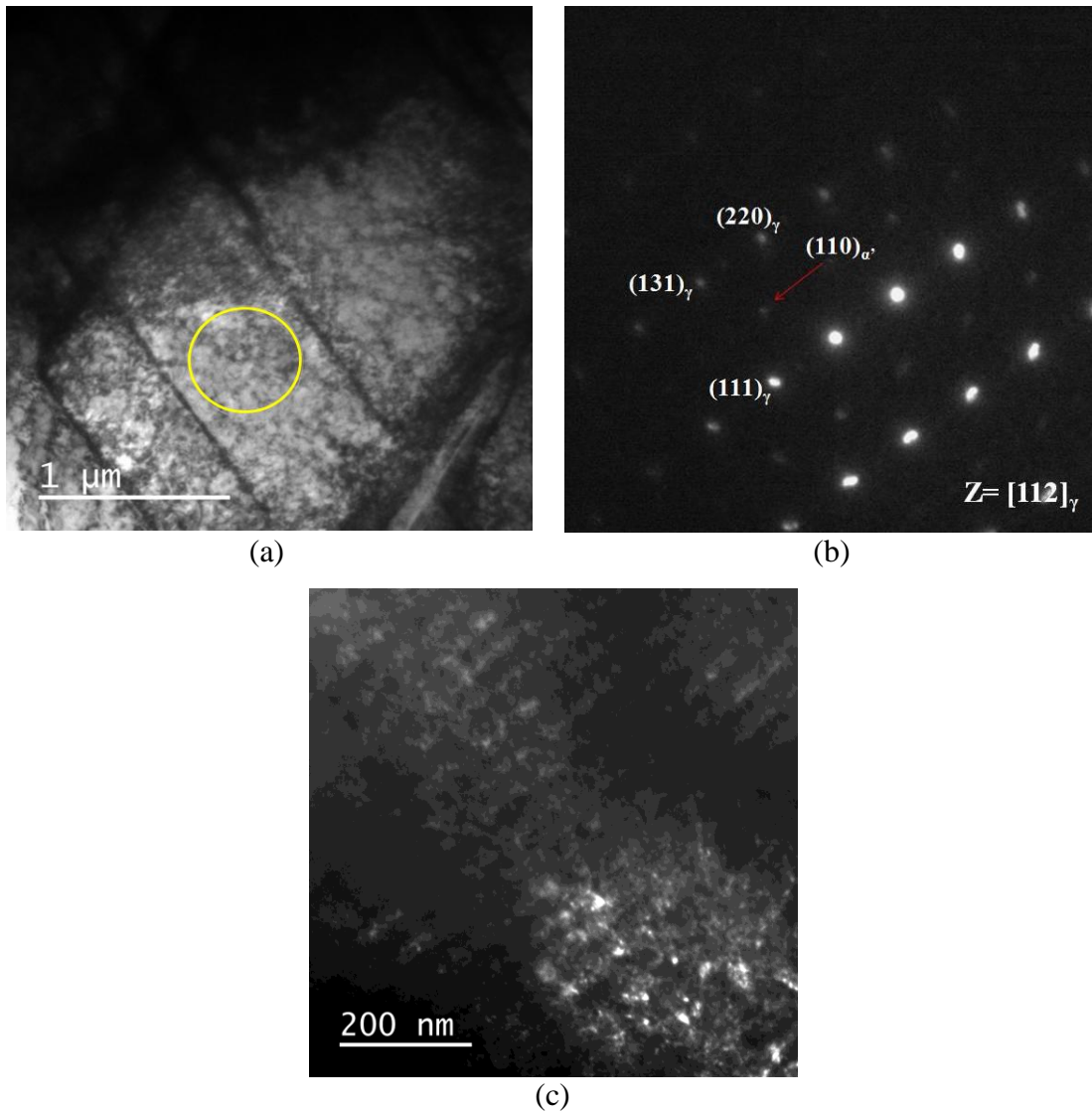
Fig. 4.25 (a) BF-TEM micrograph showing presence of the parallel shear bands. (b) SAED pattern from the marked region and (c) DF-TEM micrograph using (110) martensite reflection

Diffraction pattern corresponds to $[\bar{1}12]$ zone axis of the austenite is superimposed with the additional spots from the martensite phase. Higher magnification dark-field TEM micrograph using (110) martensite reflection is given in Fig. 4.25(c). These micrographs affirm the presence of the nano-scale shear bands between the major shear bands. Dark-field micrograph confirms the formation of the DIM parallel to those nano-scale shear bands.

4.4.4 Microstructural features in the nanocrystalline region

It is observed in the section 4.4.1 that the nanocrystalline region of the GNS layer extends to about 20 μm from the top surface and it consists of the martensite phase alone. However, during the TEM study it is observed that the morphological features change from the lath martensite to the dislocation cell type martensite in this region. Figure 4.26 shows the bright-field TEM micrographs from different layers in the nanocrystalline region.

The layer about 20 μm from the top surface (Fig. 4.26(a)) consists of lath martensite morphology. Corresponding SAED pattern is given in Fig. 4.26(b). Individual laths are having thickness in the range of 80-120 nm while having length in the range of several micrometers. Huge amount of dislocations are found inside each lath. SAED pattern shows broken rings of the martensite phase.

The layer above the lath martensite region (Fig. 4.26(c-e)) indicates the transition of the martensite morphology from the lath-type to the dislocation cell-type. It could be observed that the lath structure is getting broken as it is subjected to deformation at higher strain rate towards the surface. Hence, the dimensions of the individual laths are decreasing, continuously. There is an increase in the amount of dislocations and dislocation cells are emerging in certain locations of the microstructure.

(a)   (b)

(c)

(d)

(e)

(f)

(g)
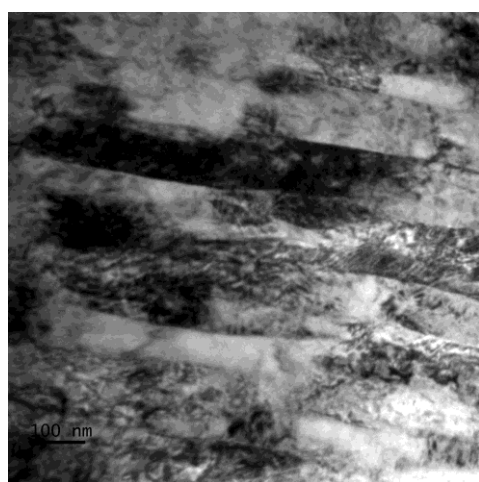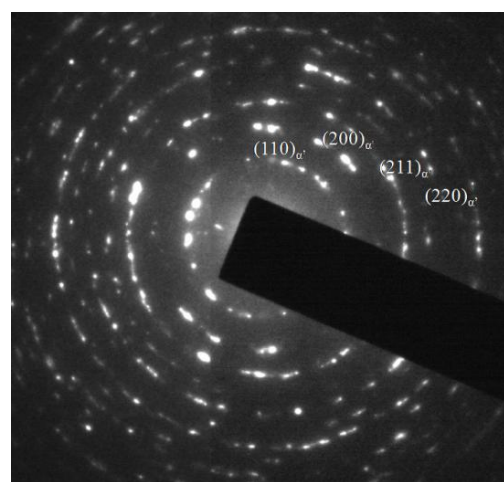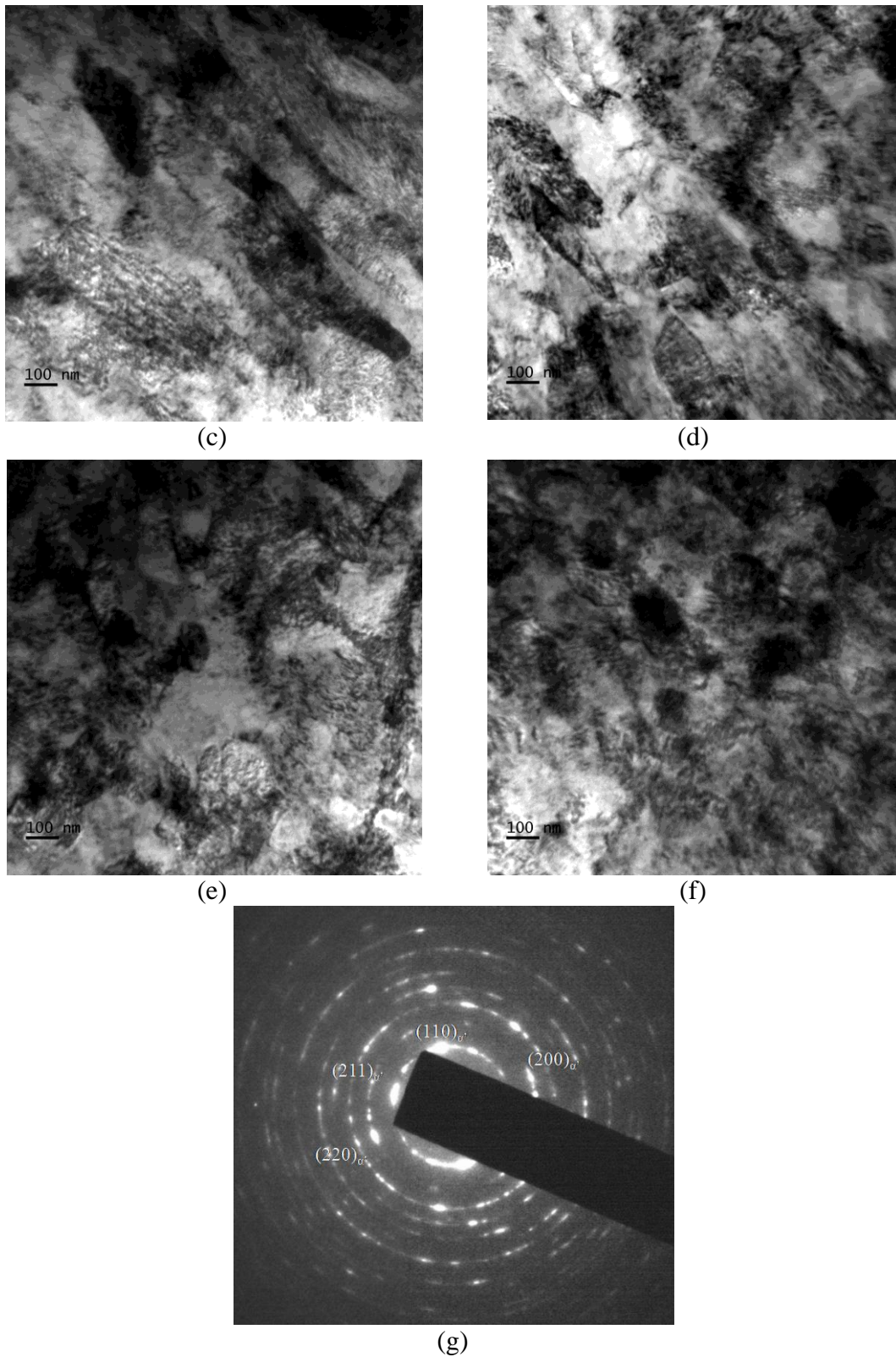
Fig. 4.26 BF-TEM micrographs (a,b) from about 20 µm depth from the peened surface and correpsonding SAED pattern (c-e) intermediate region of about 10-12 µm depth from the peened surface and (f,g) top surface and corresponding SAED patterns

The microstructure at the top most surface is shown in Fig. 4.26(f). It exhibits dislocation cell type morphology. Martensite crystallites are nearly equiaxed; diameter in the range of 100-140 nm. The SAED pattern in Fig. 4.26(g) depicts continuous ring pattern from the martensite phase affirming that microstructure consists of randomly oriented fine martensite crystallites. This kind of transformation of morphology from the lath to the dislocation cell-type is also observed and reported by Mishra et al. (Misra et al. 2010) with increasing percentage of reduction during cold rolling of AISI 301LN grade of stainless steel.

4.5 Effect of temperature on the plasma nitriding of un-peened and peened samples

Nitriding temperature has profound effect on the phase formation upon nitriding (Gil et al. 2006; Li et al. 2008; Wang et al. 2009). Higher nitriding temperature promotes the precipitation of the CrN; which in turn, reduce the corrosion resistance of the alloy. Hence, selection of right nitriding temperature is crucial for the success of the nitriding treatment. It is equally crucial when the severe deformation is employed as a pre-treatment step to plasma nitriding. Hence, in this section, the effect of temperature on the nitride layer thickness, phase formation and hardness on the surface over the nitriding temperature range of 300-500 °C is studied.

4.5.1 Nitride layer thickness

Figure 4.27 shows the cross-sectional SEM micrographs of the un-peened and the severe peened samples subjected to plasma nitriding at 300°C. No distinct nitride layer is observed in the case of un-peened sample as seen from Fig. 4.27(a). Figure 4.27(b) shows the deformation features resulting from the severe peening treatment. However, there is no indication of the nitride layer formation. This observation suggests that the nitriding temperature of 300 °C is not sufficient for diffusion of the nitrogen into the austenite matrix even with the introduction of the easy diffusion paths on the surface by severe deformation process.

<center>(a)</center>

<center>(b)</center>
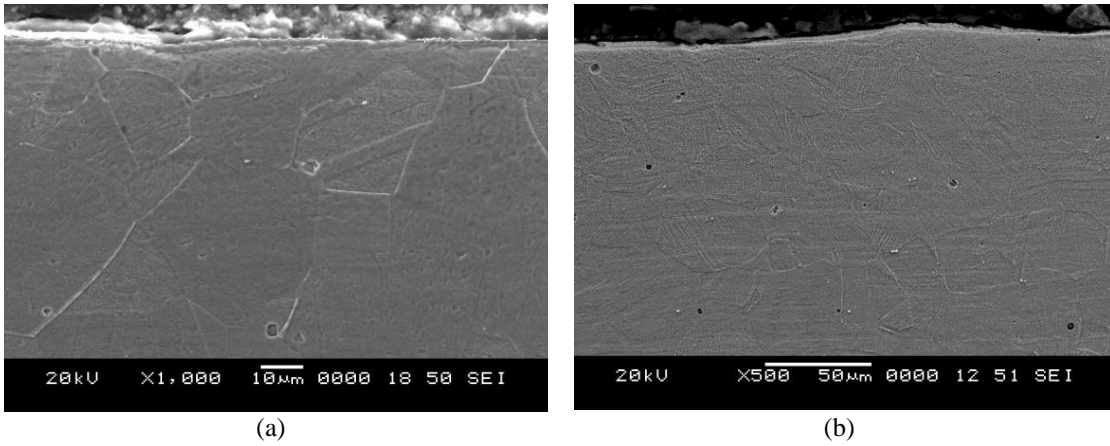
Fig. 4.27 Cross-sectional SEM micrographs of the (a) un-peened and (b) severe peened samples nitrided at 300°C

Figure 4.28 depicts the cross-sectional SEM micrographs of the un-peened and severe peened samples subjected to plasma nitriding at 400 °C. Thin continuous nitride layer of about 0.8 µm is observed in Fig. 4.28(a). In contrast, about 50 µm thick nitride layer is observed in Fig. 4.28(b). This is significantly higher than the case depth obtained upon plasma nitriding of the un-peened sample; showcasing the beneficial effects of prior surface deformation. Also, drastic change in the morphology is observed from nitride layer to substrate in the case of unpeened-nitrided sample. In contrast, the severe peened-nitrided sample shows gradual change in the morphology.

<center>(a)</center>

<center>(b)</center>
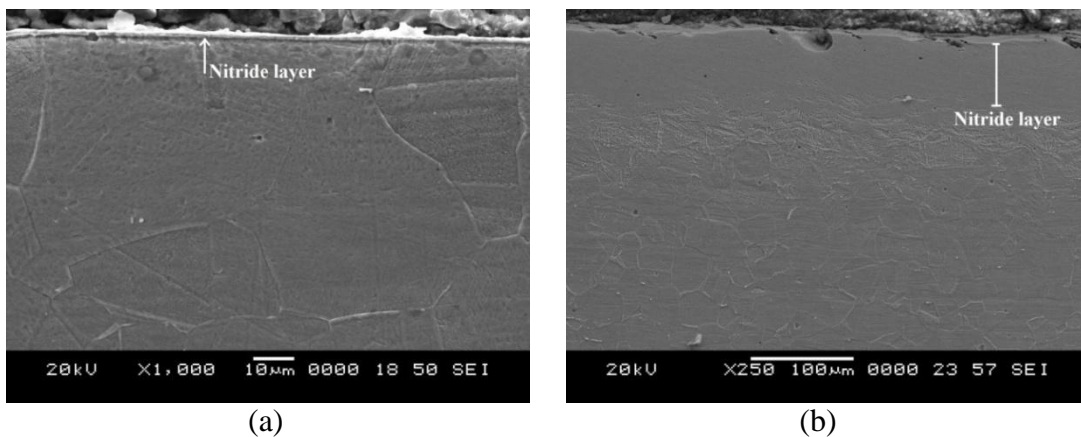
Fig. 4.28 Cross-sectional SEM micrographs of the (a) un-peened and (b) severe peened samples nitrided at 400 °C

Figure 4.29 shows the cross-sectional SEM micrographs of the un-peened and severe peened samples subjected to plasma nitriding at 500 °C. Thin continuous nitride layer of about 15 µm is observed in Fig. 4.29(a). Observation of the layer gives an indication of the presence of the second phase in the nitride layer. Severe peened

<center>68</center>

sample found to possess a nitride layer of about 28 µm thickness as depicted in Fig. 4.29(b). There is almost a two-fold increase in the thickness of the nitride layer with severe peening pre-treatment. Multiple cracks are also observed in the nitride layer.

<table>
<tr><td>(a)</td><td>(b)</td></tr>
</table>
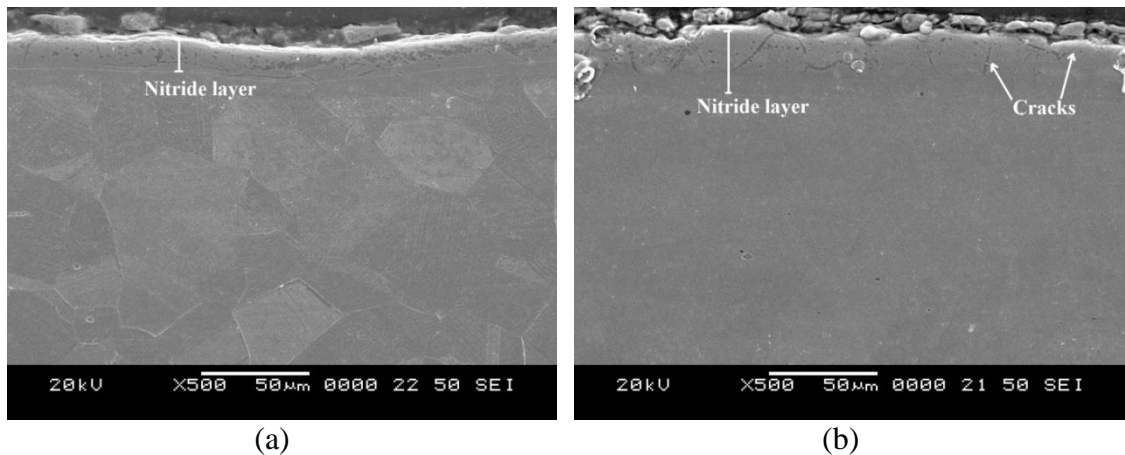
Fig. 4.29 Cross-sectional SEM micrographs of the (a) un-peened and (b) severe peened samples nitrided at 500 °C

Nitride layer thickness of all the samples are represented together in Fig. 4.30. It could be noted that highest case depth is obtained during the plasma nitriding of the severe peened sample at 400 °C. Considering the studies in the literature with shot peening pre-treatment, nitride case depth of about 20 µm was produced in the work of Ji et al. (Ji et al. 2005) upon nitriding at 400 °C for 6 hours. The work of Shen et al. (Shen et al. 2010) reported a nitride layer thickness of 5 µm after plasma nitriding at 400 °C for 4 hours. Though the work of Hashemi et al. (Hashemi et al. 2011) reports the formation of the nitride layer thickness of 50 µm, gas nitriding was carried out at 570 °C for 8 hours. Hence, considering the process parameters employed in the peening-nitriding duplex treatment, significant improvement in the nitride case depth is obtained in the present work.
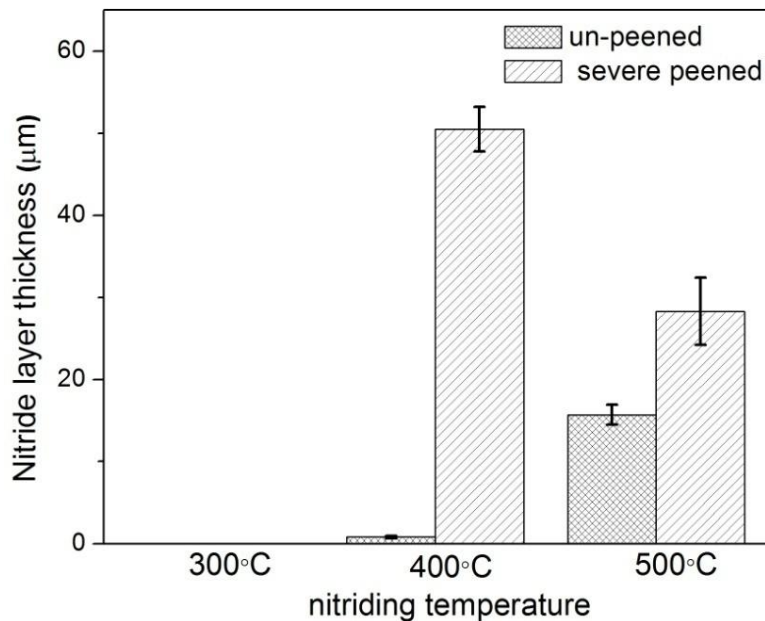
Fig. 4.30 Nitride layer thickness of the un-peened and severe peened samples subjected to plasma nitriding at 300, 400 and 500 °C, respectively

4.5.2 Phase formation details

Figure 4.31 shows the XRD patterns of the un-peened and the severe peened samples subjected to plasma nitriding at 300, 400 and 500 °C, respectively. In Fig. 4.31(a), all the peaks from the un-peened sample before nitriding corresponds to the austenite phase (JCPDS card no. 33-0397), while severe peened sample shows major peak corresponding to (110) plane of the martensite (JCPDS card no. 35-1375). Martensite is formed by the deformation induced transformation of the austenite phase (Spencer et al. 2009). It could be observed from Fig. 4.31(b) that, the phases formed upon nitriding at 300 °C are same as that of the un-peened and the severe peened samples before nitriding. This is in support to the observations from Fig. 4.27; affirming that there was no observable nitride layer formed during nitriding at 300°C.

Peaks corresponding to the S-phase are observed in Fig. 4.31(c) upon nitriding of the un-peened sample at 400 °C. S-phase is the solid solution of the nitrogen in the austenite (Fewell et al. 2000). It is also known as expanded austenite. In contrast, severe peened sample upon nitriding depicts the presence of broad peak in the 2θ range of 40-43° and a sharp peak at diffraction angle of 44.7°. The broad peak is attributed to S-phase while the sharp peak could be from the martensite phase. Precipitation of the deleterious chromium nitride was not observed at this temperature

in the case of both un-peened and severe peened samples. However, detailed TEM study will be conducted to affirm the absence of the CrN phase.

Nitriding of the un-peened samples at 500 °C in Fig. 4.31(d) showed the presence of peaks from the CrN phase (JCPDS card no. 11-0065) along with that of the S-phase. Severe peened sample showed peaks from the martensite and the CrN phase upon nitriding. This suggests that, nitriding temperature of 500 °C favours the formation of the CrN irrespective of the pre-treatment. Intensity of the CrN peaks is pronounced in the case of the severe peened sample. It is suggested that the defects produced during severe peening process aid in the diffusion of the Cr along with that of the nitrogen (Balusamy et al. 2013). Hence, it could be inferred that nitriding temperature of 500 °C should be avoided as it expected to impair the corrosion resistance of the material.
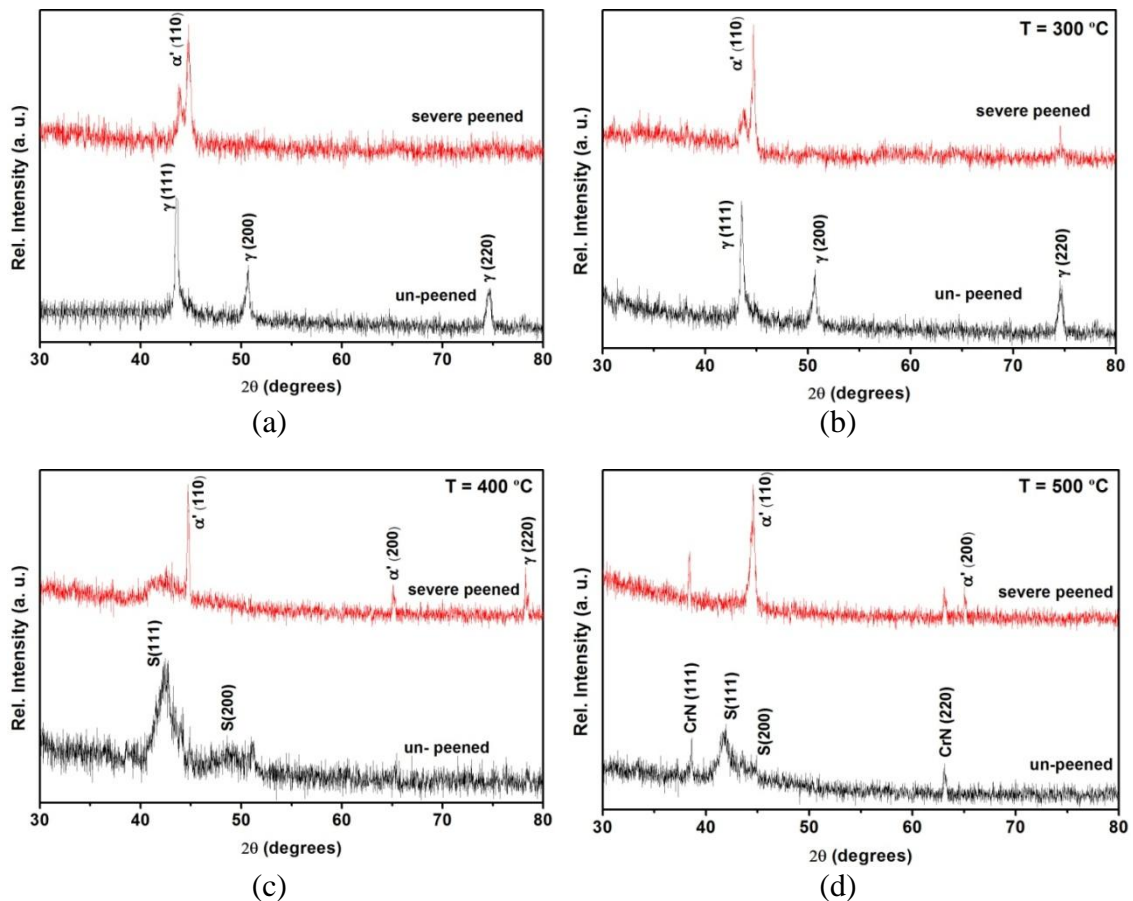
Fig. 4.31 XRD patterns of the un-peened and the severe peened samples (a) before nitriding, after nitriding for 4 hours at (b) 300 °C, (c) 400 °C and (d) 500 °C, respectively

4.5.3 Microhardness data

Figure 4.32 compares microhardness data of the un-peened and the severe peened samples nitrided at 300, 400 and 500 °C, respectively. Microhardness of the un-peened sample before nitriding is about 200 Hv. It could be observed that severe peening drastically increases the hardness of the surface due to formation of the non-equilibrium defects and the strain induced martensite. Insignificant improvement in the hardness is observed upon nitriding at 300 °C. This marginal increase could be due to bombardment of the ions during nitriding process. Significant improvement in the hardness is observed in the un-peened and the severe-peened sample, upon nitriding at 400 °C; owing to incorporation of the nitrogen into the lattices of the austenite and the martensite; respectively. Change in the hardness of the samples when nitrided at 500 °C is attributed to formation of the CrN precipitates, along with the incorporation of the nitrogen into the lattices of the austenite and martensite.
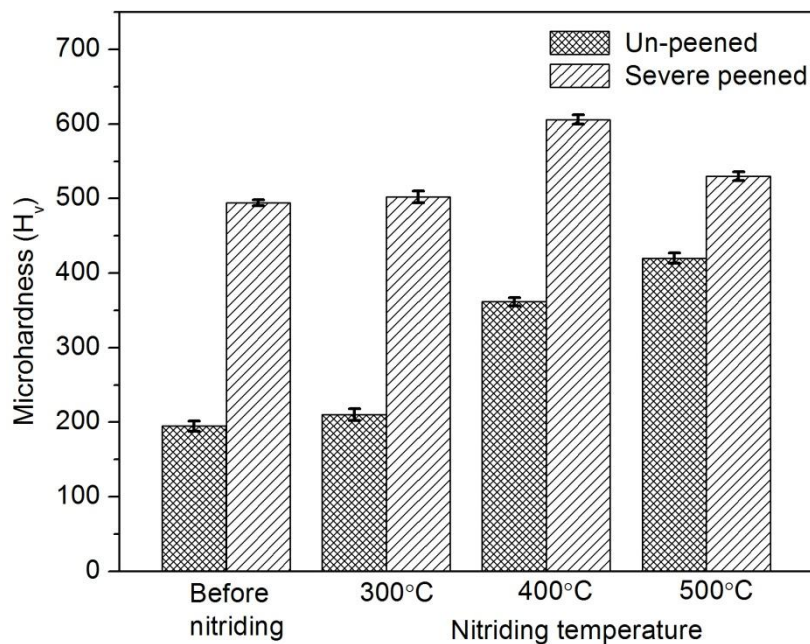
Fig. 4.32 Microhardness data of the un-peened and the severe peened samples subjected to plasma nitriding at 300, 400 and 500 °C, respectively

4.6 Effect of peening coverage on plasma nitriding at 400 °C

It is observed that 400 °C is the ideal plasma nitriding temperature for shot peened samples to harvest the beneficial effects of peening pre-treatment. In this section,

effect of shot peening coverage on nitriding kinetics is studied at this temperature. For comparison, data of nitriding of the un-peened sample is also provided.

4.6.1 Variation in the nitride layer thickness

Cross-sectional SEM micrographs of the un-peened and the peened samples after plasma nitriding as well as variation of the nitride layer thickness are shown in Fig. 4.33. Drastic improvement in the nitride layer thickness is observed; from about 1 µm in the case of the unpeened-nitrided sample to about 50 µm in the case of the severe peened-nitrided sample. This is considerably high compared to the reported literature (Hashemi et al. 2011) (Hassani-Gangaraj et al. 2014) (Ji et al. 2005) (Shen et al. 2010). It is also noted that increase in the peening coverage increases the nitride case depth. In all cases, the nitride layer appears featureless with no cracks or precipitates while the base material is attacked by the etchant during etching. Also, a gradual transition from the nitride layer to the unaffected base material is observed in the case of the pre-peened samples through a transition zone consisting of deformation features induced during the peening process.

(a)   (b)

(c)

(d)

(e)
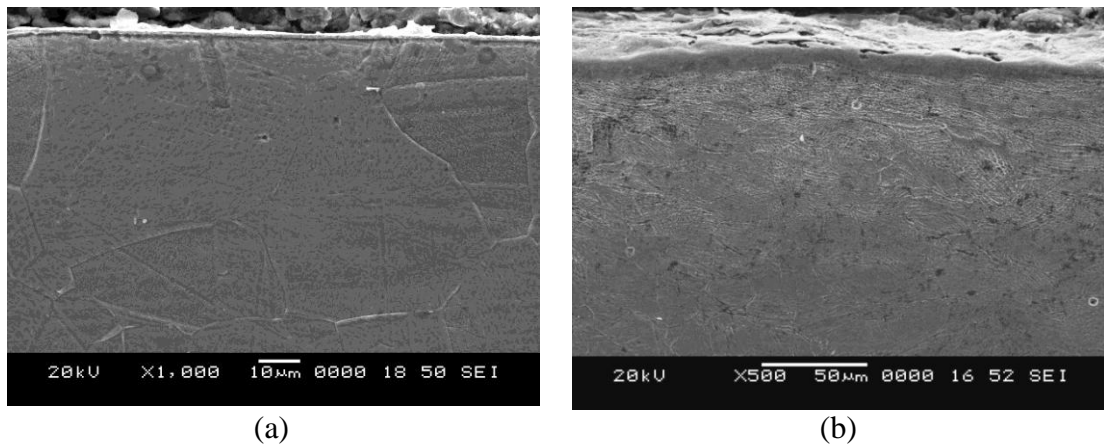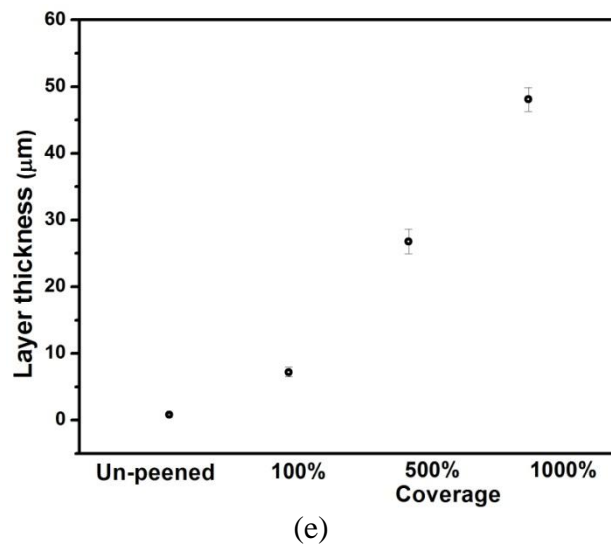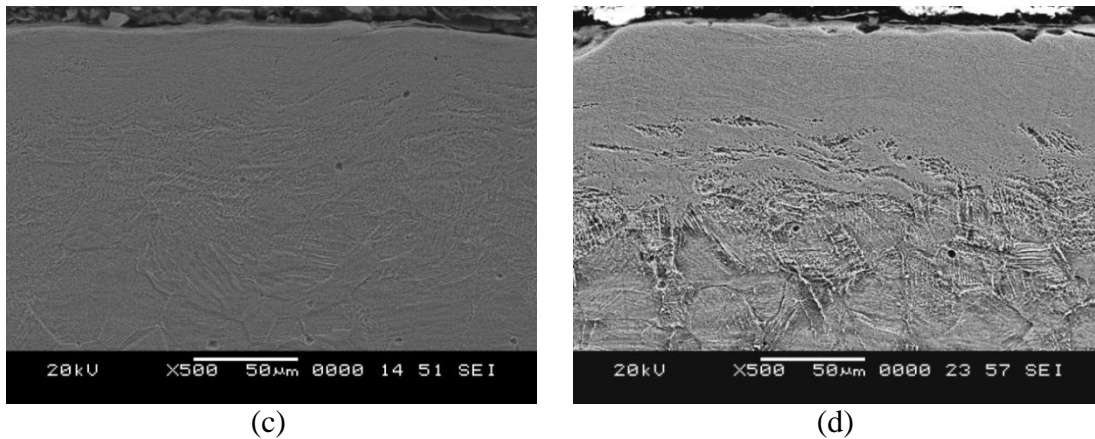
Fig. 4.33 Cross-sectional SEM micrographs of the (a) un-peened specimen and specimens peened with (b) 100% (c) 500% (d) 1000% coverage after plasma nitriding and (e) variation of the nitride layer thickness with peening coverage

4.6.2 Phase formation details

The X-ray diffraction patterns of the un-peened and the shot peened samples after plasma nitriding are shown in Fig. 4.34. The un-peened sample and the sample peened with 100% coverage indicate the formation of the expanded austenite phase; commonly called as S-phase, upon plasma nitridng treatment. It is the solid solution of the nitrogen in the austenite and is reported by many researchers during low temperature plasma nitriding of the austenitic stainless steels (Fewell et al. 2000) (Li et al. 2012) (Gontijo et al. 2006). It is interesting to note that plasma nitriding of the samples peened at 500% and 1000% coverage show the peaks corresponding to (111) and (200) planes of the marteniste along with a broad peak in the 2θ range of 40-43°

74

corresponding to the S-phase. With extensive formation of the strain induced martensite on severe peening (as seen in Fig. 4.6) and thick nitride layer during plasma nitriding (in Fig. 4.33(c) and (d)); it is reasonable to assume that the nitrogen has entered into the martensite lattice. It is widely accepted that, in austenitic stainless steels, severe deformation leads to formation of the strain induced martensite (α') on the surface while plasma nitriding alone forms expanded austenite (S-phase) (Zhang and Bell 1985). However, structural characteristics of the layer formed on the pre-deformed steel surface after plasma nitriding is still a matter of debate. Hence, as discussed in section 4.5.2, TEM studies of the severe peened- nitrided samples are conducted and results are elaborated in section 4.7. Precipitation of the deleterious chromium nitride is not observed in any of the samples.
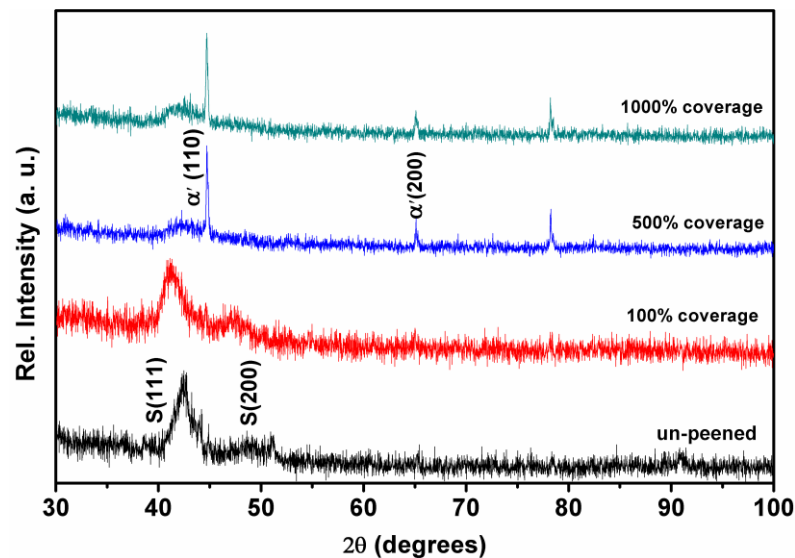
Fig. 4.34 XRD patterns of the un-peened and the shot peened samples after plasma nitriding

4.6.3 Surface roughness data

Comparison of the average surface roughness after shot peening and plasma nitriding treatments is shown in Fig 4.35. The roughness data of the peened samples are shown for the purpose of comparison. It could be observed that the average roughness value remains largely unchanged upon nitriding.
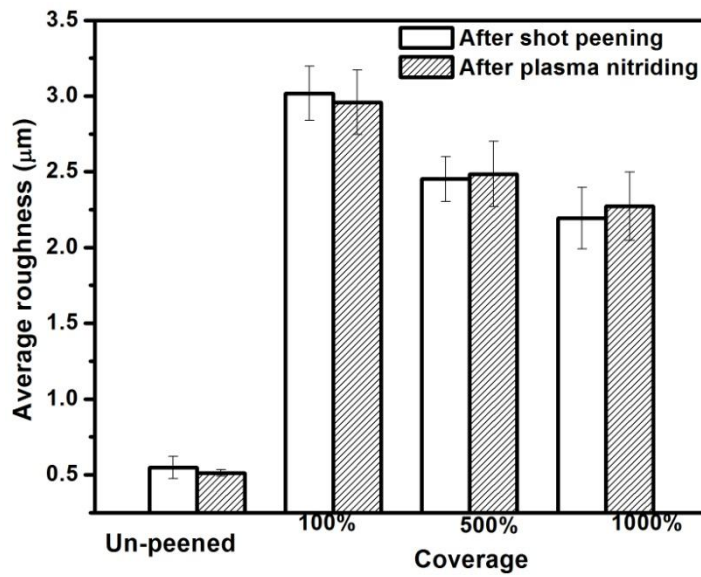
Fig.4.35 Variation of the surface roughness after shot peening and plasma nitriding treatments

4.6.4 Microhardness data

Comparison of the surface microhardness after shot peening and plasma nitriding treatments is shown in Fig 4.36. The microhardness data of the peened samples are shown for the purpose of comparison. It could be observed that the plasma nitrided counterparts show higher hardness for all the peening coverages, due to the incorporation of the nitrogen into the austenite or martensite phases. It is observed that considerable improvement in the surface hardness from about 200 Hv to about 600 Hv could be achieved by this duplex treatment.
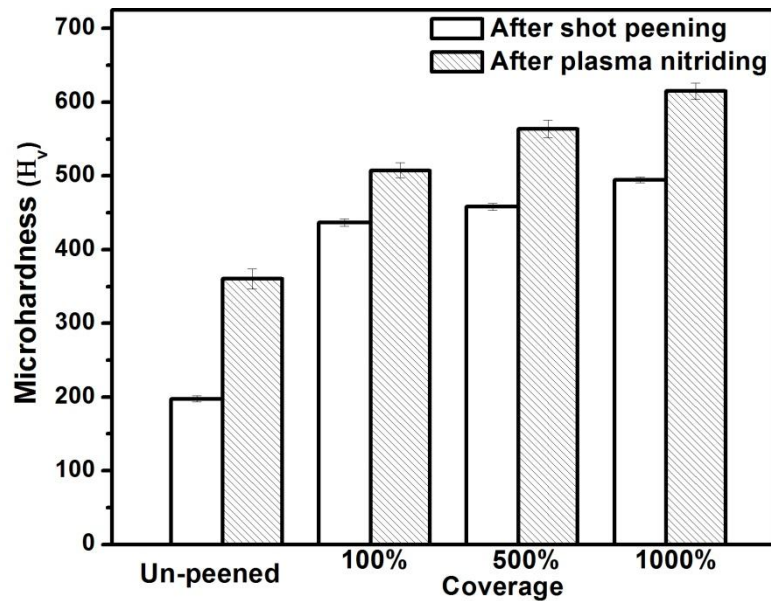
Fig. 4.36 Variation of the microhardness after shot peening and plasma nitriding treatments

4.7 Microstructural characterization of severe shot peened-plasma nitrided sample through TEM study

From the section 4.3 it is clear that surface nanocrystallization by severe shot peening could be successfully used as a pre-treatment step to enhance kinetics of plasma nitriding process. Pre-treatment step helps in achieving the thicker nitride layers at lower temperature and/or in shorter time; thus making the process more economical. In particular, peening coverage of 1000% assists in obtaining a substantially thicker nitride layer. However, the structural characteristic of the nitride layer has not been studied in-detail in the literature. The present section elaborates the microstructural characterization of the steel surface after duplex treatment using TEM study.

4.7.1 Microstructure of the surface layer

Cross-sectional SEM micrograph shown in Fig. 4.33(d) indicates a nitride layer of about 50 μm thickness. Figure 4.37 shows the TEM micrograph and corresponding SAED patterns of the top-most layer of the peened-nitrided sample. Grains in the range of 30-100 nm are seen in Fig. 4.37(a) suggesting that ultrafine grain structure obtained during shot peening is retained even after nitriding. However, dislocation density within the grains was notably less. During plasma nitriding treatment, the

77

samples were maintained at 400 °C for 4 hours. It is well established that the thermal energy assists in recombination, rearrangement and annihilation of dislocations substructures (Murr et al. 1982). This could be the reason for the observed decrease in the dislocation density. It is to be noted that the morphology of the martensite of the topmost layer remains same even after plasma nitriding.

SAED pattern in Fig. 4.37(b) indicates presence of the stronger diffraction rings corresponding to BCC crystal structure and weaker diffraction rings corresponding to FCC crystal structure. Former is attributed to martensite phase while the later rings are attributed to the expanded austenite phase based on the XRD pattern of the severe peened-nitrided sample in Fig. 4.35. The XRD pattern possesses peaks from the expanded austenite phase. Presence of expanded austenite phase is justified based on the observations of Yu et al. (2002). During plasma nitriding, nitrogen atoms are dissolved in the martensite phase. Nitrogen is an austenite stabilizer. Supersaturation of the nitrogen atoms in the lattice of the martensite decreases the transformation temperature of the martensite to the austenite. Hence, it is probable that during plasma nitriding, a small of amount of deformation induced martensite would transform back to the austenite phase. With simultaneous diffusion of the nitrogen into the lattice, the austenite will transform to expanded austenite.

(a)   (b)
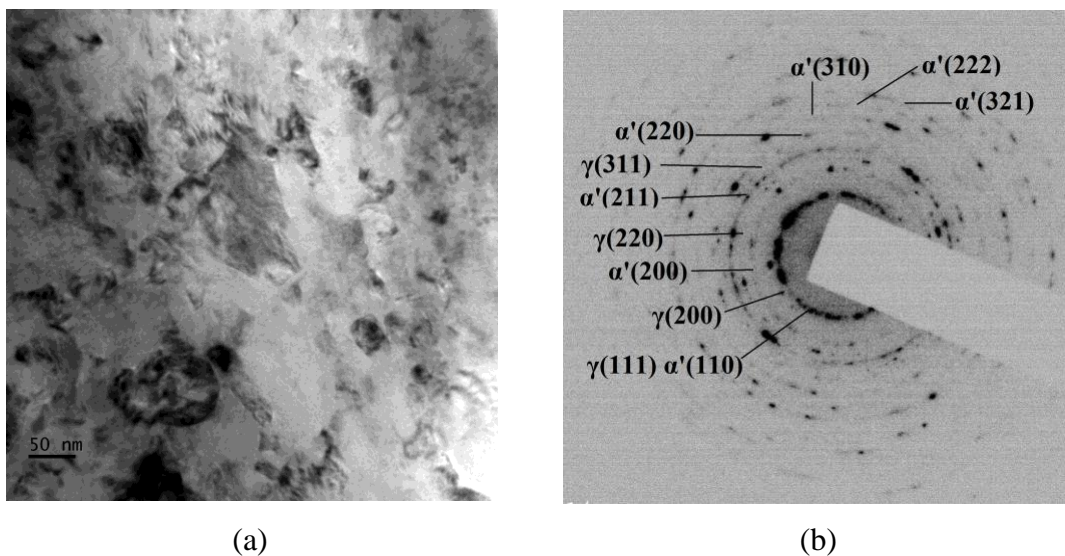
Fig. 4.37 (a) TEM micrograph and (b) corresponding SAED pattern from the top surface of the peened-nitrided sample

4.7.2 Microstructure of the sub-surface layer

Bright-field TEM micrograph and corresponding SAED pattern from 15 μm below (approximately) top layer of the peened-nitrided sample are given in Fig. 4.38. Presence of lath martensite is clearly visible in Fig. 4.38(a) with individual lath having thickness in the range of 60-100 nm. Each lath is found to consist of huge amount of dislocation sub-structures. Corresponding SAED pattern in Fig. 4.38(b) confirms presence of only the martensite phase. Precipitation of the CrN was not observed either on the top surface or in the sub-surface layer. Hence the peak corresponding to 2θ of 44.7° in the XRD pattern of the peened-nitrided sample in Fig. 4.34 could be undoubtedly attributed to the martensite.

(a)   (b)
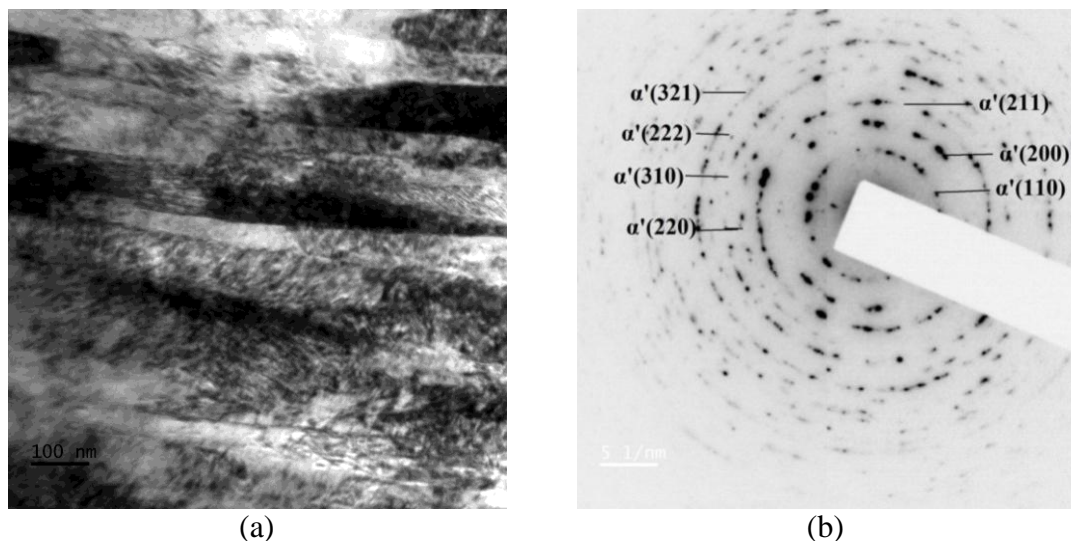
Fig. 4.38(a) TEM micrograph and (b) corresponding SAED pattern of the peened-nitrided sample from about 15 μm depth below the surface

Figure 4.39(a) depicts the bright field TEM micrograph from the region about 45 μm from the top surface. The microstructure consists of the lath martensite. SAED pattern in Fig. 4.39(b) has rings corresponding to the martensite phase. SAED pattern taken from individual lath in Fig. 4.39(c) corresponds to the martensite phase along zone axis [111]. This confirms that entire thickness of the nitride layer consist mainly of the martensite phase.

(a)   (b)

(c)
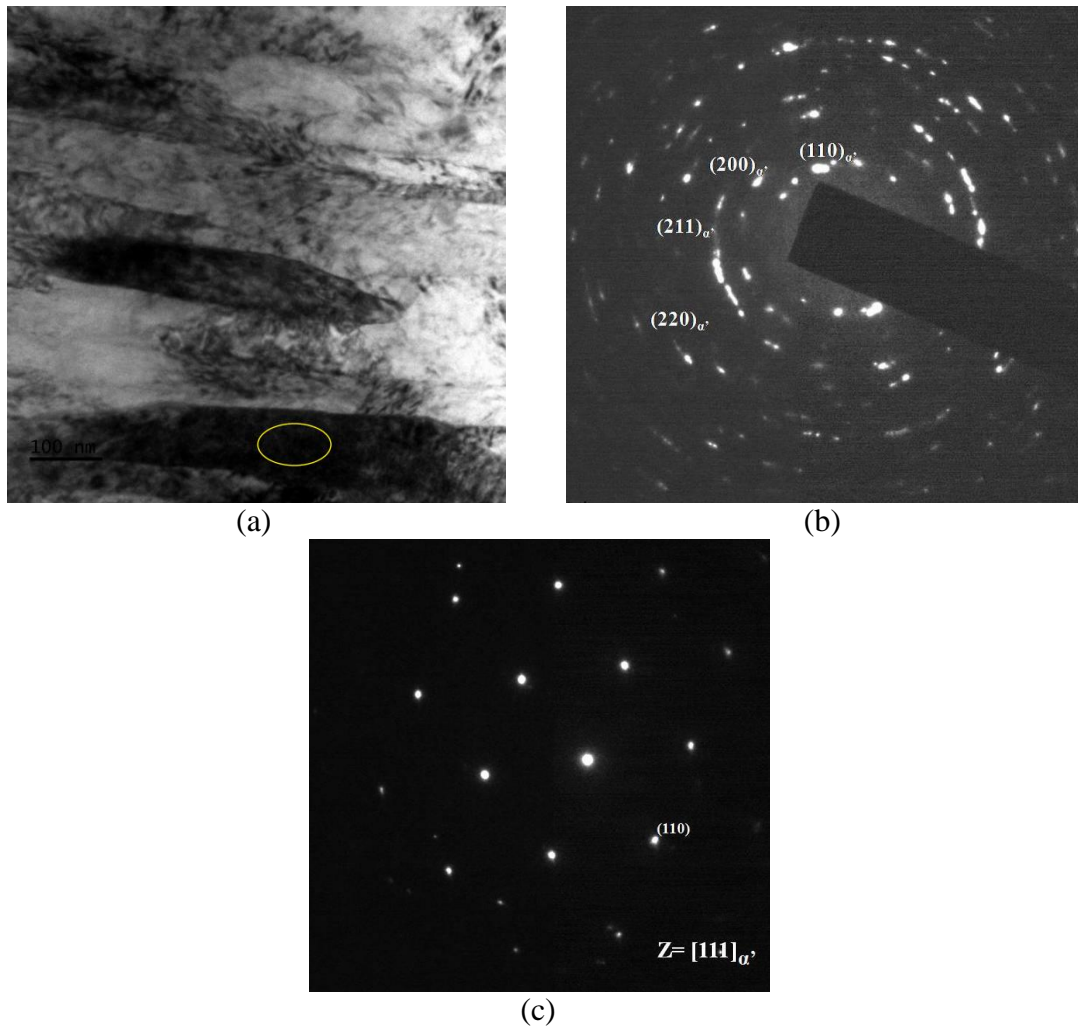
Fig. 4.39(a) TEM micrograph and (b) corresponding SAED pattern of the peened-nitrided sample from about 45 μm depth below the surface and (c) SAED pattern from the marked region

4.8 Mechanical properties of the 316L steel after shot peening and plasma nitriding

This section consists of the results from mechanical characterization of the base material and the treated surfaces. Hardness of the treated layer was measured by cross-sectional microhardness measurement. Scratch testing was carried out to assess the scratch hardness of the surface; while nanoindentaion, nano-scratch and nano-scale wear tests were carried out to study the hardness and wear properties of the treated surface at the nano-scale regime.

80

4.8.1 Hardness of the treated layer

Variation of microhardness data in the deformed region of the conventional peened, intermediate peened and severe peened surface is depicted in Fig. 4.40. For all the samples, maximum hardness is obtained at the peened surface and it found to decrease gradually as a function of depth from the treated layer. In the conventional peened sample, surface hardness is measured to be 450 H_v. It is more than twice the hardness of the base metal. However, it is observed that the hardness falls to less than 250 H_v at depth of less than 10 µm from the top surface. Surface hardness of the intermediate and severe peened sample are 478 and 497 H_v, respectively. In the case of intermediate peened sample, hardness of about 300 H_v is maintained upto 20 µm depth. In the case of severe peened sample, hardness of about 480 H_v is maintained upto 20 µm depth; which is the region of nanocrystallization. In the transition region, which extends to about 500 µm; hardness gradually decreases to about 250 H_v.
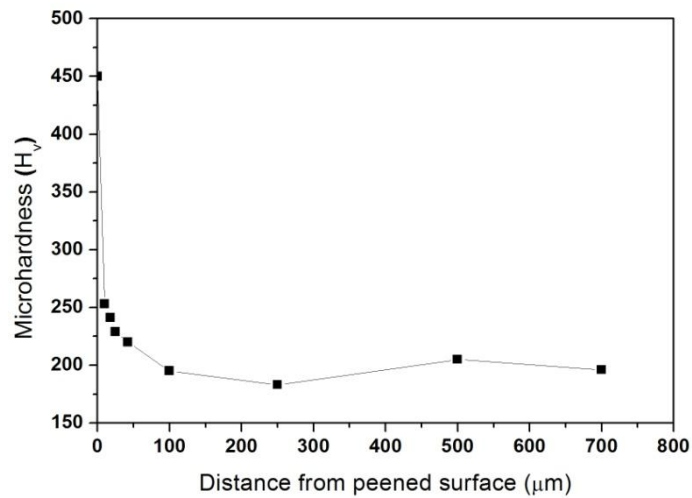
(a)
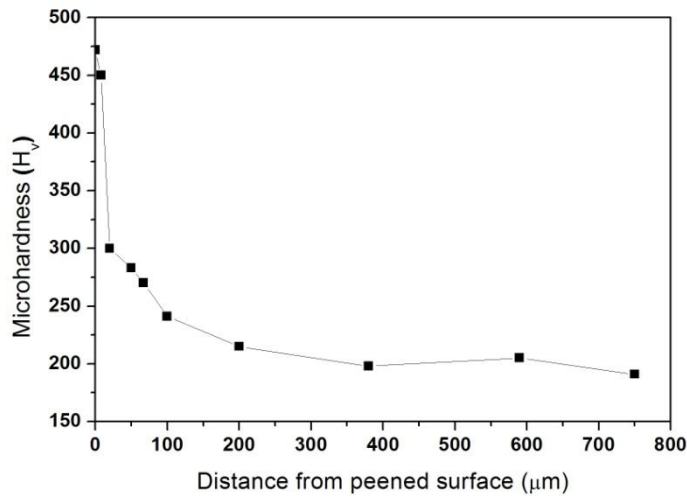
(b)
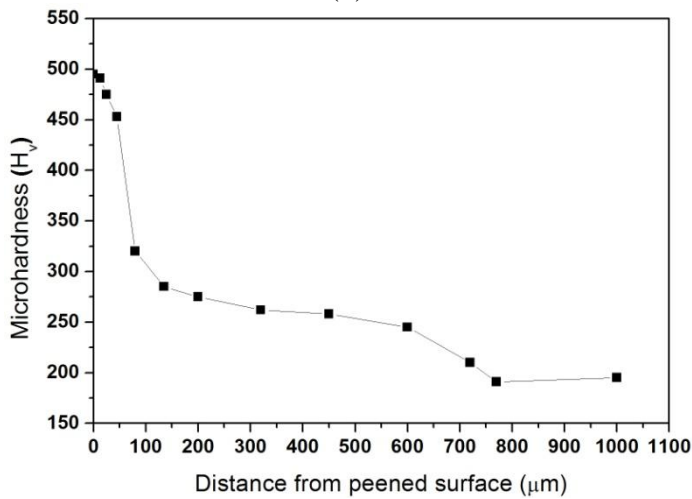
(c)

Fig. 4.40 Variation of microhardness data of the shot peened samples peened at (a) 100%, (b) 500% and (c) 1000% coverage, respectively

Variation of the microhardness data in the nitride layer of the peened-nitrided samples is depicted in Fig. 4.41. It could be observed in all the samples that maximum hardness is obtained at the surface and hardness shows only marginal decrease in the magnitude in the nitride layer. Beyond that the hardness decreases gradually with depth to the magnitude equivalent to that of the base material.
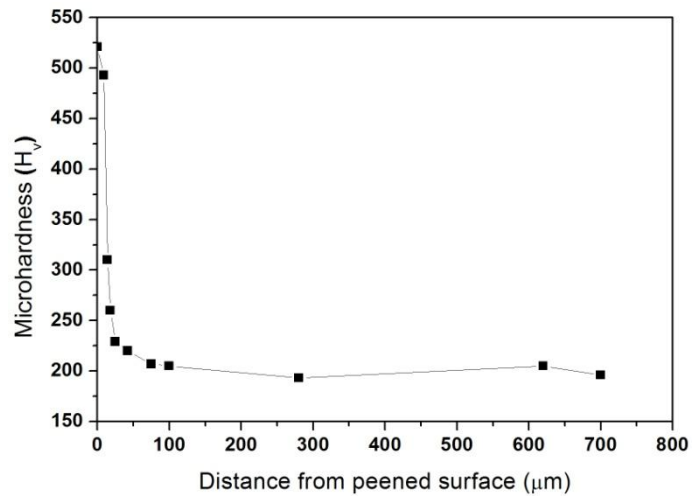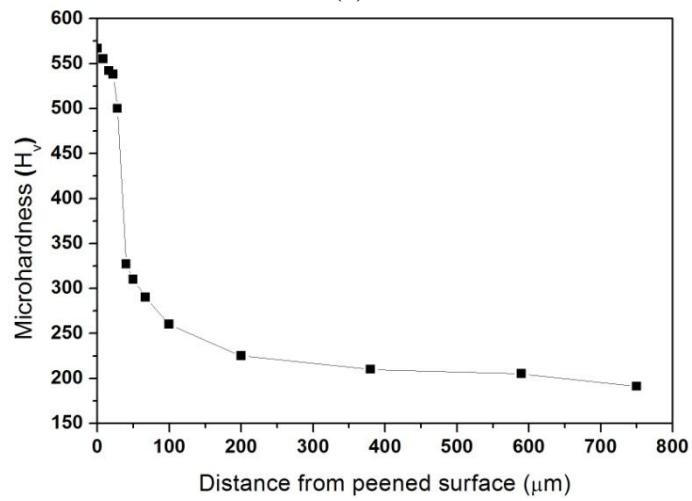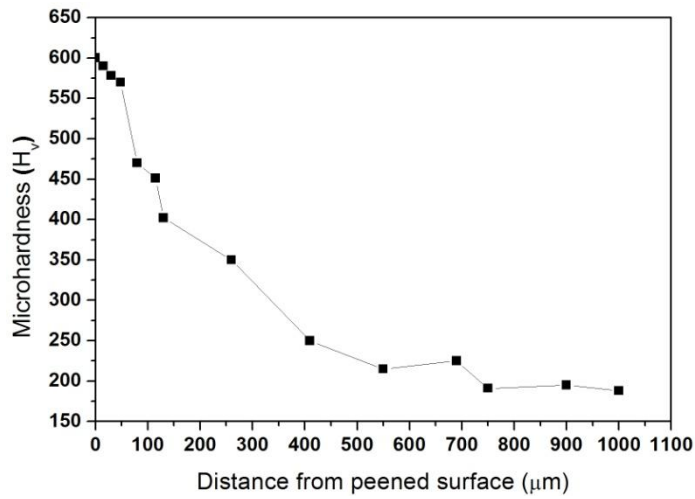
Fig. 4.41 Variation of microhardness data of the nitrided samples subjected to peening pre-treatment at (a) 100%, (b) 500% and (c) 1000% coverage, respectively

4.8.2 Scratch hardness results

SEM micrographs of the base metal, shot peened and nitrided samples after scratch test are shown in Fig. 4.42.

(a)

(b)

(c)

(d)

(e)

(f)

(g)

(h)

(i)

(j)

(k)

(l)

(m)

(n)

(o)

(p)

(q)
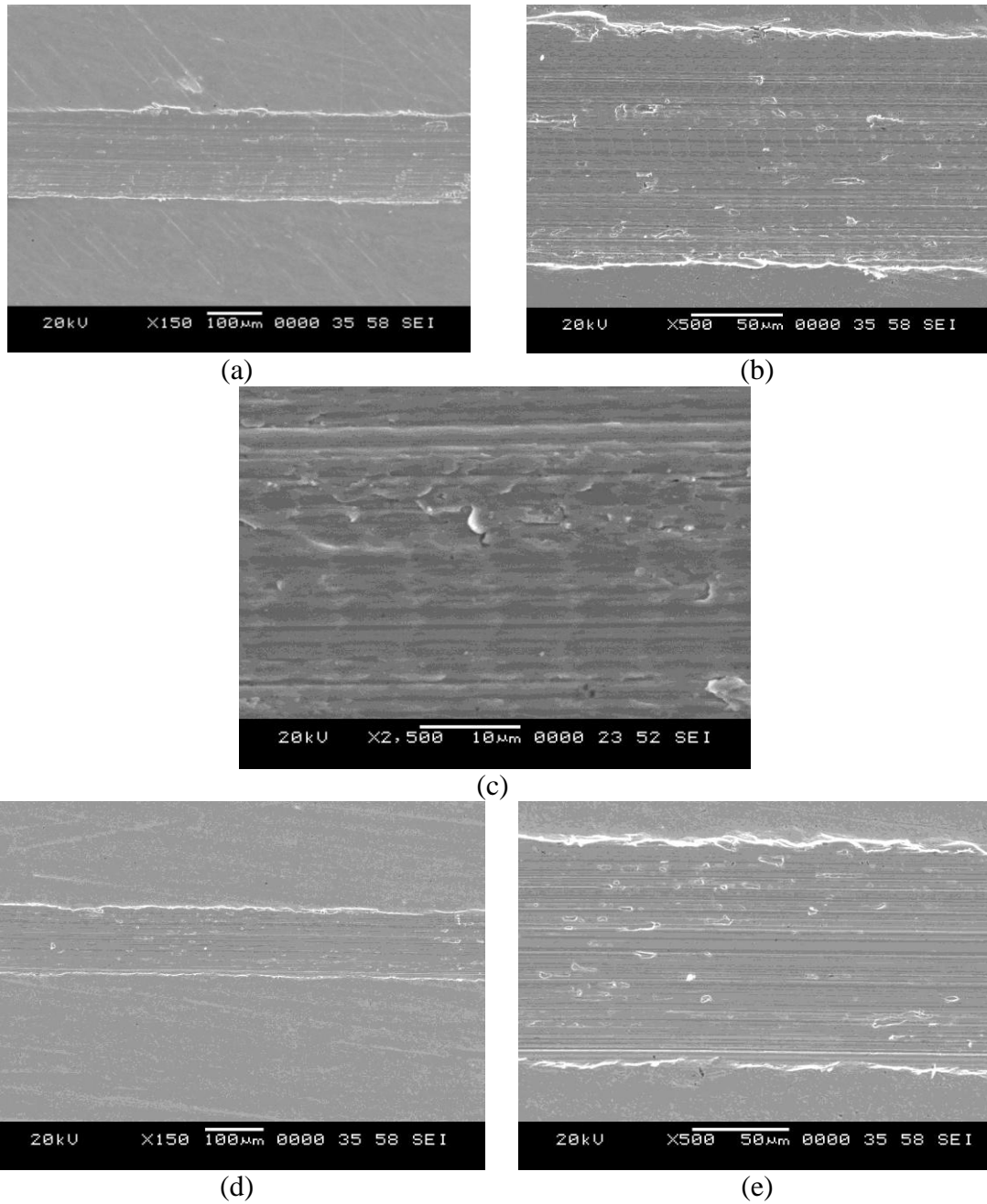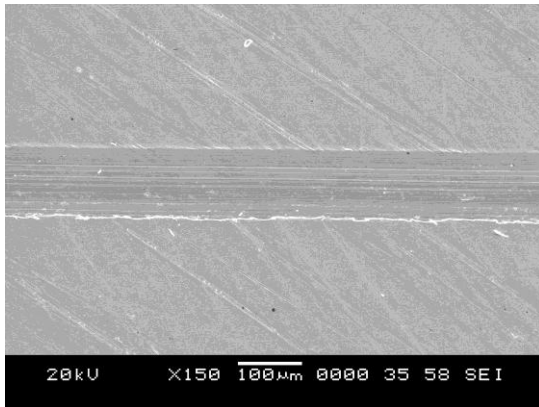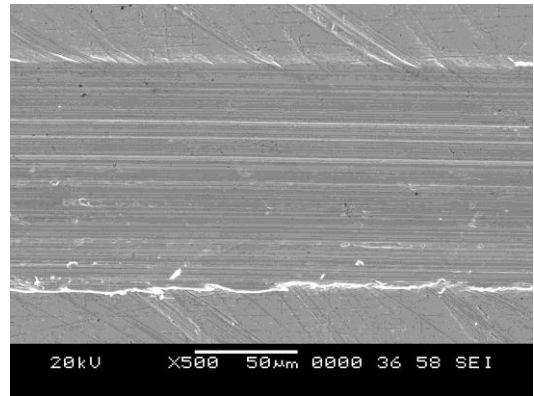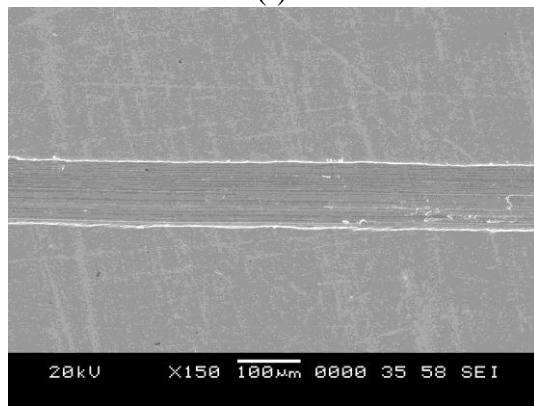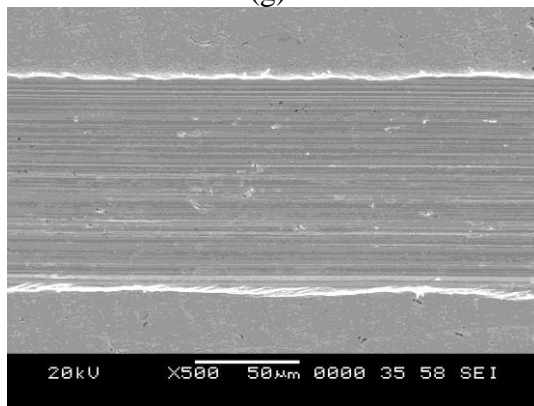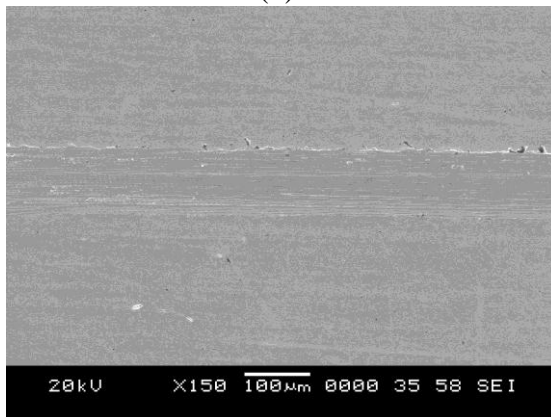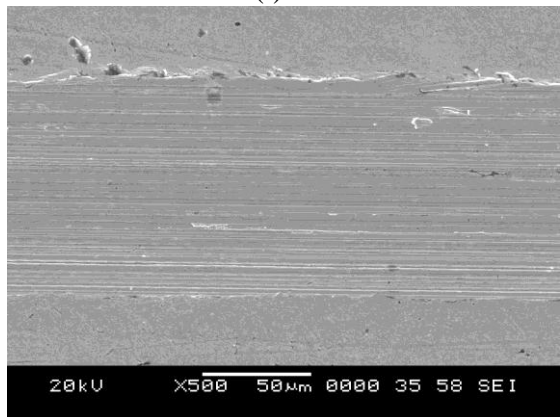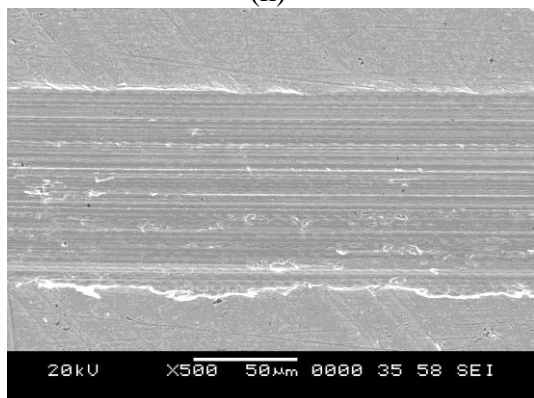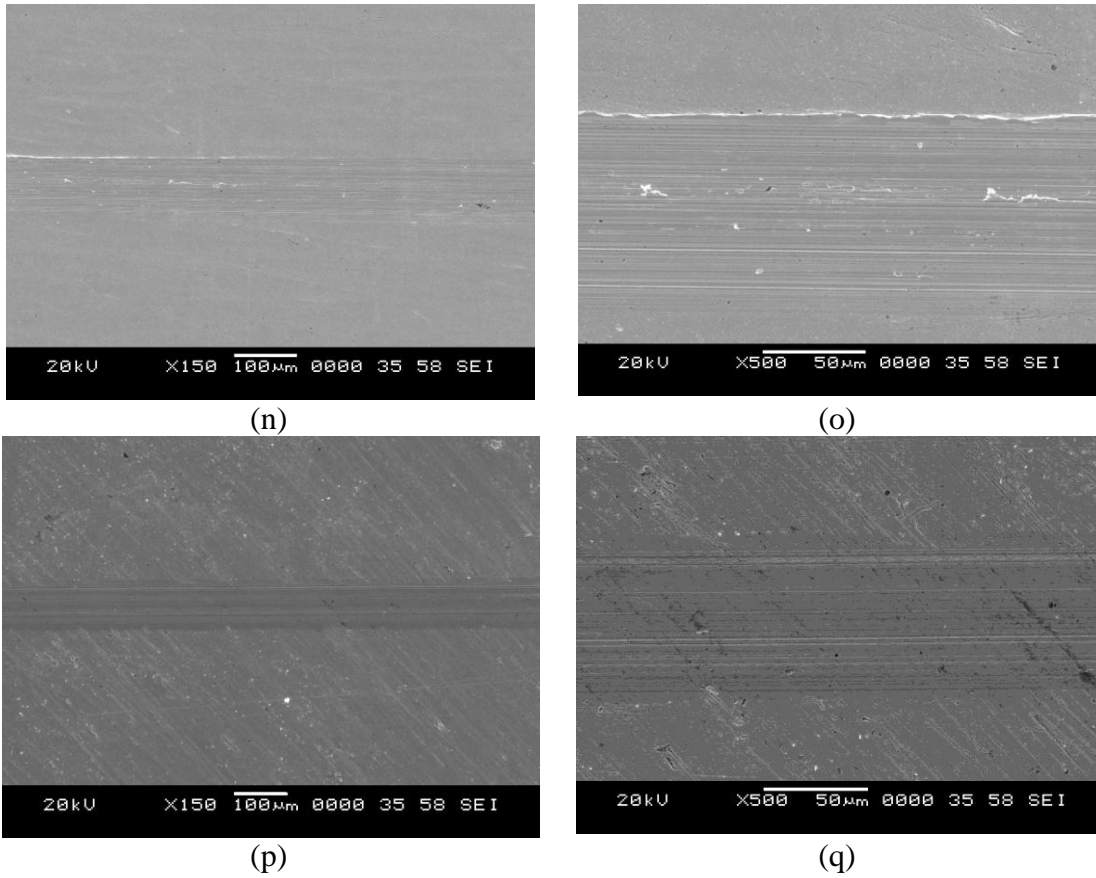
Fig. 4.42 SEM micrographs of the (a-c) base metal (d,e) unpeened-nitrided (f,g) conventional peened (h,i) intermediate peened, (j,k) severe peened, (l,m) conventional peened-nitrided, (n,o) intermediate peened-nitrided and (p,q) severe peened-nitrided samples nitrided at 400 °C for 4 hours; after scratch test at different magnifications

Scratch width is maximum for the base metal which possesses minimum microhardness at surface amongst all the samples under consideration. Material pile up is observed along the edges of the scratch track. Clear indications of the plastic flow are observed in the high magnification SEM micrograph in Fig. 4.42(c). Scratch width is minimum for the severe peened-nitrided sample. Also, there is no observable material pile-up at either side of the scratch track indicating that material in front of the scratch indenter is removed in brittle manner. Scratch width is measured using these micrographs at multiple locations and average scratch width is reported. The scratch hardness (H_s) is calculated using the formula $H_s = \frac{8F_N}{\pi b^2}$ (Beegan et al., 2007); where F_N is the normal force and b is the average scratch width. The results are summarized in Table 4.1.

Table 4.1 Results of scratch test on the base metal and the treated samples

Sample	Coverage	Scratch width (µm)	Scratch hardness (GPa)
Base metal	-	158.59	2.03
Nitrided	-	117.02	3.71
Peened	100%	105.43	4.57
	500%	103.94	4.702
	1000%	101.61	4.92
Peened and nitrided	100%	98.64	5.22
	500%	94.97	5.63
	1000%	92.16	5.98

It could be observed from Table 4.1 that the scratch hardness data of the various samples are following the trend of microhardness data. Base material is having scratch hardness of 2.03 GPa which is enhanced to 5.98 GPa in severe peened − nitrided sample. Both, in peened and nitrided samples, increasing peening coverage is found to increase the scratch hardness.

4.8.3 Nanoindentation study

In order to understand surface mechanical properties at the nano-scale regime, nanoindentation, nano-scratch and nano-scale wear tests are carried out on the base metal, severe peened samples and severe peened-nitrided samples. Load-displacement curves generated during the nanoindentation test are depicted in Fig. 4.43. Displacement at maximum load for base, severe peened and peened-nitrided samples are observed to be 2342.3, 1659.7 and 1304.6 nm, respectively.
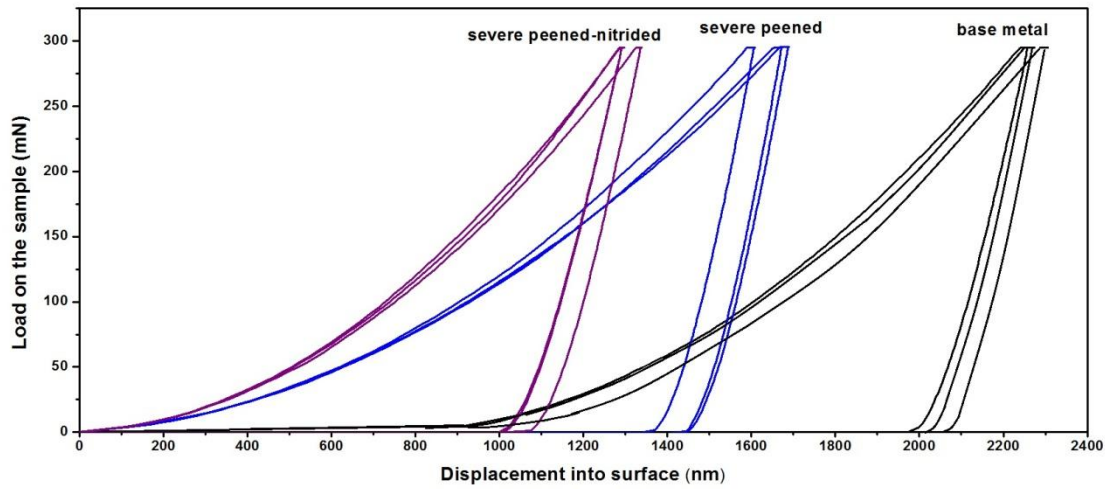
Fig. 4.43 Load-displacement curves of the base metal, severe peened and peened-nitrided sample

Hardness values obtained from the test using the Oliver – Pharr method are depicted in Fig. 4.44. It could be observed that hardness increases from 2.36 GPa for the un-peened base metal to 8.73 GPa for the severe peened-nitrided sample.
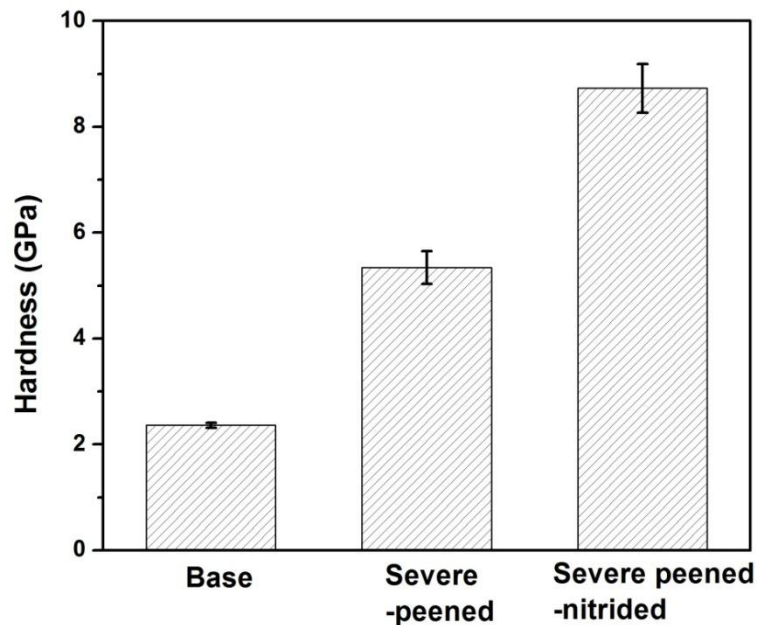
Fig. 4.44 Hardness of the base metal, severe-peened and severe peened-nitrided samples obtained from the nanoindentation test

4.8.4 Nano-scale scratch test results

Results of nano-scratch test on the base metal, the severe-peened and the peened-nitrided samples are given in Fig. 4.45. Depth of the scratch as a function of scratch

distance is plotted. Pre-scratch scan of all the three samples show that the surfaces are relatively flat. Drastic increase in the scratch depth with increasing load is observed in the base metal compared to the peened and the nitrided samples. This indicates the increased resistance offered by the peened and the nitrided layer to increasing scratch load. Base metal was found to experience the highest scratch depth of about 10800 nm for the maximum scratch load. In contrast, the severe peened sample and the peened-nitrided sample experienced about 8060 nm and 2030 nm scratch depth, respectively, at the maximum scratch load.

(a)

(b)

(c)
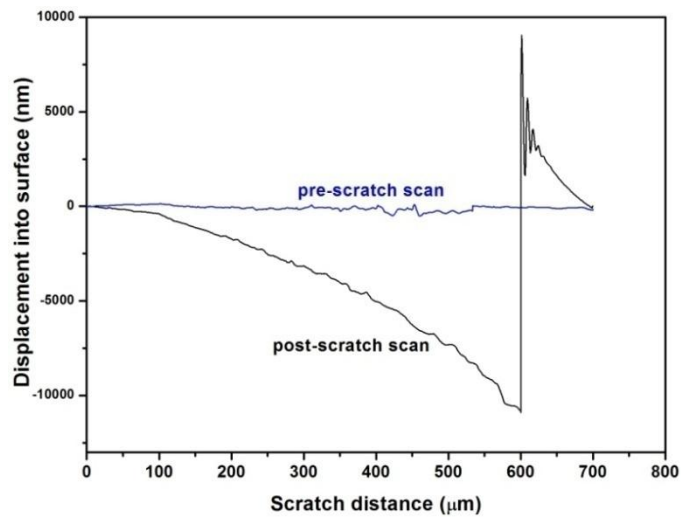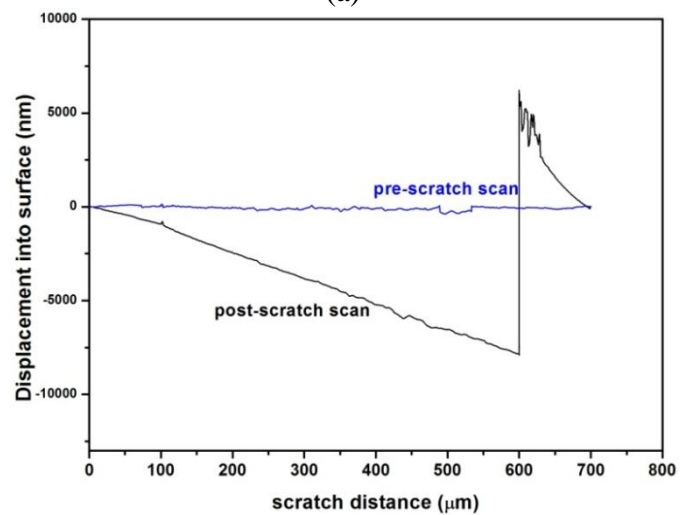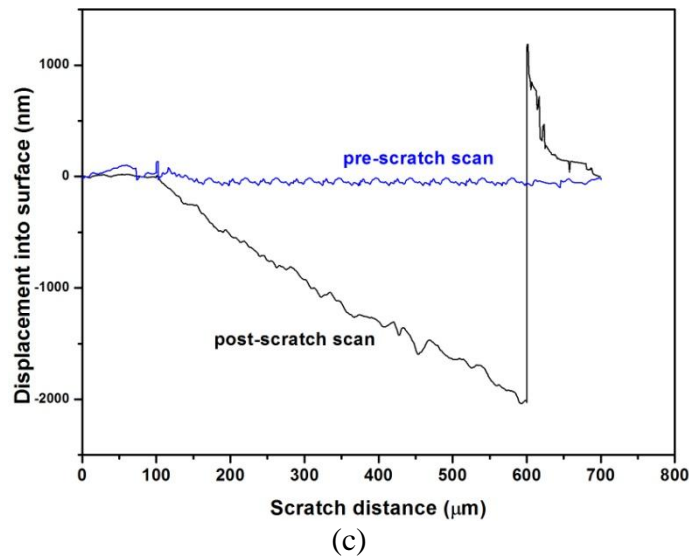
Fig. 4.45 Nano-scratch test data of (a) the base material (b) the severe peened sample and (c) the severe peened-nitrided sample, respectively

4.8.5 Nano-scale wear behavior

Results of the nano-scale wear test from the base metal, the severe-peened and the peened-nitrided samples are given in Fig. 4.46. For all the three samples, the data of displacement into the surface as a function of the scratch distance is given after 10, 20 and 30 scratches. For reference, surface profile before the wear test is also included. It could be observed that all the samples show increase in wear track depth with increase in the number of cycles. However, the highest resistance to wear is offered by severe peened-nitrided sample; while un-peened base material shows the lowest resistance. This shows that the duplex treatment comprising of severe peening and plasma nitriding successfully improves the wear resistance of the un-treated 316L stainless steel.

(a)

(b)

(c)
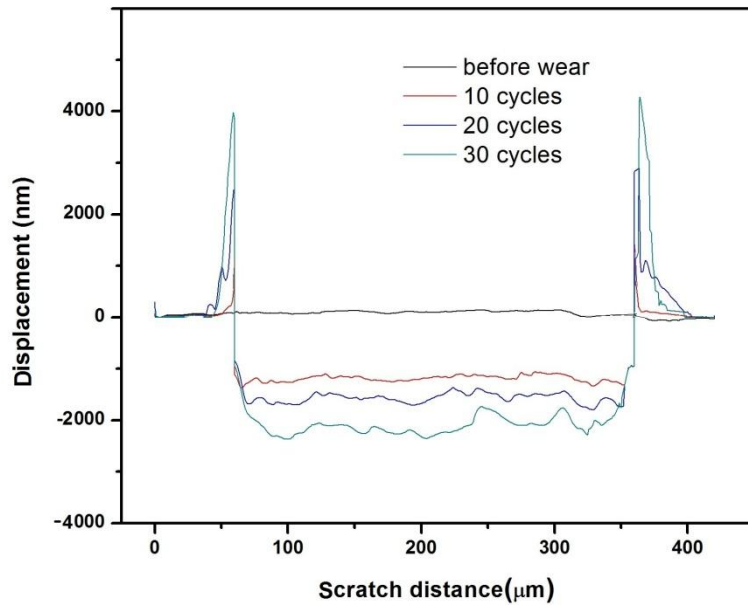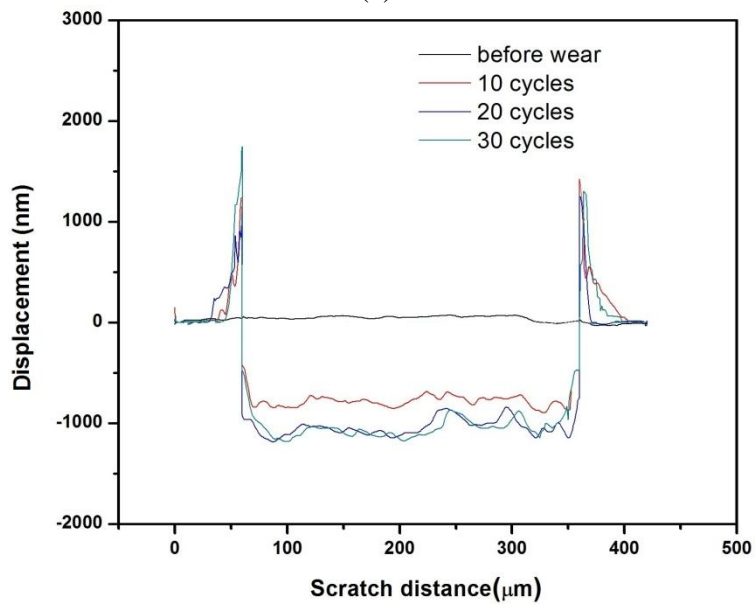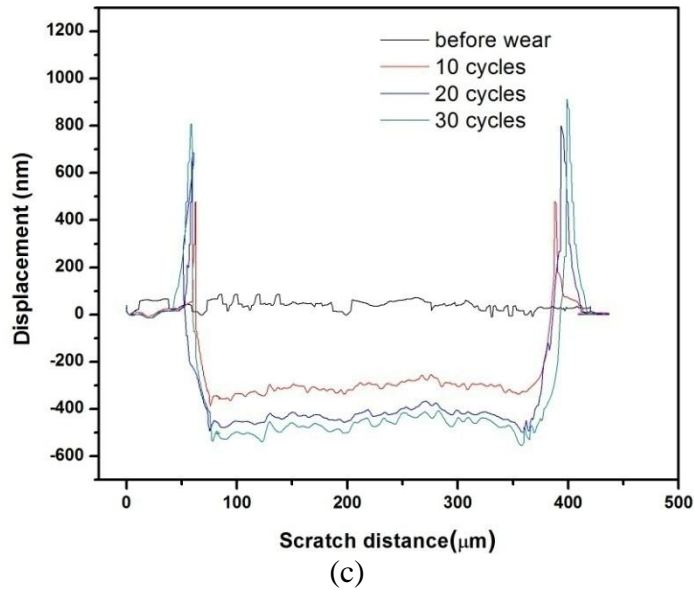
Fig. 4.46 Nano-scale wear test data of (a) the base material (b) the severe-peened sample and (c) the severe peened-nitrided sample

4.9 Summary

It is inferred from the results presented in this chapter that shot peening treatment could be successfully used as a pre-treatment step to plasma nitriding in order to achieve thicker nitride layer at shorter nitriding duration. Shot peening severity increases with increasing peening coverage, which in turn, enhance the depth of the deformed layer affected by the peening process. Plasma nitriding in the temperature range of 300-500 ℃ suggests that nitriding temperature of 400 ℃ results in significantly higher case depth for severe peened sample without precipitation of the deleterious chromium nitride phase. Detailed microstructural characterization of the shot peened samples provided insights about the nanocrystallization process and martensite nucleation; while it suggests that the nitride layer is mainly martensitic in nature in the case of the severe peened-nitrided sample. Mechanical characterization affirms the improvement in the surface mechanical properties, like, hardness, scratch hardness, wear resistance upon shot peeneing- plasma nitriding duplex treatment.

CHAPTER 5

DISCUSSION

This chapter discusses the concepts related to the results elaborated in the chapter 4. Concepts related to the nanocrystallization of the severe peened surface, deformation induced martensitic transformation, microstructural evolution during peening as well as nitriding, mechanical properties of the duplex treated surface; relevant to present study, are discussed.

5.1 Austenitic stainless steel

The austenitic stainless steels are an important class of stainless steels used in a wide verity of applications owing to distinctive properties, like, corrosion resistance, good weldability, high rate of work hardening, etc. Microstructure of the austenitic stainless steels consists of the austenite phase; having FCC crystal structure. 300-series austenitic SS grades are widely popular amongst various fields of application. Chromium and nickel are the major alloying elements in these grades.

Chromium imparts the "stainless" property; wherein a thin layer of the adherent impervious chromium oxide will be formed on the surface of the steel which provides superior corrosion resistance. However, chromium being a ferritic stabilizer, nickel is added to the alloy to stabilize the austenite phase at room temperature. Another alloying element carbon provides significant solid solution strengthening effect by being an interstitial alloying element. It also stabilizes the austenite phase. However, presence of carbon increases the tendency of the chromium carbide precipitation at high temperatures. This impairs the corrosion resistance of the alloy and this phenomenon is called sensitization (Devine, T. M. 1990). Hence, steel will be alloyed with elements, like, Mo, Nb, etc. These elements are strong carbide formers and addition of these will assist in overcoming the problem of sensitization. Thus, the austenitic steel grades produced are stabilized grades. In particular, the alloy under

consideration, AISI 316L grade contains 2.03% molybdenum. Composition of this grade is given in Table 3.1.

Austenite stainless steels are characterized by relatively low stacking fault energy; in the range 18- 45 mJ/m^2 (Lo et al. 2009). The magnitude of stacking fault energy is dependent on the composition of the steel. It has profound effect on the deformation behavior of the alloy. It is well known that the austenitic stainless steels are strengthened by cold working. Hence the stacking fault energy has a significant role in strengthening of the austenitic stainless steel grades. Schramm and Reed (1975) formula is used for estimating the stacking fault energy of the stainless steels in mJ/m^2. It is given by,

$$SFE = -53 + 6.2(\%Ni) + 0.7(\%Cr) + 3.2(\%Mn) + 9.3(\%Mo) + 12.4(\%Cu)$$

The calculated stacking fault energy of the 316 stainless steel used in present work is 54.75 mJ/m^2. It is slightly higher than the stacking fault energy of the 304 grade stainless steel due to the presence of molybdenum in the alloy.

5.2 Nanocrystallization through the shot peening technique

Process of air-blast shot peening involves bombarding the surface of the component with shots of pre-determined size and hardness, forced through the high velocity air jet from a nozzle. These shots reach the surface of the components to be shot peened and make repeated multidirectional high velocity impacts on the sample surface. This results in dimples on the metal surface as observed in Fig. 4.3. Each impact will amount to a finite amount of localized plastic deformation. Figure 5.1 depicts a schematic diagram of the impact of a shot on the sample surface.
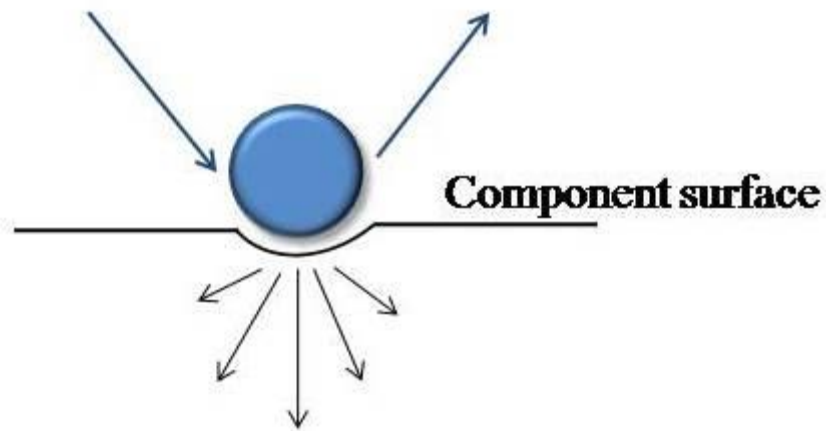
Figure 5.1 Schematic diagram of the impact of a shot on the sample surface

The plastic strain generated by the peening process is accommodated through the generation, accumulation and re-arrangement of dislocations, mechanical twins and point defects in the matrix. Additionally, it is also accommodated through the martensitic phase transformation as in the present case. A finite fraction of the point defects and dislocations get annihilated upon recombination. However, major fraction of the dislocations undergoes rearrangement to form dislocation cells. Thus, the initial grains are subdivided into a large number of sub-grains (or domains). These are separated by small angle grain boundaries. With further strain, the misorientation angles of these boundaries gradually increase to become high-angle grain boundaries. This process generates a large amount of finer grains; leading to surface nanocrystallization (Murr and Esquivel 2004, Tao and Lu 2009). It is advocated in the literature (Zhang et al. 2003, Tao and Lu 2009) that, with increase in the plastic strain, nanocrystallization is favoured in order to minimize the total energy of the system.

It is known that the degree of plastic strain is an important factor which decides the effects of shot peening on the sample. With increased coverage of peening, amount of plastic strain increases. Amount of plastic strain generated during the shot peening treatment was assessed in the study of Hassani Gangaraj et al. (2015) through numerical simulation. Shot velocity of 65 m/s, shot radius of 0.3 mm, and shot hardness of 48 HRC were used for peening. The study was conducted over a wide range of coverage from 100% to 1500%. The results of this study are relevant to the present discussion as the process parameters closely match with those used in the

present study (Elaborated in section 3.2). It was observed in the study that the average surface plastic strain after conventional shot peening with 100% coverage is around 0.5. In contrast, the average surface plastic strain after severe shot peening with 1000% coverage was increased to 7-8. This was found sufficient to bring about surface nanocrystallization. Thus, it could be concluded that higher the coverage, more is the level of the plastic strain. This is the reason for moving from conventional peening to severe shot peening for producing nanostructured surface.

In the present study, it is observed in Fig. 4.5 that depth of the deformed layer increases on increasing peening coverage. TEM study of the peened surface indicated that, upon conventional peening, the coarse austenite grains of the parent metal seen in Fig. 4.8 have found to possess deformation features, like shearbands, dislocations, etc. (as observed in Fig. 4.9 and 4.10). However, nanocrystallization is not evident. When the peening coverage is 1000%, TEM micrograph in Fig. 4.13 in section 4.3.3 clearly depicts dislocation cells in the cell size range of about 40-100 nm on the surface of the severe peened sample. This suggests that, in the present study, process parameters corresponding to severe peening have resulted in an average plastic strain of more than 7-8 and hence, lead to nanocrystallization of the surface.

5.3 Deformation induced martensitic transformation

Deformation induced martensitic transformation has significant influence on mechanical properties of the austenitic stainless steels. Transformation imparts higher degree of strain hardening during forming operations. It also significantly enhances the strength, hardness and wear resistance of the material. Also, reversion of deformation induced martensite is viewed as a technique to obtain ultra-fine grained austenitic stainless steel (Misra et al. 2010). Hence it is important to study the deformation induced martensitic transformation; under severe surface deformation condition encountered during the peening process.

During the deformation induced transformation, austenite phase having FCC crystal structure may directly transform to α' martensite (having BCC crystal structure) or it may transform through the intermediate ε-martensite phase (having HCP crystal structure). The transformation sequence depends on the composition and stacking

fault energy of the steel, austenite stability, temperature, strain rate, amount of strain, state of stress during deformation (Tian et al. 2017).

In the present study, upon shot peening, deformation induced transformation of the austenite phase to the martensite found to take place, with martensite fraction increasing with increasing peening coverage. Fraction of martensite as a function of peening coverage is shown in Fig. 5.2.
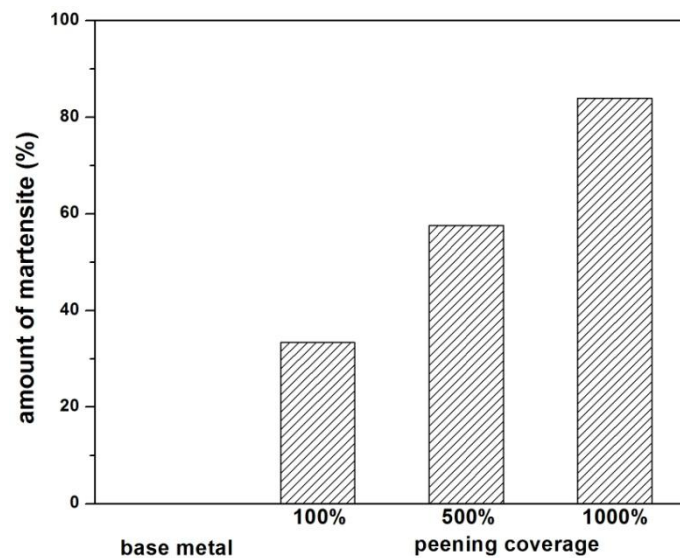
Fig. 5.2 Variation of the relative amount of martensite as a function of peening coverage

Austenite was found to transform directly to α' martensite without any indication of the ε-martensite phase (as in XRD) as seen in Fig. 4.6. Detailed TEM study in section 4.3 and 4.4 also affirms that the ε-martensite phase is not observed during the study. These results are in accordance with the results obtained by Brooks et al. 1979; Shrinivas et al. 1995; Talonen and Hänninen 2007 where α' martensite is directly formed during the deformation of the austenitic stainless steel.

5.3.1 Stress assisted and strain induced martensitic transformation

Martensite formed during deformation of the austenitic steel is termed as the 'deformation induced martensite'. This term is merely used to differentiate the martensite from that formed during the quenching treatment; without any specific reference about role of the stress or the strain that is responsible for the phase transformation. However, there are two types of deformation induced martensite;

97

namely, the stress assisted martensite and the strain induced martensite as explained by Maxwell et al. (1974) and Olson et al. (1975).

During deformation, applied stress results in martensitic transformation when the amount of stress in the specimen provides the reduction in the driving force required for the austenite phase to transform into the martensite phase. Martensite thus formed is termed as *stress-assisted* martensite. It is observed that such martensite transforms through the nucleation and growth process which results in the transformation of the unstressed and the unstrained austenite during quenching heat treatment. In contrast, the *strain-induced* martensite forms as a direct consequence of plastic deformation of the austenite phase. The microstructural features that are originated during the plastic deformation serve as nucleation sites for nucleation of the strain induced transformation.

However, it should be noted that the studies by Perdahcioglu et al. (2008) and Das et al. (2008) have suggested that all deformation induced martensite could be viewed as stress-assisted. Perdahcioglu et al. (2008) opine that the major effect of deformation on the austenitic matrix is the additional mechanical driving force that triggers the martensitic phase transformation. The strain resulting from the deformation produces deformation features in the austenite matrix; which act as potential nucleation sites. However, it is suggested that providing additional mechanical driving force has governing effect on transformation. This hypothesis is affirmed by the mathematical modeling work of Das et al. (2008). It suggests that majority of the published work correlating the plastic strain and the martensitic transformation could be re-visited by considering the thermodynamic effect of applied stress on transformation.

In majority of the literature related to peening of the austenitic stainless steels, the martensitic transformation is said to be strain induced (Bagherifard et al. 2016, Zhang et al. 2003, Shen et al. 2008, Baluswamy et al. 2013). However, in the present study, the term 'deformation induced martensite' is used throughout the thesis as it is not possible to distinguish whether martensite is formed due to mechanical driving force provided by the peening process (stress-assisted) or whether the generation of the defects during deformation helps in heterogeneous nucleation of the martensite

(strain-induced); in the context of the present work. Hence, it is relevant to use the term deformation induced martensite (DIM).

5.3.2 DIM formation

M_s is the martensite start temperature below which martensite forms spontaneously from the quenched austenite. Chemical driving force is high enough to induce the phase transformation without any deformation below this temperature. Eichelmann and Hull's empirical relation (Eichelmen and Hull 1953) given below is commonly used to predict the M_s temperature from the chemical composition.

$$Ms = 1320 - 61(\%Ni) - 42(\%Cr) - 33(\%Mn) - 28(\%Si) - 1667(\%C + N)$$

The estimated M_s temperature for 316L stainless steel is -90 °C. However, deformation induced martensitic transformation could take place at the ambient temperature with the aid of mechanical work. Martensite formation temperature upon deformation (M_d) is estimated using the relation as given by Angel (1954). Martensitic transformation takes place readily, when austenite is deformed below M_d.

$$Md\left(\frac{30}{50}\right) = 413 - 462(\%C + N) - 9.2(\%Si) - 9.5(\%Ni) - 13.7(\%Cr)$$
$$- 8.1(\%Mn) - 18.5(\%Mo)$$

Where, $Md\left(\frac{30}{50}\right)$ is the temperature at which 50 volume percentage of martensite is formed during deformation at a true tensile strain of 0.3. Calculated value of $Md\left(\frac{30}{50}\right)$ is 28.53 °C for 316SS. It is close to ambient temperature at which shot peening is carried out. But it should also be remembered that, during shot peening the temperature rises locally due to continuous impact of shots; though the peening treatment is carried out at room temperature,. However, in the present study, considerable amount of deformation induced martensite is formed at different peening coverages; as observed from Fig. 5.2. TEM observations in section 4.3 also indicate that the top surface of intermediate peened sample (in Fig. 4.12 and 4.13) and severe peened sample (in Fig. 4.14) consists of only the martensite phase. With reference to

the work of Murr et al. (1982), formation of the martensite in the present case is opined to be attributed to high strain rate encountered during the peening treatment.

5.3.3 Nucleation of DIM

Literature suggests that the formation, morphology and mechanical properties of the deformation induced martensite in austenitic stainless steels are studied by several researchers. However, limited literature is available on the mechanisms of nucleation and growth of the martensite. This is primarily due to the finer dimensions the martensite nucleus and rapid kinetics of the martensitic transformation. Specifically, mechanism of nucleation of deformation induced martensite is still a matter of debate amongst researchers.

It is largely advocated (Lecroise and Pineau 1972; Olson 1972; Zhang et al. 2003) that the deformation induced martensite nucleates solely at shear band intersections during plastic deformation. In contrast, few researchers (Das et al. 2008, Gey et al. 2005) have reported that the shear band intersections are merely the preferential sites for the martensite nucleation. However, it is reported (Shrinivas et al. 1995) that any appropriate defect structure could serve as nucleation site for the martensite nucleation. Through the in-situ TEM observations, Brooks et al. (Brooks et al. 1979) have shown that the martensite always nucleates from the favourable dislocation configurations generated by the stress associated with the transformation. These observations affirm that the nucleation of DIM is not restricted to the shear band intersections. Also, there are reports in the literature (Das et al. 2008; Gussev et al. 2013) depicting the nucleation of DIM at grain boundaries, triple junction and shear band-grain boundary intersections. It is also reported that the martensite could form parallel to shear bands (Murr et al. 1982).

In spite of the above mentioned observations by various researchers, amongst majority of the literature (Zhang et al. 2003, Baluswamy et al. 2013, Lin et al. 2006) related to the mechanism of nanocrystallization in the austenitic stainless steels upon severe peening, DIM nucleation is reported to be restricted to shear band intersections. However, it is interesting to observe that in the present study, martensite

is nucleated at multiple locations in the austenite matrix as observed in TEM micrographs presented in section 4.4.2.1. Martensite is found to nucleate at shear band intersections (in Fig. 4.18) parallel to isolated shear bands (in Fig. 4.21), within the shear band (in Fig. 4.22), across the shear band (in Fig. 4.23), at grain boundaries (in Fig. 4.24) and parallel to multiple nano-scale shear bands (in Fig. 4.25) in the matrix. These observations suggest that shear band intersections are not the sole locations for the martensite nucleation.

5.3.4 Growth of the deformation induced martensite

Limited literature addresses the growth of the deformation induced martensite. Based on the detailed transmission electron microscopy observations, Murr et al. (1982) have shown that growth of the martensite units occur due to the coalescence of the martensite embryos formed at the shearband intersections. This phenomenon results in the formation of long martensite units resembling the lath morphology. It is also justified by the work of Lee et al. (2002) that growth of the long martensite laths continue until a barrier for the growth is encountered. Growth of the martensite lath is clearly identified through TEM study in the transition region of the GNS of severe peened sample as in Fig. 4.19. This observation justifies the presence of lath martensite in the top surface of the intermediate peened sample (in Fig. 4.12(a)) and in the sub-surface region of the severe peened sample (in Fig. 4.26(a)).

It is interesting to observe that continuous layer of the lath martensite exists at a depth of about 10-15 μm below the top surface (in Fig. 4.26(a)); while dislocation cell type martensite in the top most surface (in Fig. 4.26(a)). Similar DIM morphologies are observed in the study of Misra et al. (2010). In the study, AISI 301 steel was subjected to cold rolling with increasing percentage of reduction and morphologies of deformation induced martensite were studied. It was observed that, with increase in reduction, the lath martensite morphology was changed to dislocation cell-type morphology. Based on these observations, transformation of the lath martensite to the dislocation cell-type martensite is explained though the schematic diagram in Fig. 5.3.
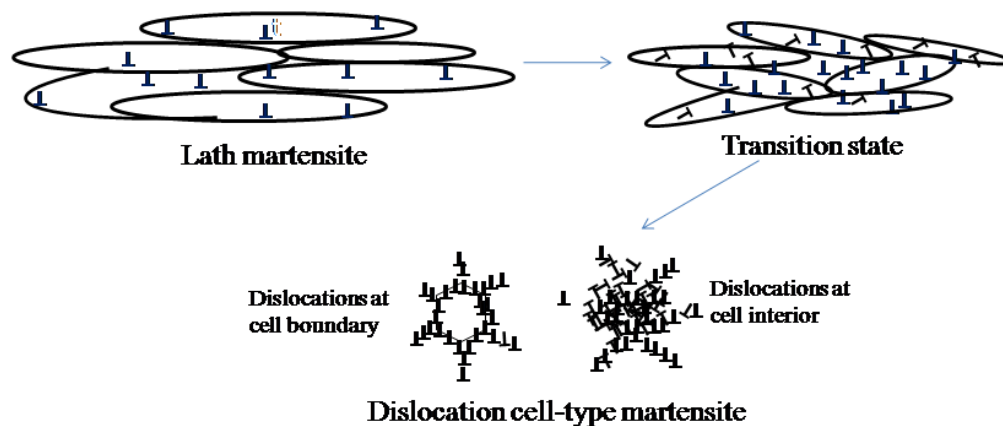
Fig. 5.3 Schematic diagram showing transition from the lath martensite to dislocation cell type martensite

Shot peening is a surface deformation technique and hence, maximum strain and strain rate are experienced by the top surface due to direct impact of the shots on the surface. At a depth more than about 500 μm from the surface, un-affected base metal consists of coarse grains which are typical of hot rolled microstructure of the austenitic stainless steels (Fig. 4.16). Upon sufficient degree of deformation, martensite transformation occurs through the nucleation and growth processes explained in the present section. This results in the lath martensite structure schematically represented in Fig. 5.3. As the sample is further deformed, width of the martensite laths decrease due to the continuous breaking up of the lath structure. This results in the crystallographic distortion and drastic increase in the dislocation density. These dislocations rearrange to give rise to blocky martensite structure. However, it is also speculated (Shrinivas et al. 1995) that the lath boundaries become unstable after growing to a critical dimension resulting in change of morphology from the lath-type to the blocky-type; under the strain during peening.

5.4 Microstructural evolution and surface nanocrystallization upon severe shot peening

Severe peening techniques, like air blast shot peening, ultrasonic peening, laser peening, etc. are widely used to increase hardness and wear resistance of the surface of the components. Specific to the austenitic stainless steels; deformation induced martensitic transformation takes place in addition to grain refinement upon severe peening. Hence, study of microstructural evolution and mechanism of

nanocrystallization are relatively complex in these classes of alloys. Different observations are made by various researchers on microstructural changes occurring during severe peening of the austenitic steels.

During ultrasonic peening of the 316L SS, Liu et al. (2000) observed that dislocation activity driven by intense localized stress is responsible for the grain refinement through the subgrain formation. It was supported by the work of Chen et al. (2011); in which ultrasonic peening of the 304 SS at strain rate below 10^3 s^{-1} was studied. Detailed microstructural investigation of the 304 SS subjected to SMAT was carried out by Zhang et al. (2003) through electron microscopy technique. It was inferred that the twin-twin intersections repeatedly sub-divide the austenite grains and also act as nucleation sites for the martensitic transformation. Closer to the surface, intersecting twins become finer in dimension leading to the formation of the nano-sized martensite crystallites having random orientations.

Lu et al. (2010) suggested that during laser shock peening of the 304 SS, grain sub-division by deformation twinning and continuous dynamic recrystallization (DRX) is responsible for nanocrystallization. Deformation induced martensite (DIM) formation was not directly observed in the study. However, Zhou et al. (2016) opine that the mechanical twins as well as the DIMs are equally responsible for grain refinement process during laser shock peening of the 304 SS. Bhagerifard et al. (2016) studied severe shot peening of the 316L SS and observed that, upon peening, the layers of DIM gets embedded in the austenite matrix. Defect density was observed to decrease due to dynamic annealing and DRX. Recent report by Bahl et al. (2017) suggested that microbands and shear bands are formed during the SMAT of 316L SS. Deformation twinning and DRX within the shear bands are responsible for nanocrystallization.

A schematic diagram of the microstructural evolution during the present study is depicted in Fig. 5.4. Figure 5.4 (a) represents the different regions of the gradient nanostructured surface layer while Fig. 5.4 (b) depicts the schematics of the microstructural evolution in GNS. During severe shot peening, the strain and strain rate experienced at the surface is markedly high and ceases as the depth from the

surface increases. Depth affected by the peening process depends on the severity of peening and the material characteristics. It could be observed from section 4.4.3 that about 500 μm of the sample from the peened surface consists of gradient in nano-structured deformation features. At a depth of 500 μm, where effect of deformation is minimal, shear bands are found in the microstructure. Moving towards the peened surface, multiple sets of shear bands will emerge. With increase in strain, the intersection of multidirectional twins takes place leading to formation of the rhombic blocks (in Fig. 4.17). These intersections repeatedly subdivide the original coarse austenite grains to finer dimensions.

(a)

(b)
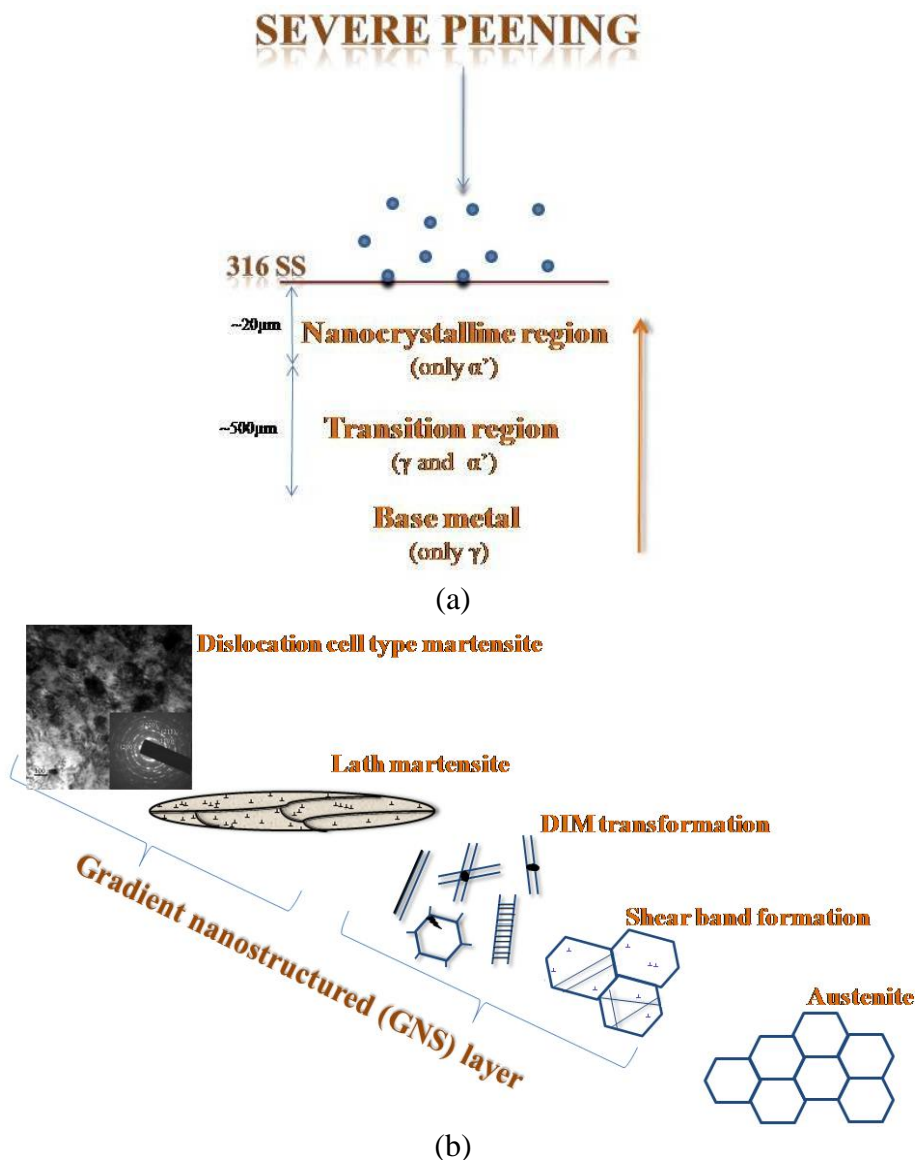
Fig. 5.4 Schematic diagrams depicting (a) different regions of the gradient nanostructured surface layer and (b) microstructural evolution in GNS

Martensite units are found to nucleate at multiple locations in the austenite matrix from a depth of about 20 μm to a depth of about 500 μm from the peened surface. These include, locations like parallel to shear band, inside the shear band, across the shear band, near the grain boundaries, etc. These martensite units grow by coalescence into laths which is the dominant morphology of the deformation induced martensite in the austenitic stainless steels (Murr et al. 1982).

Well-developed, complete layer of the lath martensite is observed at a depth of about 20 μm from the peened surface. Formation of a continuous layer of lath martensite is not observed in the previous reports on severe peening; although it is reported in austenitic steels deformed by bulk deformation techniques, like tension deformation, rolling, etc. Within a depth of about 20 μm from the surface, continuous layer of the lath structure is broken and refinement of the lath packets takes place; thus leading to the formation of the dislocation cell-type martensite (Misra et al. 2010).

To summarize, in the present study, severe shot peening generates about 500 μm thick gradient nanostructured (GNS) layer from the peened surface; refining the hot-rolled parent austenitic microstructure having grain size in the range of 40–80 μm to dislocation cell- type deformation induced martensitic structure having cell size in the range of 100–140 nm.

The gradient nanostructure (GNS) is considered to be a unique architecture in which a transition layer with graded grain size is sandwiched between a hard, wear resistant nano-scale grain structure on one side and ductile substrate having coarse grain structure on the other side. This configuration of varying grain size offers advantage of tailoring the properties of the materials. Also, these structures help in harvesting the beneficial properties (like high hardness, improved wear resistance, etc) of the ultra fine grained structure compared to their coarse grained counterparts. Gradient nanostructures also predicted to possess obvious beneficial effects during diffusion based surface modification processes.

5.5 Microstructure evolution upon plasma nitriding

This section briefs the nitride phase formation in unpeened and peened samples after 4 hours of plasma nitriding at 400 ℃. It is observed that the nitride phase/phases formed during nitriding and conventionally peened samples are similar; while those formed during intermediate and severe peened samples are similar. Hence they are discussed separately in the following sub-sections.

5.5.1 Nitriding of the un-peened and conventionally peened samples

It could be observed from Fig. 4.34 that the un-peened sample and sample peened with 100% coverage indicate the formation of the expanded austenite phase upon nitriding. It is the solid solution of nitrogen in the austenite; which is also commonly called as S-phase. It is reported to be formed by many researchers during the low temperature plasma nitriding of the austenitic stainless steels (Fewell et al. 2000) (Li et al. 2012) (Gontijo et al. 2006).

Zhang and Bell (1985) reported for the first time about the expanded austenite phase on the surface layer of the 316 SS upon low temperature plasma nitriding treatment. It is found to possess high hardness and good corrosion resistance. It is termed as S-phase by Ichii et al (1986). It is also referred to as metastable supersaturated austenite or γ_N phase. It is observed in several grades of the austenitic steel upon nitriding (Fewel et al. 2000).

Since austenite has a FCC structure, it is widely accepted (Ichii et al. 1986, Zhang and Bell 1985, Mingolo et al. 2006, Sun and Bell 1999) that the S-phase also exhibits FCC structure. Nitrogen occupies the octahedral voids in the lattice of the austenite resulting in expansion of the austenite lattice. It is observed that the positions of diffraction peaks shift in a systematic manner from the ideal FCC lattice. This has made Menthe et al. (1995) to opine that the S-phase has a tetragonal structure. However, it should be kept in mind that nitriding process involves formation of the stacking faults and high compressive residual stresses in the nitrided layer, resulting in a highly distorted and disordered FCC structure. Also, the lattice parameter of the S-phase will increase with increasing nitrogen concentration. Since, diffusion of the

nitrogen is maximum at the surface and decreases gradually, the lattice parameter of the S-phase also decreases away from the surface. These factors are analysed in detail by Sun and Bell (1999) and affirmed that the S-phase therefore has a FCC crystal structure with a gradually expanded and distorted lattice towards the surface. Thus, samples containing expanded austenite exhibit characteristic X-ray diffraction pattern. XRD peaks shift to lower diffracting angles upon nitriding. Broadening of the XRD peaks are also observed. These observations are in accordance with the XRD results of the un-peened sample and sample peened with 100% coverage presented in Fig. 4.34 of section 4.6.2.

5.5.2 Nitriding of the intermediate and severe peened samples

It is interesting to note that the plasma nitriding of samples peened at 500% and 1000% coverage show broad peak in the 2θ range of $40–43°$ and a sharp peak at diffraction angle of 44.7 degrees (in Fig. 4.34).

It is well accepted that low temperature plasma nitriding of the austenitic stainless steel results in the formation of the expanded austenite in nitride layer; as explained in section 5.5.1. In the last decade, severe plastic deformation technique has emerged as a successful pre-treatment step for enhancement of nitriding kinetics in the austenitic stainless steels. But till date, there is no agreement in views amongst the researchers about the microstructural evolution and phases formed during this duplex process. In the study of Laleh et al. (2013) Chemuki et al. (2013), no martensite is reported after SMAT pre-treatment while austenite directly transforms to S-phase after plasma nitriding. Few authors opine that the strain induced martensite formed during the deformation gets converted into expanded austenite on plasma nitriding; which further transforms into α-Fe and CrN upon nitriding at higher temperatures for longer durations (Lin et al. 2006) (Wang et al. 2006). In few cases, Fe_4N phase is also reported (Hashemi et al. 2007).

Yu et al. (2002) proposed a two- step transformation mechanism from martensite to expanded austenite. It suggests a complete transformation of the strain induced martensite to austenite initially, followed by transformation of the austenite to the S-

phase. Several studies (Baluswamy et al. 2013) (Shen et al. 2010) (Bottoli et al. 2015) have justified their results based on this theory. In a recent study (Borgioli et al. 2016) also, it has been stated that the presence of the strain induced martensite enhances the nitriding layer thickness and it transforms to expanded austenite when nitrided at lower temperatures while it promotes CrN formation at higher treatment temperatures.

Further, a study by Ferkel et al. (2003) indicated the presence of the martensite in the nitride layer. It suggests that the martensite could be due to the strain induced transformation of the austenite during prior severe deformation or due to the decomposition of the expanded austenite to martensite and CrN. The study by Ji et al. (2005) confirmed the formation of the strain induced martensite upon deformation, while phases formed after plasma nitriding were left unidentified suggesting that it could be a mixture of ferritic and/or martensitic phases along with the Fe and/or Cr nitrides. This ambiguity was due to observed broad XRD peaks in the region of 40-45° and hence, TEM analysis was strongly recommended by the authors (Ferkel et al. 2003 and Ji et al. 2005) to confirm the phases observed.

In the present investigation, there is no indication of the CrN phase, suggesting that corrosion resistance of the steel is not impaired as chromium has not diffused out from the matrix. This is distinctly different than investigations (Lin et al. 2006) (Wang et al. 2006) in which extensive formation of the CrN during nitriding is reported. XRD pattern of the nitride samples in Fig. 4.34 depicts a broad peak in the 2θ range of 40–43° and a sharp peak at diffraction angle of 44.7 degrees. The broad peak could be assigned to the (111) plane of the expanded austenite. However, there exists ambiguity in assigning the sharp peak observed in the XRD results to the martensite and/or CrN phase as (200) reflection from the CrN and (110) reflection from the martensite phase are probable in the diffraction angle of about 44°. This was intuitive to carry out a layer-by-layer TEM study of the nitride layer of the severe peened-nitrided sample.

Results of TEM study in section 4.7 confirmed that, top surface of nitride layer found to consist of nearly-equiaxed grains forming predominantly martensite phase (in Fig. 4.37). Weak diffraction rings of FCC- structure were observed in Fig. 4.37(b). These

are attributed to formation of the expanded austenite in the top surface of the nitride layer; which is evident in the XRD pattern in Fig. 4.34. During nitriding treatment, surface of the component gets enriched with nitrogen. Nitrogen being an austenite stabilizer, its supersaturation at the surface decreases the transformation temperature of the martensite to austenite, as reported by Yu et al. (2002). Hence, it is probable that during plasma nitriding, small of amount of deformation induced martensite would transform back to the austenite phase. With simultaneous diffusion of the nitrogen into the lattice, the austenite will transform to expanded austenite.

Subsurface layers were observed to possess completely martensite phase having lath morphology as observed in Fig. 4.38 and Fig. 4.39. Under the process parameters used for the duplex treatment, precipitation of the deleterious CrN is not observed. It is also evident that the major phase in the surface and subsurface layer is martensite. Hence, it is reasonable to assume that the nitrogen has entered into the martensite lattice during nitriding treatment to facilitate the formation of about 45 μm thick nitride layer. This study differs from most of the previous reports indicating that the major phase in the nitride layer is martensitic in nature.

5.6 Nitrogen diffusion during plasma nitriding treatment

5.6.1 Calculation of effective diffusion coefficient

Effective diffusion coefficient of the nitrogen (D_N) for plasma nitriding of 316L stainless steel is calculated from the equation x $\cong \sqrt{D_N t}$ where 'x' is the nitride layer thickness in meter and 't' is the duration of nitriding in seconds. Effective diffusion coefficient of the nitrogen through the austenite lattice at 400 °C could be theoretically calculated using the equation $D_N = D_0 \, exp(\frac{-Q}{RT})$; where D_0 is the pre-exponential constant and Q is the activation energy. It is calculated to be 9.919 x10^{-18} m^2/s; considering the magnitudes of D_0 and Q for the diffusion of the nitrogen into the lattice of γ–Fe as 9.1x10^{-5} m^2/s and 167 kJ/mol, respectively (Saker et al. 1991).

The nitride case depth of the un-peened sample after 4 hours of nitriding is calculated to be 0.315 μm. Order of the case depth matches closely with the experimental nitride

layer thickness of 0.83 ± 0.09 μm for the un-peened sample after plasma nitriding as seen in Fig. 4.33. Observed increase in the thickness (experimental value is approximately 2.5 times estimated value) is attributed to the lowering of the activation energy during the plasma nitriding process (Moskalioviene et al. 2011). However, the nitride layer thickness of the peened samples after nitriding at 400 °C for 4 hours is given in Table. 5.1. These are distinctly higher than the case depth predicted from the equation.

Table 5.1 Nitride layer thickness of the pre-peened samples after plasma nitriding at 400 °C for 4 hours

Peening coverage	Nitride layer thickness (μm)
100%	7.2
500%	26.8
1000%	53.2

Effective diffusion coefficients of the nitrogen in un-peened and peened samples at 400 °C are calculated using nitriding layer thickness and are reported in Table 5.2. The theoretical effective diffusion coefficient is given for reference.

Table 5.2 Effective diffusion coefficients of the nitrogen in un-peened and peened samples

Condition	Effective diffusion coefficient (m^2/s)
Theoretical	9.919×10^{-18}
Un-peened	4.14×10^{-17}
100% peened	3.6×10^{-15}
500% peened	4.9×10^{-14}
1000% peened	1.6×10^{-13}

It is observed that effective diffusion coefficient for the diffusion of nitrogen through the un-peened sample upon plasma nitriding is slightly higher than that of the theoretically calculated value. It could be attributed to the marginal reduction of the activation energy during plasma processes (Dimitrov et al. 1998). In contrast, effective diffusion coefficient for the severe peened sample is about five orders in magnitude higher than the theoretical diffusion coefficient for the nitrogen at nitriding temperature of 400 °C. Severe deformation leads to nanocrystallization of the coarse grain structure on the surface of the base metal; along with the formation of the non-equilibrium defects, like dislocations, deformation twins, stacking faults, etc. (Bahl et al. 2017; Zhang et al. 2003; Zhou et al. 2016).

Ultra fine-grained structure and non-equilibrium defects collectively enhance the nitrogen diffusion kinetics by serving as easy diffusion paths. During nitriding of the un-peened sample, lattice diffusion prevails as the nitrogen diffuses through the coarse grained austenite phase. In contrast, diffusion through the grain boundaries, dislocation (pipe diffusion) and other defect structures are prominent during nitriding of severe peened sample (Tong 2003). Additionally, deformation induced transformation of the austenite to martensite takes place at the surface and subsurface regions as seen in Fig. 5.2. Martensite being the open structure; further enhances the diffusion of the nitrogen (Yu et al. 2002).

It is also important to note that the precipitation of the deleterious chromium nitride is not observed. In plasma nitriding of the austenitic stainless steels, prevention of CrN precipitation is a major challenge. Formation of the CrN reduces the availability of the chromium in the steel matrix and adversely affects the corrosion resistance. Higher nitriding temperature favors the CrN precipitation; while lower nitriding temperature results in thin nitride layers. It is reported that even the studies in which the surface nanocrystallization was used as a pre-treatment step to reduce plasma nitriding temperature have faced the problem of chromium nitride precipitation (Baluswamy et al. 2013) (Shen at al. 2010). It was reasoned that the surface defects formed due to the prior deformation facilitate faster diffusion of the Cr as well. However, lower nitriding temperatures and nitriding durations might be responsible for the prevention of the CrN formation. This is one of the highlights of the present report.

Diffusion of the nitrogen in the steels depends mainly on the lattice structure, grain size, chemical composition and defect density. Undeformed 316L grade consists of coarse austenite grains. Austenite being the close packed structure, diffusion of the nitrogen is difficult. In the undeformed state, the defect density will be typical of the hot rolled steel. Since, the grain size is in the range of $40 - 80$ μm, relative contribution of grain boundaries to the overall diffusion is also insignificant. Hence, though expanded austenite phase forms on the surface upon plasma nitriding at 400 ℃, the thickness of the nitride layer will be less than a micrometer as seen from the SEM micrograph in Fig. 4.33(a). In contrast, shot peening induces ultrafine grains on the surface, higher dislocation density, higher fraction of the grain boundaries, triple junctions, etc. which provide easy path for the diffusion of the nitrogen during plasma nitriding. Also, formation of the strain induced martensite aids in the faster diffusion of the nitrogen as diffusion coefficient of the nitrogen in the martensite is more than that in the austenite (Yu et al. 2002). These factors are responsible for the higher effective diffusion coefficient as well as observed improvement in the nitride layer thickness.

5.6.2 Role of easy diffusion paths in improving the diffusion kinetics

It is well-established that the diffusion in crystalline materials takes place along a number of diverse paths. These include crystal lattice, grain boundaries, dislocations, free surfaces, etc. Out of these, all are considered to be lattice defects except the crystal lattice. All these defects are associated with more open structure and it is shown experimentally that the jump frequency for the diffusing atoms migrating along these defects is higher than that for diffusion through the lattice (Porter and easterling 1992). These defects are considered to be high diffusivity paths. Hence, nanocrystalline and/or deformed metal will show higher rate of diffusion compared to its well-annealed, coarse grained counterpart. This phenomenon is exploited in enhancing the diffusion kinetics during the diffusion based surface modification techniques, like nitriding, carburizing, boronizing, etc. through prior deformation.

It is observed in section 4.5.1 that significant enhancement in nitriding layer thickness occurs with shot peening pre-treatment. It is also discussed in section 5.6.1 about the

enhanced effective diffusion coefficient of pre-peened samples compared to their un-peened counterparts. This clearly reveals the beneficial effect of shot peening pre-treatment.

It is also interesting to note that the case depth obtained in the present study with severe peening pre-treatment and plasma nitriding for 4 hours at 400 °C is considerably high compared to other studies with similar process parameters. Case depth obtained was limited to 5 µm in the work of Shen et al. (2010) when plasma nitriding was carried out at 400 °C for 4 hours with shot peening pre-treatment. Here, peening was carried out using steel shots of 0.8 mm diameter; for duration of 5 minutes. In the work of Ji et al. (2005), the nitride layer thickness achieved was about 20 µm in spite of nitriding at 400 °C for 6 hours. Here the shot peening pre-treatment was carried out in a planetary ball mill for 50 minutes using steel shots of 10 mm diameter. Nitride layer thickness of 50 µm is reported in the work of Hashemi et al (2011) with shot peening pre-treatment. However, gas nitriding was carried out at 570 °C for 8 hours.

5.6.2.1 Diffusion along the grain boundaries

Relative ease with which diffusion takes place through the free surface, grain boundary and lattice are indicated by the respective diffusion coefficients:

$D_s > D_b > D_l$ where, D_s, D_b, and D_l are the diffusion coefficients related to free surface, grain boundary and defect-free lattice, respectively. Though the diffusion along free surface is higher, the total boundary area is significantly higher than that of the free surface in bulk materials. Hence, role of the grain boundary as high diffusivity path is considered prominently.

It is well-understood that at the grain boundary, atomic arrangement is random. This implies that the number of defects is more in grain boundary compared to the grain interior. Hence, during diffusion, the resistance offered by the grain boundary for the diffusing atom is less than that of the lattice. The total flux of atoms during diffusion will be the sum of flux of atoms diffusing through the lattice and that of the grain boundary (Porter and easterling 1992).

$$J = J_b\,\delta/d + J_l$$

Where J_b and J_l are the flux through the grain boundary and the lattice, respectively.

We know that,

$J_b = -D_b\,dc/dx$ and

$J_l = -D_l\,dc/dx$

Hence, $J = -\dfrac{D_b\delta + D_l d}{d}\,\dfrac{dc}{dx} = -D_{app}\,\dfrac{dc}{dx}$

where D_{app} is the apparent diffusion coefficient.

Therefore, $D_{app} = D_l + D_b\,\delta/d$

$D_{app}/D_l = 1 + (D_b\delta/D_l d)$

where δ is the width of the grain boundary and d is the grain size. Relative significance of the grain boundary diffusion over that of the lattice diffusion depends on the ratio of $D_b\delta/D_l d$. It is observed that the grain boundaries will contribute significantly to the total flux when $D_b\delta$ is more than $D_l d$. The effective width of the grain boundary is about 0.5 nm (Porter and easterling 1992).

Diffusion of the elements in bulk polycrystalline material occurs through the crystal lattice. This is aided by lattice point defects, like vacancies and interstitials. In coarse grained materials, grain size may vary between 10-1000 μm. Hence, relative contribution of the grain boundaries towards diffusion will be less compared to their nano-grained counterparts (Tong et al. 2003). However, in the case of nanostructured materials, grains are refined to the nano-scale regime. This drastically increases the fraction of the grain boundary area. In the present case, grain size is refined to about 80-100 nm owing to surface nanocrystallization upon severe peening (in Fig. 4.26). This brings about a drastic enhancement in the diffusion through the grain boundaries. This makes diffusion through grain boundary as a significant diffusion mechanism in nanocrystalline materials.

5.6.2.2 Diffusion through the dislocation

Literature on severe peening-nitriding duplex treatment suggests that, there are studies in which grain refinement upto 10-15 nm was achieved by different peening techniques. It is observed in the work of Laleh et al. (2013) that, upon SMAT process, the grain size is refined to the scale of 10-15 nm as confirmed by the TEM study. In the work of Baluswamy et al. (2013), grain size in the range of 12-23 nm is obtained upon SMAT treatment; calculated by using XRD. However, improvement in the nitride layer thickness of the pre-peened samples after plasma nitriding was observed to be less compared to the results reported in the present study; for the similar process parameters employed. Similarly, in the work of Lin et al. (2006), nanostructured surface containing grains of about 100 nm are obtained after SMAT treatment. But plasma nitriding for 4 hours at 400 °C has produced a nitride layer thickness of 10 μm.

In the present study, bright-field TEM micrograph presented in Fig. 4.26 depicts that the dislocation cell type martensite is obtained on the top surface of the severe shot peened sample. Cell size was observed to be in the rage of 80-100 nm; which is considerably high compared to the values reported in the above paragraph. However, the improvement in the nitride layer thickness observed in the present study is significantly high. About 50 μm case depth is observed in the severe peened sample after plasma nitriding for 4 hours at 400 °C. This suggests that diffusion along grain boundary is not the only decisive factor in diffusion of the nitrogen during plasma nitriding.

It could be observed from the TEM micrographs presented in Fig. 4.13, 4.14 and 4.26 that huge amount of dislocations are present in the top surface of the severe shot peened sample. This suggests that diffusion through the dislocation also contributes significantly to the diffusion of the nitrogen during plasma nitriding treatment. In fact, the diffusion through the grain boundaries can also be explained in terms of the dislocation structure at the boundaries. Hence, higher case depth obtained in the present study is attributed to the paramount influence of the dislocations in acting as

high diffusivity paths for the diffusion of the nitrogen during plasma nitriding treatment.

Diffusion through the dislocation is a short-circuit diffusion often referred to as pipe diffusion. The name comes from the fact that the dislocations effectively acts as pipe along which atoms can diffuse with a diffusion coefficient D_p (Love, G. R. 1964). Properly oriented grain edge can also act as a pipe. The relative cross-sectional area of the dislocation and the matrix phase decides the contribution of the dislocation to the total diffusion. This is illustrated through a schematic diagram in Fig. 5.5.
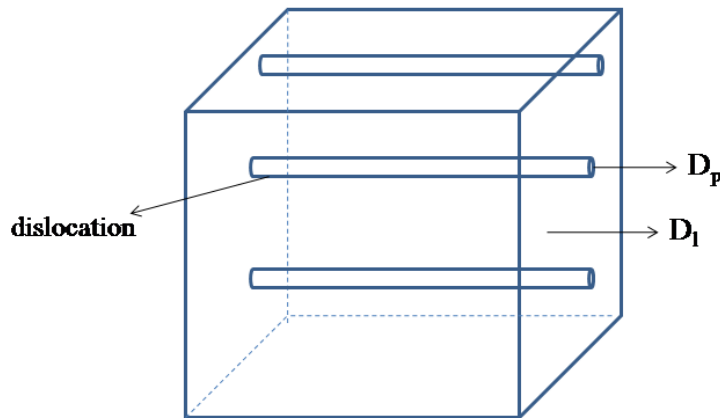
Fig. 5.5 Schematic diagram of diffusion through the dislocation in the matrix

Diffusivity through a single crystal containing dislocations is given by

$$\frac{D_{app}}{D_l} = 1 + g.\frac{D_p}{D_l}$$

where g is the cross-sectional area of dislocation (which is assumed as a pipe) per unit area of the matrix. D_l and D_p are the diffusion coefficients of the lattice and the dislocation, respectively(Porter et al. 2009). Dislocation density of the well annealed metallic material is about 10^5 dislocations per square millimeter. It is mentioned that at temperatures below half the homologous temperature, the term $g.\frac{D_p}{D_l}$ is significantly high and the relative contribution from the dislocation to total flux will be significant compared to the diffusion occurring through the lattice.

Dislocation density plays a major role in the relative significance of the pipe diffusion to the total diffusion flux. During severe plastic deformation techniques, like shot

peening, the dislocation density increases to as high as 10^{16} dislocations per m^{-2}. These dislocations may be in isolated or aligned in the form of dislocation forest, dislocation cells, sub-boundaries (low angle boundaries), etc.

It is well established that the dislocations are associated with strain fields. The strain field of an edge dislocation has a dilatational component. The work of Love, G. R. (1964) indicates that the segregation of vacancies occur at the vicinity of the edge dislocation. Because of this segregation, the empty lattice sites will be available to the flux of the diffusing atoms. Hence, favourable lattice strain fields around the dislocation would enhance the motion of the diffusing species. This, in turn, will accelerate the rate of diffusion.

5.7 Mechanical properties

Plasma nitriding is one of the widely accepted diffusion based surface modification technique used for the austenitic stainless steels, results in the formation of a hard and wear resistant nitride layer upon treatment. The pre-treatment step of shot peening also adds to increase in hardness. In the present study, the effect of duplex treatment is assessed through microhardness, nanoindentation and nanoscale wear tests. Understanding the mechanical properties of the treated surface is vital to meet requirements of targeted applications in aerospace, medical and automotive industries.

5.7.1 Microhardness test

Indentation hardness testing is classified as quasi-static hardness, in which a stylus is pressed into a surface under a certain normal load. The resultant depth or the diameter or diagonal of indentation is used to calculate the hardness number. In the present study, microhardness test by using the Vickers indenter is performed to compute the hardness when subjected to quasi-static loading.

Microhardness data of the base metal, peened, nitrided and peened-nitrided samples are given in Fig. 4.36 of section 4.6.4. Compared to the average base metal microhardness of 197.6 Hv, peened samples show a drastic improvement in the surface hardness due to effect of the peening. With increase in the peening coverage,

the defect density on the surface increases along with the grain refinement. It is also observed that the deformation induced martensitic transformation takes place upon peening and the relative fraction of the martensite increases with increase in the peening coverage as observed in Fig 5.2 of section 5.3. It could be observed from bright-field TEM micrographs that the coarse austenite grain structure of the parent metal (in Fig.4.8(a)) is changed to dislocation cell type martensite structure on the surface of the severe peened sample (in Fig.4.26(f)). Martensite aids in faster diffusion of the nitrogen compared to the austenite; due to relatively open structure. These factors are collectively responsible for the improvement in the surface microhardness.

Effect of increase in the deformed layer, as observed by the cross-sectional SEM micrographs in Fig. 4.5 of section 4.2.3, is manifested in the cross-sectional microhardness data in Fig. 4.40 of section 4.8.1. With increase in the peening coverage, depth of the deformed layer will increase and consequently, the microhardness data also shows gradual increase.

Upon nitriding, further improvement in the surface microhardness is observed. Nitrogen goes in to the interstitial sites of the austenite and/or martensite in the un-peened and peened samples during the plasma nitriding treatment. This results in lattice strain which contributes to the increase in hardness.

5.7.2 Scratch hardness test

Scratch hardness testing is carried out to measure the resistance of the treated surfaces to permanent deformation under the action of a single point (stylus tip) scratch loading. It is a complimentary testing method to the quasi-static hardness tests. In contrast to quasi-static hardness tests, the diamond indenter moves tangentially along the surface during the scratch testing. The state of stress that the material experiences during the motion of the stylus will be different compared to that produced under a quasi-static indenter. It is opined that the scratch hardness numbers are more appropriate measure of the wear resistance of the material. This test assesses the damage resistance property of the treated surface to the two-body abrasion conditions.

The resistance of a material to abrasion by a single point may be affected by its sensitivity to the strain rate of the deformation process. Therefore, this test is conducted under a low stylus traversing speed. Use of a slow scratching speed also minimizes the possible effects of frictional heating. This test uses measurements of the residual scratch width after the stylus has been removed to compute the scratch hardness number. Therefore, it reflects the permanent deformation resulting from scratching and not the instantaneous state of combined elastic and plastic deformation of the surface.

The results of scratch hardness are consolidated in Table. 4.1 in section 4.8.2 found to follow the same trend as that of microhardness data presented in Fig. 4.36 of section 4.6.4. However, the magnitude of scratch hardness values is higher than those of the microhardness. Comparison of the microhardness and scratch hardness data is given in Fig. 5.6. Microhardness is expressed in the unit of GPa by multiplying the magnitude in VHN by factor of 9.81. It could be observed that the difference between magnitudes of microhardness and scratch hardness data decreases with increase in the hardness.

Fig. 5.6 shows that the shot peened alloy is harder than the nitrided alloy. This is because, nitriding of austenitic stainless steels results in S-phase (expanded austenite: which is solid solution of nitrogen in FCC- Fe) which is a soft phase compared to the microstructure (fine grains, deformation induced martensite, large amount of non-equilibrium defects, etc.) produced during the shot peening treatment. Only nitriding of pure iron (α-Fe) produces hard, iron nitride layer (white layer). Also, the nitride layer thickness of un-peened sample after nitriding is about 1µm. So during the microhardness and scratch hardness testing, effect of bulk material also could have contributed to lower magnitude.
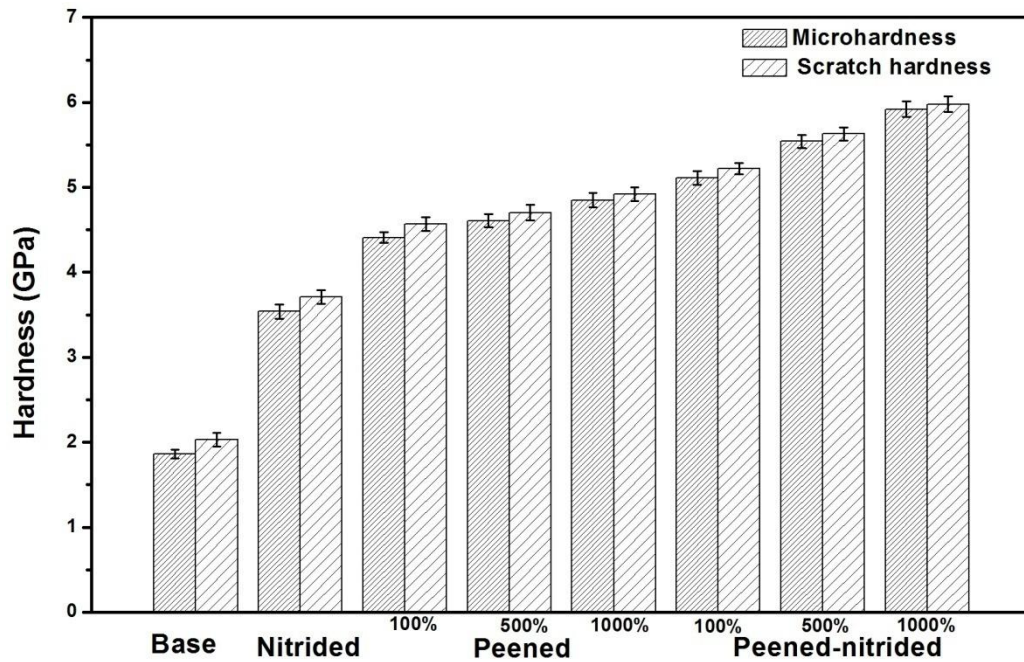
Fig. 5.6 Comparison of the microhardness and scratch hardness data of the base metal and the treated samples

5.7.3 Nano-scale hardness test

For general purpose applications, hardness of the austenitic stainless steels subjected to shot peening as well as nitriding treatment are evaluated through macro/micro quasi-static hardness testing. But under certain surface treatments, the depth of indentation in the case of macro-scale hardness tests will be more than the deformed layer itself. Then, the hardness data obtained from the test will be less than the actual hardness on the surface. This necessitates the use of nano-scale tests to assess the surface hardness and wear resistance.

It is elaborated in the section 4.4 and section 4.7 that the severe peened and severe peened-nitrided samples possess gradient nanostructured layers, respectively. This necessitates the nano-scale hardness and wear tests despite the treated surfaces being evaluated by microhardness. Hence, to evaluate the surface properties in the hardness and scratch tests are conducted on the base metal, severe peened and severe peened-nitrided samples using the nanoindenter.

Surface hardness of the base metal, severe peened and peened-nitrided samples obtained from microhardness, scratch hardness and nanoindentation are summarized in Fig 5.7. It could be observed that hardness value obtained from nanoindentation is marginally higher than that of microhardness and scratch hardness value. However, in the case of the severe peened and nitrided samples, the nano-scale hardness magnitude is significantly higher.
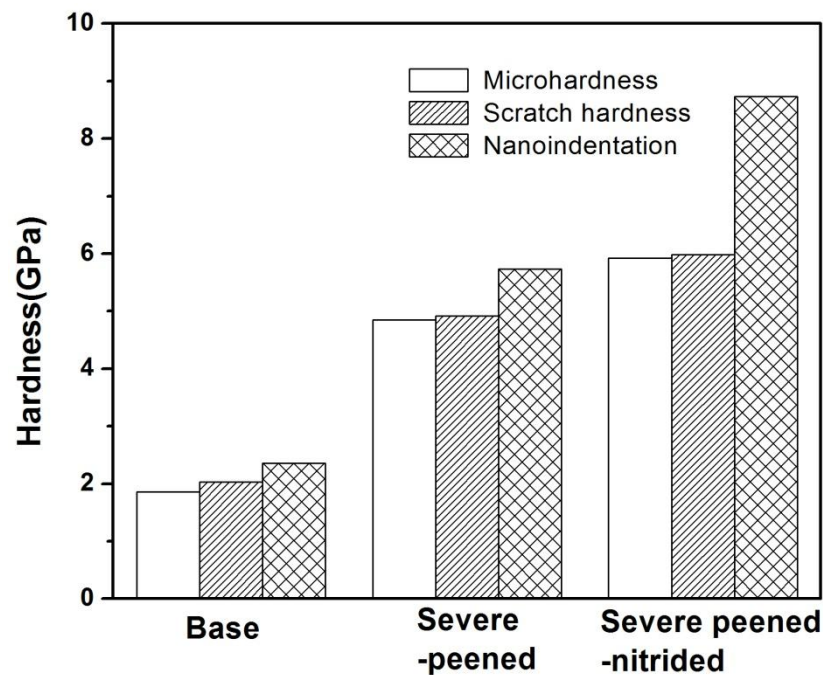
Fig. 5.7 Comparison of hardness from nanoindentation, microhardness and scratch hardness of the base metal, severe peened and peened-nitrided samples

Base metal consists of coarse grained austenite structure in bulk as well as the surface of the sample. Hence, the microhardness, scratch hardness as well as the nanohardness magnitude are almost similar. In contrast, the severe peened sample consists of fine martensite cell structure on the surface while sub-surface consists of lath martensite. Huge amount of dislocations are also seen in the martensite cells. Similarly, the severe peened- nitrided sample consists of fine martensite crystallites while sub-surface shows the lath martensite structure. Hence, nanoindentation yielded significantly higher hardness value compared to the microhardness and scratch hardness magnitudes. It can be recalled that nanoindentation yields higher values than the corresponding microhardness magnitudes. However, in case of severe peened and

peened-nitrided samples, this magnitudes are notably higher due to the reason stated above.

The results of the nanoscratch and nano-scale wear studies elaborated in section 4.8.4 and 4.8.5 also indicates the significant improvement in the surface wear properties upon severe peening as well as peening-nitriding duplex treatment. It is relevant to recall that precipitation of the deleterious chromium nitride phase is not observed under these process parameters. Hence, an increase in wear resistance and hardness without considerable loss of corrosion resistance will aid towards better performance of this grade of stainless steel under suitable application.

5.8 Summary

The chapter briefs that plastic strain experienced during the severe peening results in the grain refinement or surface nanocrystallization. Nucleation of the deformation induced martensite could take place at different locations in the austenite matrix where the appropriate defect structure is available. Growth of these nuclei into lath martensite occurs; which further transforms into dislocation cell type morphology under the continued action of peening stresses. Nitriding treatment results in formation of the nitrogen enriched austenite/martensite depending on the dominant phase on the surface of the treated sample. The gradient nanostructured layer aids in faster diffusion of the nitrogen through the introduction of easy diffusion paths; in contrast to the base metal. These microstructural and morphological changes are also reflected in the surface properties of the treated samples.

CHAPTER 6

CONCLUSIONS

In the present work, AISI 316L grades are subjected to plasma nitriding in the temperature range of 300-500 ℃ for a duration of 4 hours with air-blast shot peening pre-treatment. The aim of the pre-treatment step is to bring about surface nanocrystallization and increase the non-equilibrium defect density on the surface and in the sub-surface region so as to enhance the diffusion kinetics of plasma nitriding process. Peening coverage is used as a measure of severity of the peening process and its effect on the formation of gradient nanostructured layer, deformation induced martensitic transformation and subsequent plasma nitriding is assessed. Based on the experimental results obtained and the discussion presented the following conclusions are drawn:

- Moving from conventional peening to severe peening found to increase in the shot peening coverage, increases depth of layer affected by peening process, enhances the grain refinement and increases the relative amount of DIM while the surface roughness found to follow the opposite trend.

- TEM study shows that typical hot rolled austenitic microstructure having grain size in the range of 40-80 μm is refined to fine martensite crystallites with cell size in the range of 100–140 nm on the surface of the severe peened sample.

- Severe shot peening generates about 500 μm thick gradient nanostructured (GNS) layer; characterized by the presence of nanocrystallized region and deformation features, like shearbands, multiple shearband intersections, rhombic blocks, etc.

- Nucleation of DIM is not limited to shear band intersections. Martensite units found to nucleate at multiple locations in the austenite matrix, like parallel to shear bands, within the shearbands, across the shearbands, at the grain boundary, etc.

- Coalescence of the martensite nuclei leads to formation of a continuous layer of lath martensite, at about 15-20 μm from the peened surface. Lath morphology changes over to dislocation cell type morphology due to breaking up of martensite laths by the high strain rate, multi-directional impact of shots at the topmost surface.

- Shot peening treatment is successfully used as pre-treatment to plasma nitriding to achieve thicker nitride layers at shorter nitriding duration. Increase in peening coverage enhances the depth of the deformed layer. However, beneficial effects of the pre-treatment can be harvested by selection of appropriate plasma nitriding temperature.

- Nitriding temperature of 300 °C is insufficient to facilitate formation of the continuous nitride layer in 4 hours inspite of the high defect density on the severe peened surface. Nitriding at 500 °C results in precipitation of the deleterious CrN phase; in both un-peened and severe peened samples.

- Pronounced effect of pre-treatment on nitride layer thickness is obtained at 400 °C; from less than 1 μm for the un-peened sample to about 50 μm for the severe peened sample, without CrN precipitation. Detailed TEM study suggests that the nitride layer is observed to be formed largely by incorporation of the nitrogen into martensite lattice; contrary to majority of the reports.

- Mechanical characterization affirms the improvement in the surface mechanical properties, like, microhardness, scratch hardness, wear resistance in the severe peened-nitrided sample.

Scope for the future work

In the present study, 5 mm thick hot-rolled AISI 316L grade stainless steel sheets are subjected to plasma nitriding in the temperature range of 300-500 ºC for a duration of 4 hours. Air-blast shot peening is used as a pre-treatment step to improve the diffusion kinetics. Peening severity is varied by varying the peening coverage and its effect on surface nanocrystallization and subsequent nitriding is studied. Based on the results of

microstructural and mechanical characterization, following studies could be considered for future work.

- Apart from peening coverage, Almen intensity is the measure of peening severity practiced in industry. Hence, a similar study could be carried out to assess the effect of Almen intensity on the plasma nitriding kinetics of AISI 316L grade sheets.

- Effect of air-blast shot peening on other diffusion based surface modification techniques, like carburizing, boronizing, nitrocarburizing, etc.

- Study could be extended to various grades of ferrous and non-ferrous grades of alloys which require surface engineering techniques to improve the wear resistance of the surface.

- Detailed TEM study of the samples subjected to different peening/ surface severe deformation techniques can be done to acquire deeper insights on the nucleation and growth of the deformation induced martensite.

REFERENCES

Altenberger, I., Scholtes, B., Martin, U. and Oettel, H. (1999). "Cyclic deformation and near surface microstructures of shot peened and deep rolled austenitic stainless steel." *Mater. Sci. Eng. A.*, 264 (1-2), 1-16.

Angel, T. (1954). "Formation of martensite in austenitic stainless steels." *J. Iron Steel Inst.*, 177, 165-174.

Arifvianto, B., Wibisono, S. K. A. and Mahardika, M. (2012). "Influence of grit blasting treatment using steel slag balls on the subsurface microhardness, surface characteristics and chemical composition of medical grade 316L stainless steel." *Surf. Coat. Technol.*, 210, 176–182.

Azar, V., Hashemi, B. and Rezaee Yazdi, M. (2010). "The effect of shot peening on fatigue and corrosion behavior of 316L stainless steel in Ringer's solution." *Surf. Coat. Technol.*, 204(21–22), 3546–3551.

Bagheri, S. and Guagliano, M. (2009). "Review of shot peening processes to obtain nanocrystalline surfaces in metal alloys." *Surf. Engg.*, 25(1), 3–14.

Bagherifard, S., Ghelichi, R. and Guagliano, M. (2010). "A numerical model of severe shot peening (SSP) to predict the generation of a nanostructured surface layer of material. " *Surf. Coat. Technol.*, 204(24), 4081–4090.

Bagherifard, S., Ghelichi, R. and Guagliano, M. (2012). "Numerical and experimental analysis of surface roughness generated by shot peening." *Appl. Surf. Sci.*, 258(18), 6831–6840.

Bagherifard, S., Slawik, S., Fernández-Pariente, I., Pauly, C., Mücklich, F., and Guagliano, M. (2016). "Nanoscale surface modification of AISI 316L stainless steel by severe shot peening." *J. Mater. Des.*, 102, 68–77.

Bahl, S., Suwas, S., Ungar, T., and Chatterjee, K. (2017). "Elucidating microstructural evolution and strengthening mechanisms in nanocrystalline surface induced by surface mechanical attrition treatment of stainless steel." *Acta Mater.,* 122, 138–151.

Balusamy, T., Narayanan, T. S. N. S., Ravichandran, K., Park, I. S. and Lee, M. H. (2013). "Plasma nitriding of AISI 304 stainless steel: Role of surface mechanical attrition treatment." *Mater. Charact*., 85, 38–47.

Beegan, D., Chowdhury, S., Laugier, M., (2007). "Comparison between nanoindentation and scratch test hardness (scratch hardness) values of copper thin films on oxidised silicon substrates." *Surf. Coat. Technol*. 201, 5804–5808.

Blawert, C., Weisheit, a., Mordike, B. L. and Knoop, R. M. (1996). "Plasma immersion ion implantation of stainless steel: austenitic stainless steel in comparison to austenitic-ferritic stainless steel." *Surf. Coat. Technol*., 85(1–2), 15–27.

Borgioli, F., Galvanetto, E. and Bacci, T. (2016). "Low temperature nitriding of AISI 300 and 200 series austenitic stainless steels." *Vacuum*, 127, 51–60.

Bottoli, F., Winther, G., Christiansen, T. L. and Somers, M. A. J. (2015)."Influence of plastic deformation on low-temperature surface hardening of austenitic stainless steel by gaseous nitriding." *Metall. Mater. Trans. A.,* 46(6), 2579–2590

Brooks, J. W., Loretto, M. H., and Smallman, R. E. (1979). "In-situ observations of the formation of martensite in stainless steel." *Acta Metall*., 27(12), 1829–1838.

Chemkhi, M., Retraint, D., Roos, A., Garnier, C., Waltz, L., Demangel, C. and Proust, G. (2013). "The effect of surface mechanical attrition treatment on low temperature plasma nitriding of an austenitic stainless steel." *Surf. Coat. Technol*., 221, 191–195.

Chen, A. Y., Ruan, H. H., Wang, J., Chan, H. L., Wang, Q., Li, Q., and Lu, J. (2011). "The influence of strain rate on the microstructure transition of 304 stainless steel." *Acta Mater*., 59(9), 3697–3709.

Das, A., Sivaprasad, S., Ghosh, M., Chakraborti, P. C., and Tarafder, S. (2008). "Morphologies and characteristics of deformation induced martensite during tensile deformation of 304 LN stainless steel." *Mater. Sci. Eng. A.*, 486(1–2), 283–286.

Devine, T. M. (1990). "The mechanism of sensitization of austenitic stainless steel." *Corr. Sci.* 30 (2-3), 135-151.

Dimitrov, V. I., Haen, J. D., Knuyt, G., Quaeyhaegens, C., and Stats, L. M. (1998). "A method for determination of the effective diffusion coefficient and sputtering rate during plasma diffusion treatment." *Surf. Coat. Technol.*, 99, 234–241.

Dossett, J. and Totten, G.E. (2013). "Steel Heat Treating Fundamentals and Processes" Vol. 4A, ASM handbook, ASM international.

Eichelman, G. H. and Hull, F. C. (1953). "The effect of composition on the temperature of spontaneous transformation of austenite to marteniste in 18-8 type stainless steel." *Trans. Amer. Soc. Metals*, 77, 45-55.

Fargas, G., Roa, J. J., and Mateo, A. (2015). "Effect of shot peening on metastable austenitic stainless steels." *Mater. Sci. Eng. A.*, 641, 290-296.

Ferkel, H., Glatzer, M., Estrin, Y., Valie, R. Z., Blawert, C. and Mordike, B. L. (2003). "RF plasma nitriding of severely deformed iron-based alloys." *Mater. Sci. Eng. A*, 348, 100–110.

Fewell, M. P., Mitchell, D. R. G., Priest, J. M., Short, K. T. and Collins, G. A. (2000). "The nature of expanded austenite." *Surf. Coat. Technol.*, 131, 300–306.

Gatey, A. M., Hosmani, S. S., Figueroa, C. A., Arya, S. B. and Singh, R. P. (2016). "Role of surface mechanical attrition treatment and chemical etching on plasma nitriding behavior of AISI 304L steel." *Surf. Coat. Technol.*, 304, 413-424.

Gey, N., Petit, B., and Humbert, M. (2005). "Electron backscattered diffraction study of ε/α′ martensitic variants induced by plastic deformation in 304 stainless steel." *Mater. Sci. Trans. A.*, 36, 3291-3299.

Gil, L., Bruhl, S., Jimenez, L., Leon, O., Guevara, R. and Staia, M. H. (2006). "Corrosion performance of the plasma nitrided 316L stainless steel." *Surf. Coat. Technol.*, 201, 4424–4429.

Gontijo, L. C., Machado, R., Miola, E. J., Casteletti, L. C., Alcântara, N. G. and Nascente, P. A. P. (2006). "Study of the S phase formed on plasma-nitrided AISI 316L stainless steel." Mater. Sci. Eng. A, 431(1–2), 315–321.

Gujba, A. K. and Medraj, M. (2014). " Laser peening process and its impact on materials in comparison with shot peening and ultrasonic and impact peening." *Materials.*, 7, 7925-7974.

Gussev, M. N., Busby, J. T., Byun, T. S., and Parish, C. M. (2013). "Twinning and martensitic transformations in nickel-enriched 304 austenitic steel during tensile and indentation deformations." *Mater. Sci.Eng. A*, 588, 299–307.

Hashemi, B., Rezaee Yazdi, M. and Azar, V. (2011). "The wear and corrosion resistance of shot peened-nitrided 316L austenitic stainless steel." *Mater.Des.,* 32(6), 3287–3292.

Hassani-Gangaraj, S. M., Cho, K. S., Voigt, H. J. L., Guagliano, M. and Schuh, C. A. (2015). "Experimental assessment and simulation of surface nanocrystallization by severe shot peening." *Acta Mater.*, 97, 105–115

Hassani-Gangaraj, S. M., Moridi, A., Guagliano, M. and Ghidini, A. (2014). "Nitriding duration reduction without sacrificing mechanical characteristics and fatigue behavior: The beneficial effect of surface nano-crystallization by prior severe shot peening." *Mater. Des.,* 55, 492–498.

Huang, H. W., Wang, Z. B., Lu, J., and Lu, K. (2015). "Fatigue behaviors of AISI 316L stainless steel with a gradient nanostructured surface layer." *Acta Mater.*, 87, 150–160.

Ichii, K. and Fugimura, K. (1986). " Structure of the Ion-nitrided Layer of 18-8 Stainless Steel." *Technol. Rep. Kansai Univ.*, 27, 135–144

Ji, S. J., Wang, L., Sun, J. C. and Hei, Z. K. (2005). "The effects of severe surface deformation on plasma nitriding of austenitic stainless steel." *Surf. Coat. Technol*., 195(1), 81–84.

Laleh, M., Kargar, F. and Velashjerdi, M. (2013). "Low-temperature nitriding of nanocrystalline stainless steel and its effect on improving wear and corrosion resistance." *J. Mater. Eng. Perform.,* 22(5), 1304–1310.

Larisch, B. and Spies, H. J., (1999). "Plasma nitriding of stainless steels at low temperatures." *Surf. Coat. Technol*., 116, 205-211.

Lecroise, F. and Pineau, A. (1972). "Martensitic transformations induced by plastic-deformation in Fe-Ni-Cr-C system." *Metall. Trans*., 3, 387–396.

Lee, W. S., and Lin, C.F. (2002). "Effects of prestrain and strain rate on dynamic deformation characteristics of 304L stainless steel: Part 2 - Microstructural study." *Mater. sci. tech*., 18, 869–876.

Li, G., Peng, Q., Li, C., Wang, Y., Gao, J., Chen, S. and Shen, B. (2008). "Effect of DC plasma nitriding temperature on microstructure and dry-sliding wear properties of 316L stainless steel." *Surf. Coat. Technol*, 202, 2749–2754.

Li, J., Zhao, G., Chen, H., Huang, Q., Ma, L. and Zhang, W. (2017) "Hot deformation behavior and microstructural evolution of as-cast 304L antibacterial austenitic stainless steel." *Mater. Research Exp.*, 5, 255-261.

Li, Y., Wang, L., Xu, J. and Zhang, D. (2012). "Plasma nitriding of AISI 316L austenitic stainless steels at anodic potential." *Surf. Coat. Technol*., 206(8–9), 2430–2437.

Li, Y., Zhang, S., He, Y., Zhang, L. and Wang, L. (2014). "Characteristics of the nitrided layer formed on AISI 304 austenitic stainless steel by high temperature nitriding assisted hollow cathode discharge." *Mater. Des*., 64, 527–534.

Liang, W. (2003). "Surface modification of AISI 304 austenitic stainless steel by plasma nitriding." *Appl. Surf. Sci*., 211(1–4), 308–314.

Lin, Y., Lu, J., Wang, L., Xu, T. and Xue, Q. (2006). "Surface nanocrystallization by surface mechanical attrition treatment and its effect on structure and properties of plasma nitrided AISI 321 stainless steel." *Acta Mater.,* 54(20), 5599–5605.

Liu, G., Lu, J. and Lu, K. (2000)."Surface nanocrystallization of 316L stainless steel induced by ultrasonic shot peening." *Mater. Sci. Eng. A*, 286(1), 91–95.

Liu, J. L., Umemoto, M., Todaka, Y. and Tsuchiya, K. (2007). "Formation of a nanocrystalline surface layer on steels by air blast shot peening." *J. Mater. Sci.*, 42(18), 7716–7720.

Lo, K. H., Shek, C., H. and Lai, J. K. L. (2009) "Recent developments in stainless steels." *Mater. Sci. Eng. R.,* 65 (4-6), 30-104.

Love, G. R. (1964). "Dislocation pipe diffusion." *Acta Metall.*, 12 (6), 731- 737.

Lu, J. Z., Luo, K. Y., Zhang, Y. K., Sun, G. F., Gu, Y. Y., Zhou, J. Z., Ren, X. D., Zhang, X. C., Zhang, L. F., Chen, K. M., Cui, C. Y., Jiang, Y. F., Feng, A. X., and Zhang, L. (2010). "Grain refinement mechanism of multiple laser shock processing impacts on ANSI 304 stainless steel." *Acta Mater.*, 58(16), 5354–5362.

Mahagoankar, S. B., Brahmankar, P. K. and Seemikeri, Y. C. (2008). "Effect of shot peening parameters on microhardness of AISI 1045 and 316L material." *Int. J. Adv. Manf. Tech.,* 38, 563-574.

Marchev, K., Cooper, C. V., Blucher, J. T. and Giessen, B. C. (1998). "Conditions for the formation of a martensitic single phase layer in ion-nitrided 316L austenitic stainless steel." *Surf. Coat. Technol.*, 99 (3), 225-228.

Maxwell, P. C., Goldberg, A. and Shyne, J. C. (1974). "Stress-assisted and strain-induced martensites in Fe-Ni-Cr alloys." *Metall. Trans.*, 5 (6), 1305-1318.

Menthe, E. and Rie, K. T. (1999). "Further investigation of the structure and properties of austenitic stainless steel after plasma nitriding." *Surf. Coat. Technol.*, 116–119, 199–204.

Menthe, E., Bulak, A., Olfe, J., Zimmermann, A. and Rie, K. T. (2000). "Improvement of the mechanical properties of austenitic stainless steel after plasma nitriding." *Surf. Coat. Technol.*, 133–134, 259–263.

Mingolo, N., Tschiptschin, A. P. and Pinedo, C. E. (2006). "On the formation of expanded austenite during plasma nitriding of an AISI 316L austenitic stainless steel." *Surf. Coat. Technol.*, 201, 4215–4218.

Misra, R. D. K., Nayak, S., Mali, S. A., Shah, J. S., Somani, M. C., and Karjalainen, L. P. (2010). "On the significance of nature of strain-induced martensite on phase-reversion-induced nanograined/ultrafine-grained austenitic stainless steel." *Metal. Mater. trans. A.*, 41(1), 3–12.

Moskalioviene, T., Galdikas, A., Rivière, J. P. and Pichon, L. (2011). "Modeling of nitrogen penetration in polycrystalline AISI 316L austenitic stainless steel during plasma nitriding." *Surf. Coat. Technol.*, 205(10), 3301–3306.

Murr, L. E., Staudhammer, K. P., and Hecker, S. S. (1982). "Effects of strain state and strain rate on deformation-induced transformation in 304 stainless steel: Part ii. microstructural study." *Metall. Trans A.*, 13(4), 627–635.

Murr, L. E. and Esquivel, E. V. (2004). "Observations of common microstructural issues associated withdynamic deformation phenomena: Twins, microbands, grain size effects, shear bands and dynamic recrystallization." *J. Mater. Sci.*, 39 (4), 1153-1168.

Naraghi, R., Hedström, P., and Borgenstam, A. (2011). "Spontaneous and deformation-induced martensite in austenitic stainless steels with different stability." Steel Research International, 82(4), 337–345.

Nishimoto, A. and Akamatsu, K. (2009). "Effect of pre-deforming on low temperature plasma nitriding of austenitic stainless steel." *Plasma Processes and Polymers*, 6(SUPPL. 1), 306–309.

Oliver, W. C. and Pharr, G. M. (1992). "An improved technique for determining hardness and elastic modulus using load and displacement sensing indentation experiments." *J. Mater. Research.* 7(6), 1564-1583.

Olson, G. B. (1972). "A mechanism for the strain-induced martensitic transformations* nucleation of." *J. Less Common Metals*, 28(1), 107–118.

Olson, G. B., and Cohen, M. (1975). "Kinetics of strain-induced martensitic nucleation." *Metal. Trans. A*, 6(3), 791–795.

Perdahcioglu, E. S. Geijselaers, H. J. and Groen, M. (2008). "Influence of plastic strain deformation induced martensitic transformation." *Scripta Mater*. 58 (11), 947-950.

Porter, D. A. and Easterling, K. E. (1992). "Phase transformations in metals and alloys." Second edition, Chapman and Hall, London.

Pye, D. (2003). "Practical nitriding and ferritic nitrocarburizing" ASM international.

Ronald, T., Retraint, D., Lu., K. and Lu, J. (2006). "Fatigue life improvement through surface nanostructuring of stainless steel by means of surface mechanical attrition treatment." *Scri. Mater*., 54, 1949-1954.

Ronald, T., Retraint, D., Lu., K. and Lu, J. (2007). "Enhanced mechanical behavior of a nanocrystallised stainless steel and its thermal stability." *Mater. Sci. Eng. A.,* 445, 281-288.

Saker, A., Leroy, C., Michel, H., and Frantz, C. (1991). "Properties of sputtered stainless steel-nitrogen coatings and structural analogy with low temperature plasma nitrided layers of austenitic steels." *Mater. Sci. Eng. A*., 140(C), 702–708.

Samandi, M., Shedden, B. A., Smith, D. I., Collins, G. A., Hutchings, R. and Tendys, J. (1993). "Microstructure, corrosion and tribological behavior of plasma immersion ion-implanted austenitic stainless-steel." *Surf. Coat. Technol*., 59(1–3), 261–266.

Schramm, R. E. and Reed, R. P. (1975). "Stacking fault energies of seven commercial austenitic stainless steels." *Metall. Trans. A.*, 6 (7), 1345.

Shen, L., Wang, L., Wang, Y. and Wang, C. (2010). "Plasma nitriding of AISI 304 austenitic stainless steel with pre-shot peening." *Surf. Coat. Technol.*, 204(20), 3222–3227.

Shrinivas, V., Varma, S. K., and Murr, L. E. (1995). "Deformation-induced martensitic characteristics in 304 and 316 stainless steels during room-temperature rolling." *Metall. Trans A.*, 26(3), 661–671.

Spencer, K., Véron, M., Yu-Zhang, K., and Embury, J. D. (2009). "The strain induced martensite transformation in austenitic stainless steels: Part 1– Influence of temperature and strain history." *Mater. Sci. Tech.*, 25(1), 7–17.

Staudhammer, K. P.L. E. M. . and S. S. H. (1983). "Nucleation and evolution of strain-induced martensitic embryos and substructure in stainless steel : A transmission electron microscope study." *Acta Metal.*, 31(2), 267–274.

Stinville, J. C., Villechaise, P., Templier, C., Riviere, J. P. and Drouet, M. (2010). "Plasma nitriding of 316L austenitic stainless steel: Experimental investigation of fatigue life and surface evolution." *Surf. Coat. Technol.*, 204 (12-13), 1947-1950.

Sun, Y. and Bell, T. (1998). "Sliding wear characteristics of low temperature plasma nitrided 316 austenitic stainless steel." *Wear*, 218(1), 34–42.

Sun, Y., Li, X. Y. and Bell, T. (1999). "X-ray diffraction characterisation of low temperature plasma nitrided austenitic stainless steels." *J. Mater. Sci.*, 4, 4793–4802.

Surface Engineering, Vol. 5, ASM Handbook, ASM International.

Talonen, J., and Hänninen, H. (2007). "Formation of shear bands and strain-induced martensite during plastic deformation of metastable austenitic stainless steels." *Acta Mater.*, 55(18), 6108–6118.

Tao, N. R. and Lu, K. (2009). "Nanoscale structural refinement via deformation twinning in face-centered cubic metals." *Scripta Mater.*, 60(12), 1039–1043.

Tao, N. R., Zhang, H., Lu, J., and Lu, K. (2003). "Development of Nanostructures in Metallic Materials with Low Stacking Fault Energies During Surface Mechanical Attrition Treatment (SMAT)." *Mater. Trans.*, 44(10), 1919–1925.

Thangaraj, B., T. S. Nellaiappan, S. N., Kulandaivelu, R., Lee, M. H. and Nishimura, T. (2015). "A facile method to modify the characteristics and corrosion behavior of 304 stainless steel by surface nanostructuring toward biomedical applications." *ACS Appl.Mater. Interf.*, 7(32), 17731–17747.

Tian, Y., Gorbatov, I., Borgenstam, A., Ruban, A., V. and Hedstrom, P. (2017). "Deformation microstructure and deformation induced martensite in austenitic Fe-Cr - Ni alloys depending on stacking fault energy." *Metall. Mater. Trans. A.*, 48 (1), 1-7.

Tong, W. P. (2003). "Nitriding iron at lower temperatures." *Science*, 299 (5607), 686–688.

Unal, O. and Varol, R. (2014). "Almen intensity effect on microstructure and mechanical properties of low carbon steel subjected to severe shot peening," *Appl. Surf. Sci.*, 290, 2014, 40–47.

Wang, J., Xiong, J., Peng, Q., Fan, H., Wang, Y., Li, G. and Shen, B. (2009). "Effects of DC plasma nitriding parameters on microstructure and properties of 304L stainless steel." *Mater. Charact.*, 60(3), 197–203.

Wang, T., Yu, J. and Dong, B. (2006). "Surface nanocrystallization induced by shot peening and its effect on corrosion resistance of 1Cr18Ni9Ti stainless steel." *Surf. Coat. Technol.*, 200 (16–17), 4777–4781.

Wu, Y. and Yan, M. (2011). "Effects of lanthanum and cerium on low temperature plasma nitrocarburizing of nanocrystallized 3J33 steel." *J. Rare Earths*, 29(4), 383–387.

Yang, H. P., Wu, X. C., Min, Y. A., Wu, T. R. and Gui, J. Z. (2013)." Plasma boriding of high strength alloy steel with nanostructured surface layer at low temperature assisted by air blast shot peening." *Surf. Coat. Technol*., 228, 229–233.

Yu, Z., Xu, X., Wang, L., Qiang, J. and Hei, Z. (2002). "Structural characteristics of low-temperature plasma-nitrided layers on AISI 304 stainless steel with martensite layer." *Surf. Coat. Technol.*, 153, 125–130.

Zhang, H. W., Hei, Z. K., Liu, G., Lu, J., and Lu, K. (2003). "Formation of nanostructured surface layer on AISI 304 stainless steel by means of surface mechanical attrition treatment." *Acta Mater.,* 51(7), 1871–1881.

Zhang, Z. L. and Bell, T. (1985). "Structure and corrosion resistance of plasma nitrided stainless steel." *Surf. Eng*., 1(2), 131–136.

Zhou, L., He, W., Luo, S., Long, C., Wang, C., Nie, X., He, G., Shen, X., and Li, Y. (2016). "Laser shock peening induced surface nanocrystallization and martensite transformation in austenitic stainless steel." *J. Alloy. Comp*., 655, 66–70.

LIST OF PUBLICATIONS

Journals:

Jayalakshmi, M., Ramachandra Bhat, B., and Udaya Bhat, K. (2016). "Microstructural characterization of low temperature plasma-nitrided 316L stainless steel surface with prior severe shot peening." **Journal of Materials and Design**, 108, 448–454.

Jayalakshmi, M., Ramachandra Bhat, B., and Udaya Bhat, K. (2017). "Effect of the shot peening coverage on surface nanostructuring of 316L stainless steel and its influence on low temperature plasma-nitriding" **Materials Performance and Characterization,** 6(4), 1-11.

Jayalakshmi, M., Prashant Huilgol, B. Ramachandra Bhat and Udaya Bhat K. "Insights into formation of gradient nanostructured (GNS) layer and deformation induced martensite in AISI 316L stainless steel subjected to severe shot peening" **Surface and Coatings Technology**, 344, 295-302.

Conference Proceedings:

Jayalakshmi, M., B. Ramachandra Bhat and Udaya Bhat K. (2018). "Enhanced cell adhesion on severe peened-plasma nitrided 316L stainless steel" **Proceedings of the International conference on Design, Materials and Manufacturing**, 1943, Page: 861-864.

Poster presented

Jayalakshmi, M., B. Ramachandra Bhat, Suma Bhat and Udaya Bhat K. (2018). "Effect of nitriding temperature on plasma nitriding of AISI 316L Stainless steel subjected to severe shot peening." International conference on advanced materials for stratergic sectors (ICAMPS 2018), 25-27th November, Thiruvananthapuram.

BIO DATA

Name	: Jayalakshmi M.
Father's name	: M. Seetharama Poojary
Date of birth	: 29-04-1989
Permanent address	: #6-15-598/2, Rajalakshmi Nilaya,
	Pangal Compound,
	Opposite Mannagudda Gurji,
	Mangalore-575003
	Dakshina Kannada Dist. Karnataka
Mobile	: +91-9731446456
E-mail ID	: jayalakshmi.nitk@gmail.com

Academic qualification:

Bachelor of Engineering (B.E.) in Metallurgical and Materials Engineering, from National Institute of Technology Karnataka (NITK), Surathkal (2010).

Master of Technology (M.Tech) in in Metallurgical and Materials Engineering, from Indian Institute of Technology Madras (IITM), Chennai (2012).

Work Experience:

Scientist/Engineer- SC, Liquid Propulsion Systems Center (LPSC) Valiamala, Indian Space Research Organisation (ISRO) from 20-06-2018 to present.